8-3-2021

AN EXAMINATION OF THE INFLUENCE OF DISTILLATION ON THE COMBUSTION BEHAVIOR OF APPARENTLY EQUIVALENT SURROGATE FUELS

Jay A. Lefkowitz
Rowan University

AN EXAMINATION OF THE INFLUENCE OF DISTILLATION ON THE COMBUSTION BEHAVIOR OF APPARENTLY EQUIVALENT SURROGATE FUELS

By
Jay A. Lefkowitz

A Thesis

Submitted to the
Department of Mechanical Engineering
College of Engineering
In partial fulfillment of the requirement
For the degree of
Master of Science in Mechanical Engineering
at
Rowan University
June 12, 2018

Thesis Advisor: Francis M. Haas, Ph.D.

Committee Members:
Krishan Bhatia, Ph.D.
Thomas Merrill, Ph.D.

Abstract

Jay Lefkowitz
AN EXAMINATION OF THE INFLUENCE OF DISTILLATION ON THE COMBUSTION BEHAVIOR OF APPARENTLY EQUIVALENT SURROGATE FUELS
2016-2018
Francis M. Haas, Ph.D.
Master of Science in Mechanical Engineering

Use of surrogates to emulate the combustion behaviors of prevaporized real fuels has been widely demonstrated in the literature. However, many combustion applications utilize atomized fuel sprays, and for these configurations, the assumption of fuel property homogeneity in prevaporized fuel combustion is tenuous. This work uses a simplified distilling droplet model to demonstrate a real potential for vaporization-coupled deviations from the single-valued combustion property targets used to characterize prevaporized combustion behaviors. To verify the model-based observations, flame blowout measurements from a custom-built annular spray burner rig are measured. Sets of essentially equivalent prevaporized jet fuel and gasoline surrogates suggested in the literature, and four nC9 surrogates composed of varying proportions of chemically similar n-alkanes are tested to examine blowout threshold variations driven by distillation behavior. The differing volatility characteristics of these surrogates emphasizes the influence of volatility on certain combustion behaviors (e.g., blowout) in a spray combustion environment. Noted variations in blowout limits (and also allowing for other limiting combustion behaviors not studied here) highlights the need to consider the coupling between distillation and combustion behavior.

Table of Contents

Table of Contents (Continued)

List of Figures

Figures Page

List of Figures (Continued)

Figures Page

List of Figures (Continued)

Figures Page

List of Tables

Tables Page

Chapter 1

Motivation

The goal of this work is to explore the effect preferential vaporization may have on the combustion behavior of real fuel surrogates. The fuel surrogates considered here are comprised of a limited number (<6) of pure component chemical species in specific proportions designed to mimic a corresponding real fuel's combustion behavior. This chapter will describe the motivation for creating fuel surrogates and the logic behind examining the effect preferential vaporization may have by

1. Exploring the complexity of real fuels and the variety among similar fuels,
2. Evaluating current surrogate formulation techniques, and
3. Identifying possible issues when using these surrogate fuels in real applications.

1.1 Complexity of Real Fuels

Petroleum-derived fuels are the chief energy source for the majority of modern propulsion applications. Common propulsion fuels such as gasoline, diesel, and kerosene-based jet fuels, are each derived from crude oil and differentiated by volatility. The crude oil these fuels are derived from is a naturally occurring substance found deep underground and formed over millions of years from decomposing organic material that results in a mixture of thousands of chemical components [1-11]. The crude oil itself is not a single composition, but consists of many varieties based on location and extraction methods which yield different quantities of desirable products [1-3, 5, 12].

In order to refine crude oil to produce fuels with the desired properties, modern oil refineries use complex processes to create the highest yields of the most in-demand fuels. A crude oil refinery is broken down into three main processes: separation, upgrading, and

conversion. The initial separation process of refinery breaks the crude into broad categories which are manipulated in later processes to create the largest quantities of the most in-demand fuels. This initial separation is most commonly achieved through fractional distillation. This is a process where refineries heat crude oil within a distillation column, creating a stratification of chemical species based on boiling point (volatility). As the components vaporize and separate, they are subsequently captured and condensed, creating regimes of mixtures differentiated by volatility. Figure 1 presents a simple illustration of fractional distillation; the broad categories of fuels shown are known as straight-run fuels [1-3, 13, 14].

Figure 1

Simplified Fractional Distillation Column With Straight Run Fuels and Associated Characteristics [78]

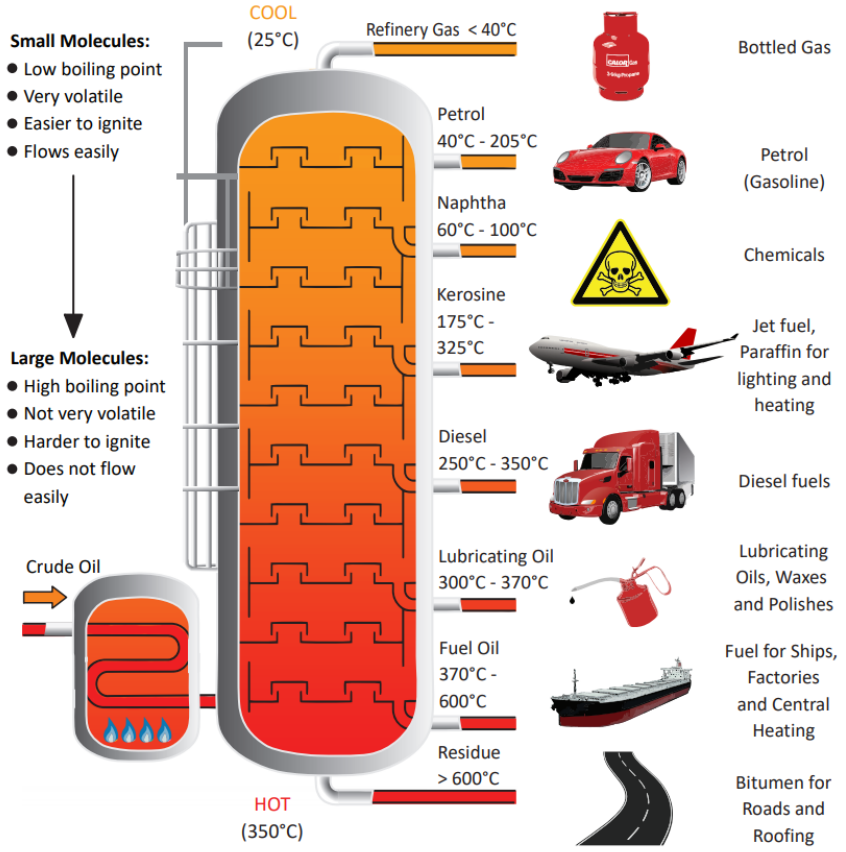

These straight-run fuels do not represent a static recipe, but rather a range of chemical species that share similar volatility. In turn, this generally correlates to similar molecular weight, density, viscosity and other physical characteristics [1-3, 13]. Volatility and carbon chain length are very closely correlated. To illustrate this, Figure 2 (a) shows distillation results of some hydrocarbon mixtures in the gasoline range. As the mixture is heated, the lower chain length (lighter) hydrocarbons generally distill off first indicating they are more volatile than their longer (heavier) counterparts. Keeping the volatility-

carbon chain length correlation in mind, these straight-run fuels can be categorized into general regimes. Figure 2 (b) highlights the chain length separation between common fuels isolated by fractional distillation.

Figure 2

(a) Distillation Curve and Associated Carbon Number Progression of a Hydrocarbon Fuel in the Gasoline Range [2]. (b) Carbon Number Regimes With Common Fuels Highlighted From [79]

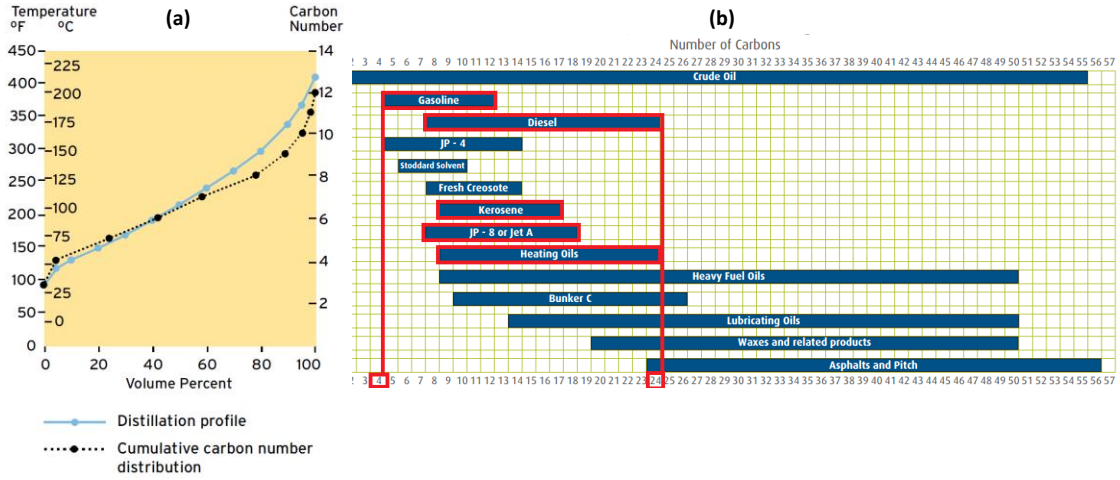

Further refining of these straight-run fuels is necessary to create mixtures that satisfy the stringent performance standards required by modern engines (e.g., ASTM D4814 for automotive gasoline [2], ASTM D975 for diesel [1], and ASTM D1655 for aviation turbine fuels [3]). To create commonly used propulsion fuels various blending recipes are created to give the desired qualities for reactivity, emissions, safe storage, lubrication, anti-icing, etc. [1-3, 7, 15]. The final products of the refining process are engineered mixtures of numerous chemical species in varying proportions within their

respective volatility/carbon chain length ranges. The jet and diesel fuel gas chromatography–mass spectrometry (GC-MS) data given in Figure 3 reveal the vast number of chemical species present in either of these fuels, which share a similar molecular weight range. The GC-MS spectrometry identifies chemical abundance by heating a substance and passing it through a narrow tube (column), which separates chemical species by volatility and diffusion rate, after which abundance is determined [12]. The time scale on the x-axis represents heat addition, which is ramped during the GC-MS separation process, as time progresses the molecules are vaporized based on boiling point creating a scale of volatility. We can assume that the least volatile fuels (longest to vaporize) are also the largest. This chromatogram in Figure 3 reveals some distinction between these two fuels, indicating that the diesel contains greater concentrations of less volatile components as compared to the jet fuel.

Figure 3

GS-MS Spectrometry of Jet Fuel #4 And Diesel Fuel #5 [12]

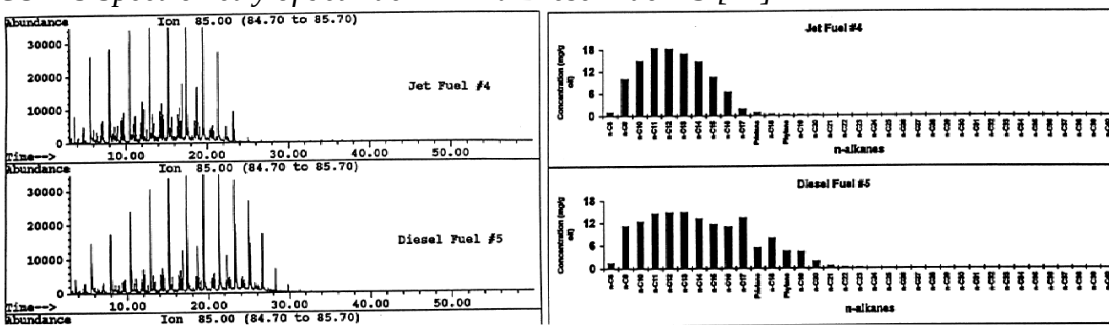

Furthermore, speaking to the chemical composition variety among similar fuels, blend recipes change seasonally, geographically, and by performance requirements (e.g., winter blend, summer blend, arctic blend, regular, premium, etc.) which indicates there is no set recipe for a given fuel. Gasoline serves as an excellent example since it is domestically the most widely used civilian fuel [2]. Focusing on performance and seasonal changes in Figure 4 (a) and (b) we can see that the blend recipe changes both fuel composition and performance.

Figure 4

(a) Species Concentration Represented by Carbon Number for Regular and Premium Grade Gasoline. (b) Distillation Curves Highlighting Seasonal Changes in Gasoline Vaporization Behavior [2]

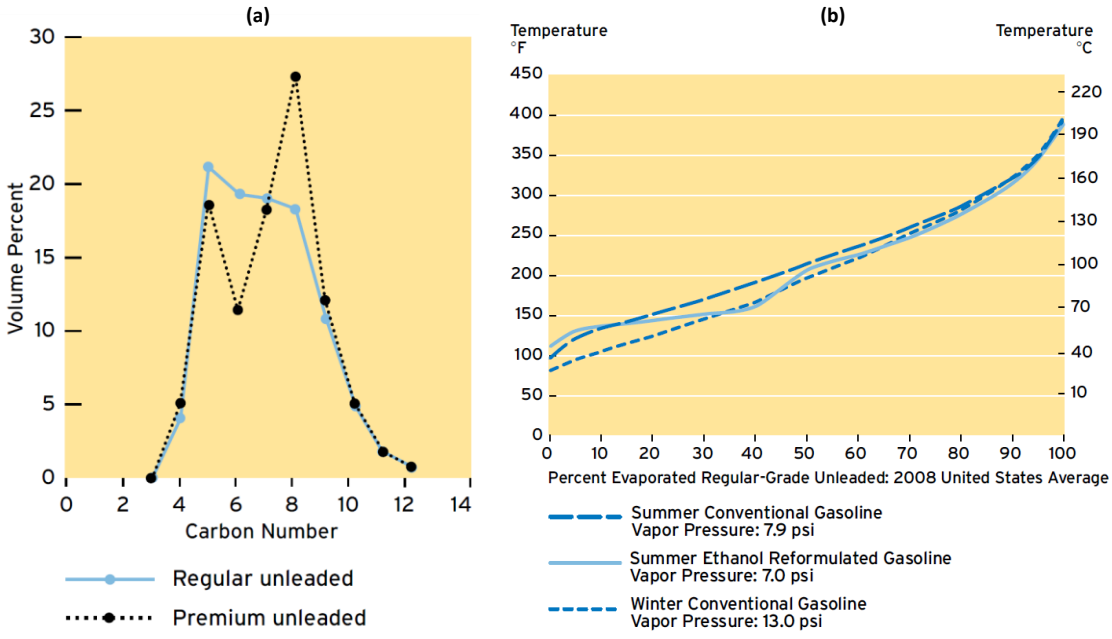

Figure 4 (a) describes the difference in chemical speciation between regular and premium gasoline; here, the most obvious deviation in composition is between carbon

numbers 5 through 9. Refineries edit the formulas of fuels to achieve some desired performance metrics. In gasoline, a key performance metric is Research Octane Number (RON), which is an indicator of reactivity, specifically, resistance to autoignition. Larger RON numbers indicate a less reactive fuel, which is desirable in spark ignition gasoline engines to reach higher compression ratios without knocking [2, 9, 16, 17]. If we consider that the RON scale is defined by n-heptane (a 7 carbon molecule with a RON of 0) and iso-octane (an 8 carbon molecule with a RON of 100), then hypothetically , panel (a) could describe a (slight) reduction of heptane and an addition of iso-octane into the premium fuel to achieve the desired quality of autoignition resistance. This observation highlights the inconsistency in chemical composition among different grades of the same fuel.

Figure 4 (b) illustrates the ASTM D86 distillation for three blends of gasoline. The ASTM D86 method is the standard for gauging fuel vaporization performance [14, 18-21] and will be described in detail in later sections. Briefly, this distillation method involves heating a fuel in a closed environment at atmospheric pressure, collecting the vapors, and then cooling and condensing them downstream. Incremental temperature measurements of the upstream mixture are taken as the condensed mixture accumulates. Analysis of complex fuels such as those indicated in Figure 4 (b) above using this method gives some insight into the vaporization behavior of such mixtures. Since only vapors ignite [2, 3, 22], vaporization character is essential in gauging many desired performance metrics, such as cold starting. Figure 4 (b) additionally illustrates performance differences between these blends, specifically in the early stages of vaporization, which is representative of startup behavior. We observe that the winter mix is more volatile than the summer blend, which is essential in colder weather for in cylinder vaporization performance [2, 5, 9].

A final observation to make pertaining to petroleum fuel variation is that the regulations and tests which verify these fuels are based on non-uniform government standards such as the volatility control tests CEN EN 228 (Europe), ASTM D4814 (USA), and JIS K2202 (Japan) [2, 9]. Additionally, these tests verify fuel behavior and not fuel composition, so individual batches of fuel may contain varying concentrations of chemical species [1-3, 5, 6, 9, 11, 12, 23, 24] yet still fit performance criteria.

With this information, we can make two general statements about petroleum fuels as they are generally used for propulsion:

1. These fuels are complex mixtures of hundreds of chemically distinct components, and

2. There is no set standard recipe (composition) for these fuels, but rather a set of standard behaviors a fuel must satisfy to be classified as an acceptable fuel.

The variable compositional nature of these fuels creates consistency and complexity issues for combustion researchers and engine designers alike. Combustion researchers require consistent test fuels to mitigate effects of batch-to-batch compositional discrepancy on experimental results. Engine designers desire efficient computational fluid dynamics models to predict engine performance prior to prototype fabrication, which can reduce development costs. To achieve models of complete chemical fidelity, the hundreds of unique chemical species and the resulting thousands of combustion reaction intermediates must be fully tabulated. However, these intermediates change both spatially and temporally as the reaction progresses according to the fuel composition and combustion environment. The immense amount of data required to develop and validate

these models is infeasible due to the sheer computational overhead and a lack of knowledge on every specific intermediate reaction [4, 5, 7, 8, 11, 23, 25].

1.2 Surrogate Fuel Formulation Techniques

To remedy these intrinsic problems with real fuel, many studies [4-11, 23, 25-30] have used surrogate fuels composed of a limited number of chemical species in specific proportions with the intention of mimicking real fuel combustion behavior. In many cases, these surrogate recipes/formulation techniques are mixed/created through matching some ensemble of combustion properties (CPs). These CPs, such as research octane number (RON), derived cetane number (DCN), hydrogen-to-carbon (H/C) ratio, lower heating value (LHV), molecular weight (MW), and threshold sooting index (TSI), quantify key combustion behaviors related to reactivity, sooting, global transport phenomena, thermodynamic potential, etc. For surrogate formulation, the CPs of real fuels become combustion property targets (CPTs) to which surrogate CPs are matched, with the presumption that real fuel and surrogate will share similar combustion behaviors. The nature of CPT matching can lead to non-unique surrogate formulations, i.e., several surrogates may emulate the target real fuel, resulting in an effective equivalence [4, 7, 9, 11, 23, 26, 27, 29, 31]. Despite apparent success in matching behavior of surrogates to real fuels for prevaporized conditions [7, 9, 10, 18, 23, 29, 32, 33], this study focuses on the principal limitation of the prevaporized assumption – namely that many applications of combustion frequently involve two-phase fuel flow. This in turn suggests the properties of the liquid fuel and its liquid-to-vapor transition may be important in development of surrogates for real fuels used in such application.

1.3 Surrogate Fuel Real Application Challenges

In particular, aero-propulsion combustion utilizes atomized liquid fuel sprays. This fuel spray must go through a phase change from liquid to vapor to burn because only vapors participate directly in combustion. This phase change is governed by many properties of the fuel, as well as the combustion environment, including but not limited to fuel cloud density, volatility, fuel density, reactivity, heat feedback, etc. [4, 22, 24, 34-38]. Simply considering that as a fuel droplet vaporizes, its most volatile components come off first indicates stratification of chemical and combustion properties may be induced. This phenomenon is known as preferential vaporization. While preferential vaporization occurs in real fuels, as seen by gasoline's distillation curve (Figure 4(b)), its composition of hundreds of distinct chemical components largely mitigates property stratification. In the case of a surrogate fuel composed of a limited number of chemical species (<6), the effect of preferential vaporization on property stratification may be much greater. The possibility of significant chemical and associated property stratification in non-prevaporized circumstances may invalidate the surrogate's real fuel emulation ability as determined by matching of CPTs for prevaporized combustion.

To determine preferential vaporization's impact on a surrogate's ability to emulate real fuel, this work examines the problem both computationally and experimentally. Chapter 2 presents and demonstrates a simple batch distillation model which offers insight into the stratification of chemical species and associated combustion properties as a fuel droplet distils. Chapter 3 discusses the development and testing of an annular burner rig designed to compare flame liftoff and blowout combustion behaviors of fuel. The experimental results obtained by the burner rig are presented in chapters 4 (pure

components) and 5 (surrogate fuel blends). In chapter 6, the measurements obtained from this rig are critically evaluated to determine how well effectively equivalent surrogates emulate each other's combustion behavior and the impact that property stratification has on surrogate fuel performance.

Chapter 2

Numerical Distillation Model

This chapter will describe the simplified numerical approach taken to qualify the possible combustion property stratification that may occur as a result of preferential vaporization in multicomponent mixtures containing species of varying volatility. This chapter will explain the:

- Phenomenological model used to simplify complex spray combustion environments and its relation to ASTM D86 distillation.
- Mathematical algorithms implemented to computationally resolve the simplified model.
- Validation of the mathematical model through pure component property evaluation.
- Ability of the model to predict combustion behavior of a real fuel and surrogate tested in an optical engine.
- Preferential vaporization and associated property stratification effects on multicomponent surrogate fuels that are experimentally tested in later chapters of this study.

2.1 Phenomenological Model

The goal of the distillation model described in this chapter is to provide some insight into the possible chemical species and accompanying property stratification that may occur during the vaporization and subsequent combustion of a multicomponent fuel mixture. In this model, the distillation process and combustion environment are significantly simplified due to the complex nature of spray combustion environments. Spray combustion environments are still not fully understood by the research community

because of their multidimensional nature [22, 36, 37, 39]. Briefly, spray combustion involves chemical equilibrium, energy conservation, chemical kinetics, transport phenomena, stability limits, boundary layer interaction, multiphase considerations, spray cloud density, droplet geometry, and droplet interaction, among other factors [22, 36]. These numerous factors make it necessary to simplify our model. Additionally, this study is searching for qualifying insight into multicomponent fuel vaporization and not exact quantitative results that may be achieved, to a degree, with more advanced and computationally expensive models [4, 31, 35, 39]. This model will be able to incrementally determine the chemical compositions of each fuel phase as it distills. The application of linear blending rules will allow us to infer combustion properties in a similar method used in surrogate formulation techniques such as [7, 9, 10, 26, 29].

In order to achieve the goal of a relatively simplistic distillation model while still maintaining sufficient detail to remain relevant to real applications, we first had to form a physical understanding of the fuel that would be vaporizing. We began with a complex fuel spray that would be expected in a real application, we then isolated a single droplet and negated complexities such as internal swirl, micro explosion, heat/mass transfer barriers, etc., expected in atomized droplets [22, 36]. Further, we considered the droplet to be in effective isolation, not interacting or influenced by other droplets or the surrounding droplet cloud. Figure 5 provides an illustration of our simple droplet model. The droplet consists of a liquid interior, surrounded by a vapor envelope. This droplet closely relates to how an actual droplet would behave during vaporization dictated by droplet heating phenomenon [22, 35, 39].

Figure 5

Illustration of the Simple Isolated Droplet Model Considered in the Distillation Program

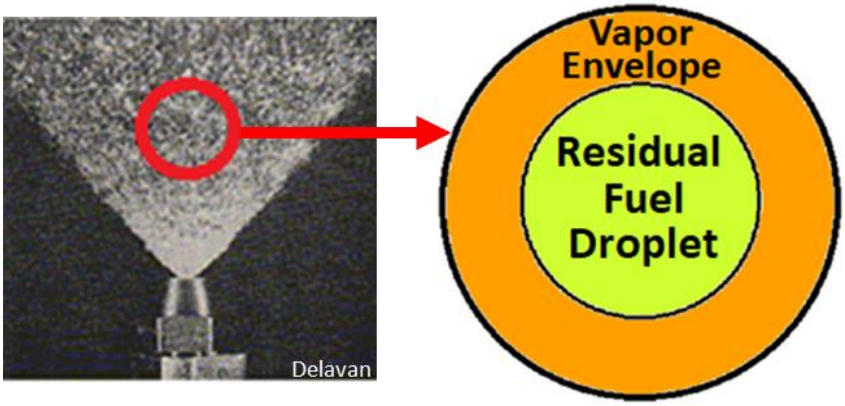

Note. The model represents a single droplet in a dense fuel spray and consists of a liquid interior, which vaporizes and deposits chemical species into the vapor envelope. The fuel spray graphic is from [64].

With consideration of our physical representation, we then formulated a process to numerically "distill" the droplet based on the standard ASTM D86 petroleum distillation method. The D86 method is applicable to real fuel distillation as it is one of the qualifying tests that real fuels undergo as seen in the earlier Figure 4 (b). This method is the standard for evaluating real fuel's distillation behavior [2, 20, 21], so numerically simulating it should provide insight into how preferential vaporization, specifically, component volatility, may affect a real multicomponent mixture. Figure 6 provides a cartoon illustrating the ASTM D86 process.

Figure 6

Visualization of ASTM D86 Batch Distillation

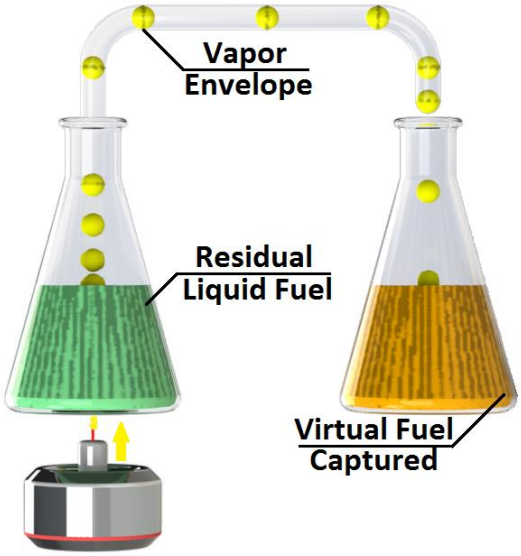

Note. The flame represents the energy input to vaporize the liquid fuel, which is subsequently captured and condensed.

ASTM D86 distillation is a process in which a liquid fuel is incrementally heated at atmospheric pressure. As the temperature of the liquid fuel increases, vapor forms and exists an actively heated container, to be subsequently captured and condensed. Temperature measurements of the residual liquid fuel (Figure 6) are taken in increments based on volumetric percent distilled to indicate vaporization behavior. The result, plotted as a function of volume percent distilled and temperature is known as the distillation curve [2, 15, 20, 21]. The distillation curve indicates how the fuel will vaporize, which is useful in determining fuel performance in different combustion environments. Figure 7 shows

how Chevron deconstructs the distillation curve for useful performance metrics for a gasoline fuel [2].

Figure 7

Chevron's Deconstruction of the Distillation Curve With Key Performance Metrics Highlighted [2]

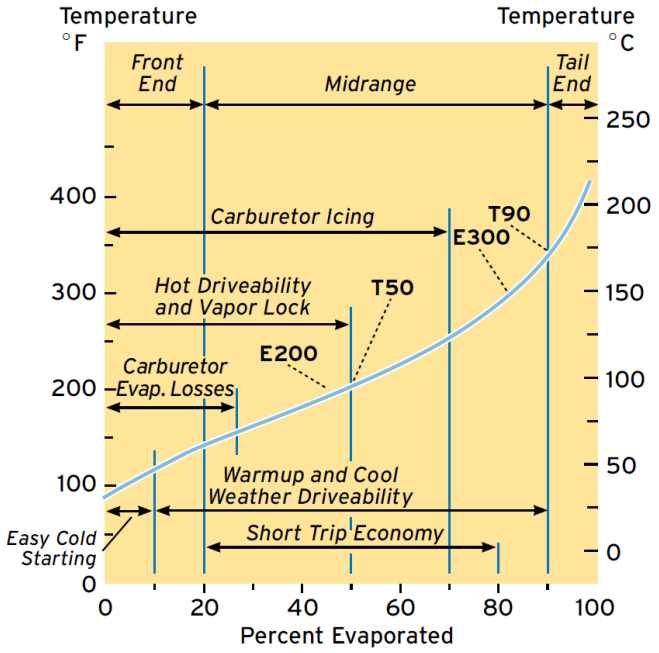

Note. Key landmarks appearing along the curve include E200 and E300 corresponding to volume percent evaporated at 200°F and 300°F as well as T50 and T90 corresponding to the fuel temperature at 50% and 90% volume distilled.

This figure isolates key performance metrics directly correlated to how a fuel distills. Distillation performance indicators provide refineries with the necessary constraints for fuel blend formulation, seen earlier in Figure 4 (a) and (b), such as winter and summer blends as well as performance grade manipulation (regular, premium) [1-3,

21, 40]. Key constraints on a fuel's distillation behavior are on the front and tail ends. Observing Figure 4 (a), we see that performance grade manipulation on fuels designed for the same season have very similar front and tail ends, with carbon number variation generally in midrange distillation. The front end is essential in cold starting and cold operation because it demands increased fuel volatility to vaporize at lower temperatures, allowing the fuel to combust and the engine to start. Volatility must also be limited in the front end to not exceed vapor lock limits which occur when fuel vaporizes in the delivery system rendering fuel pumps inoperable. The tail end restriction is adhered to for fuel economy and emissions. The fuel must be volatile enough to completely vaporize in order to utilize all the chemical energy stored within. Additionally, unburnt hydrocarbons are extremely harmful to the environment so, again the fuel must be volatile enough at the tail end to completely vaporize and combust. The midrange area offers refineries some play, but key points such as E200, E300, T50 and T90 must still be within the acceptable limits determined by performance requirements (e.g. quick warm-up, drivability, power, acceleration, etc.) [1-3, 40].

2.2 Mathematical Algorithm

With a defined physical and distillation representation, mathematical formulas could be derived through the application of assumptions valid within the isolated spherical droplet and D86 distillation realm. To begin forming a mathematical representation of the distillation process, we first had to confine our scope for the combustion process. We define fuel vaporization as an equilibrium-limited process, so we are not heat or mass transfer limited, this is indicative of ideal combustion [22]. During combustion, chemical heat release is the driving reaction force [22], so we ignore cooling effects from co-flow air and

radiative heat transfer. This assumption is reasonable if we consider the environment to be at a quasi steady-state which additionally designates an isobaric environment. The liquid fuel surrogate is also assumed to be an ideal mixture, and the vapor behaves as an ideal gas. This specifies that the mixture is completely miscible and non-azeotropic, which is reasonable, being that most hydrocarbons are miscible with each other. There do exist some hydrocarbons with azeotropic relationships, but they are typically minor [41], so the assumption holds. Lastly, incorporating that during combustion the surface of a droplet must be close the boiling temperature for vaporization to occur [22, 34, 35, 39] we can apply a system of equations to create our iterative batch distillation program.

The base equation behind the program's solver is a form of Antoine's equation described in Equation 1.

$$\mathrm{Ln}\, P_{vp_i} = A_i + \frac{B_i}{C_i + T} \tag{1}$$

Here, A_i, B_i, and C_i are the known Antoine coefficients that are obtained experimentally for each component i [42, 43], T is temperature. In our program, the coefficients are obtained from [43] and are taken with a 1 kilopascal reference. P_{vp_i} is the vapor pressure of a component at a given temperature T, measured in kelvin (K). If we have some known chemical component at a given temperature, we could use the Antoine equation to determine its vapor pressure. To take this a step further, consider a multicomponent mixture and Raoult's Law, given in Equation 2

$$P_i = P_{vp_i} x_i \tag{2}$$

Raoult's Law states that the partial pressure (P_i) of a component in a mixture is equal to its vapor pressure (P_{vp_i}) in relation to its mole fraction (x_i). The last relationship necessary to complete our solver's distillation logic is Dalton's law of partial pressures described in Equation 3

$$P_T = \sum_{i=1}^{n} P_i \tag{3}$$

Dalton's law states that the total vapor pressure (P_T) is equal to the sum of each component's partial pressures (from 1 to n components). Combining Raoult's (Equation 2) and Dalton's (Equation 3) Laws we arrive at Equation 4 which equates the relation between vapor pressure, molar concentration, and partial pressure to the total pressure.

$$P_T = \sum_{i=1}^{n} P_{vp_i} x_i \tag{4}$$

If we now substitute in the Antoine equation (Equation 1) solved for the partial pressure we arrive at the core algorithm for the distillation program, described by Equation 5

$$P_T = \sum_{i=1}^{n} e^{A_i + \frac{B_i}{C_i + T}} x_i \tag{5}$$

If we apply the assumption that vaporization occurs when the vapor pressure of a liquid is greater than, or equal to the ambient pressure as described in [13] and [44] we can solve Equation 5 for the mixture's bubble temperature (T) by setting the total vapor pressure (P_T) equal to any known pressure (atmospheric for D86). The bubble temperature is akin to surface temperature [22], thus, it is indicative of the mixture's (droplet's) temperature, assuming complete droplet mixing. We can now re-input the mixture's temperature into the Antoine's equation (Equation 1) to solve for each component's vapor pressure and subsequently extract their partial pressures. Lastly, the distillation program progresses iteratively with a set fraction of the initial mixture's molar content distilled per step. Knowing the moles distilled per step (T_m, Equation 6) and the partial pressure of each component (P_i), we can calculate the amount vaporized of each component (V_i, Equation 7) and the remaining liquid composition ($x_{(i+1)}$, Equation 8).

$$T_m = (\%\text{MoleStep}) * (\text{Initial Moles}) \tag{6}$$

$$V_i = P_{vp_i} T_m \tag{7}$$

$$x_{(i+1)} = x_i - V_i \tag{8}$$

Note here that the total moles distilled per step (T_m) is constant through the distillation process because we take a constant molar percent on each iteration. This was implemented to reduce complexity, but other distillation progressions such as those based on the d^2 Law or other more complex physical relationships could also be applied. Here, we believe that the additional complexity adds little to the overarching goal of

understanding preferential vaporization's effect on multicomponent mixtures. The final step in this process, once distillation has been resolved, is to apply the previously discussed linear blending rules to extract the combustion property (CP) evolution along the fuel's distillation trajectory. The equation for linear blending is described below in Equation 9.

$$CP_{mix} = \sum_{i=1}^{n} CP_i \, x_i \tag{9}$$

Before using this program to distill multicomponent fuel mixtures, we first evaluated the Antoine equation-based core solver. Research indicates that the equation is an adequate method for resolving multicomponent fuel distillation for temperatures not exceeding 85% of any component's critical temperature [42]. Further, [44] observes that the Antoine equation method for predicting temperature dependent vapor pressures is within +/- 1% of reported data. Through observing some arbitrary sample mixtures at atmospheric pressure, the calculated distillation curve, in general, was within the critical temperature limits for the Antoine equation. With confidence that the solver exists within the bounds of validity for the Antoine equation, the program was tested against published NIST values [45] for various well-studied pure components' boiling points which can be seen in section 2.4. Results show agreement to within a few kelvin between predicted and published values, indicating that the program is properly determining component volatility. The logic diagram, annotated code, and sample input files can be found in Appendix A. While more advanced programs exist, which may more accurately predict distillation behavior and CP evolution [4, 31, 35, 37], the Antoine equation is adequate for the scope

of this study, which is to give insight into preferential vaporization's effect on multicomponent fuel distillation, not direct quantitative valuation. Further, the simplicity of linear blending is appropriate because (1) we are only looking for a qualitative approximation of CP evolution and (2) linear blending is common among various surrogate formulation studies, specifically, the studies that will be experimentally tested here [9, 29].

2.3 Realistic Comparison & Scope Specification

Taking a step back from the mathematical theory and reapplying our basic model framework of a spherical droplet and the ASTM D86 distillation method, we observe that with some manipulation this program can predict the evolution of the three distinct chemical mixtures expected during ASTM D86 distillation as seen in Figure 6. The program can determine the liquid composition (x_i), the vapor envelope composition (V_i), and if we summed the vapor envelope composition throughout distillation, we could also acquire the condensed fuel composition. Each of these stages are unique, with dynamic compositions as distillation progresses. This makes their differentiation essential to extracting meaningful combustion properties. We consider that the condensed fuel composition will not exist during combustion since the vapor envelope will be consumed in the flame. Thus, we treat it as a "virtual" stage as it is considered elsewhere [29]. Applying this to a basic understanding of the combustion environment, we can visualize this as the vapor envelope being blown off the surface of the liquid at each distillation interval, thus it leaves the system; analogous to being consumed during combustion. With that, we are left with the residual liquid and vapor envelope stages correlating to our spherical droplet model (Figure 5). The distinction between these two stages is key since

their chemical composition and combustion properties are unique. To highlight the spatiotemporal shifts in composition and accompanying properties we formulated a ternary plot for some three component mixture, as described by Figure 8.

Figure 8

Distillation-Resolved Composition and CP Trajectories for the Residual Liquid and Vapor Envelope Stages of a Representative Ternary Mixture/Surrogate

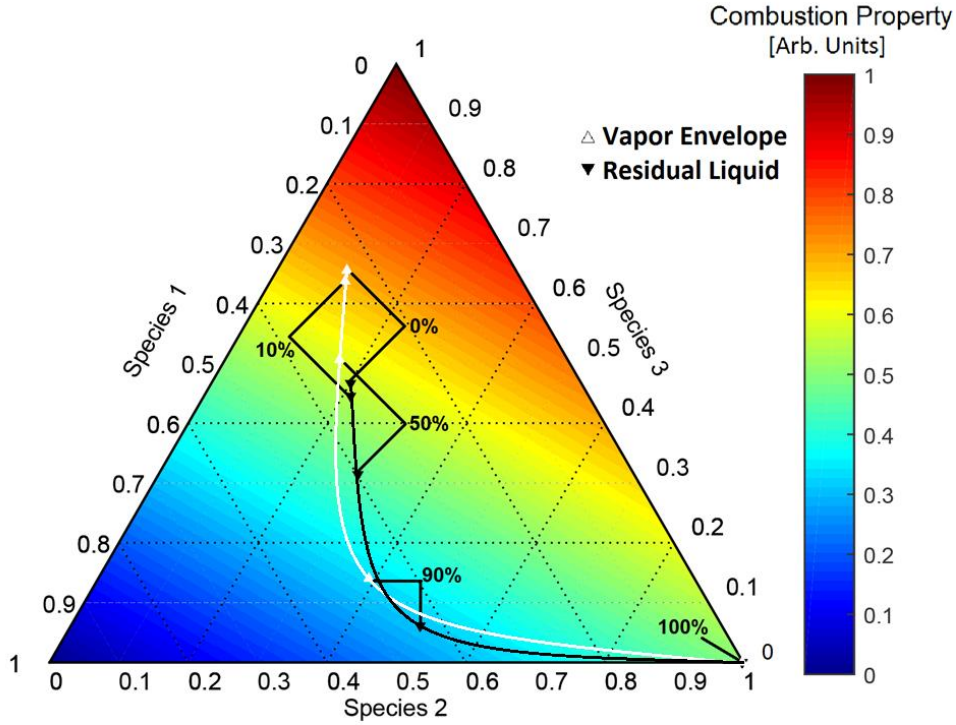

Note. Position indicates composition as fraction of volume distilled, color represents some arbitrary CP.

On the ternary plot, position represents the concentration of the three species simultaneously, and color represents some combustion property which is determined by the aforementioned linear blending rules. As the fuel distils, both liquid fuel composition

(black line) and vapor envelope composition (white line) evolve along separate trajectories in which the combustion property of interest is almost never equal between liquid and vapor phases. We further highlight this CP differentiation in Figure 9 by reapplying our spherical droplet model to the hypothetical distillation-resolved CPs revealed in the ternary plot. The unique combustion properties of liquid and vapor illustrated in this hypothetical example strongly suggests that preferential vaporization effects can be important in surrogate fuel formulation.

Figure 9

Representative Spherical Droplet Model Progressing Into Residual Liquid Fuel Droplet and Vapor Envelope Stages Through Equilibrium-Limited Vaporization

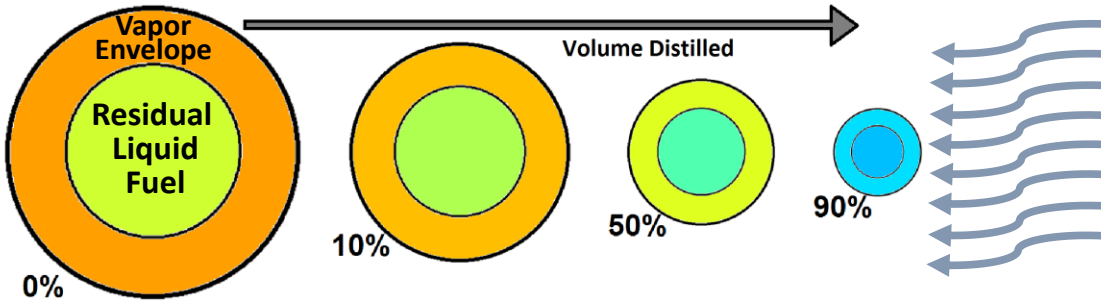

Note. Color indicates some arbitrary CP and corresponds to Figure 8.

What we observe is that the liquid and vapor exhibit varying combustion properties (represented by color) for the majority of distillation. At this point, a key distinction must be made in order to evaluate the stage which most closely represents behavior in real combustion. As stated earlier, only vapor is consumed in the flame so, combustion properties for the remainder of this study are based on type and abundance of species

deposited in the vapor envelope. This assumption fits well with our previous analysis of the combustion environment since the vapor is what is leaving the system, i.e., consumed during combustion.

The takeaway from this model is that we can resolve species progression throughout a mixture's distillation trajectory and its corresponding combustion property progression through applying linear blending rules. With a firm understanding of how the distillation program solves composition and accompanying properties, as well as accepting that its simplicity only allows for a qualitative understanding of these properties, we can begin computationally "distilling" surrogates of real fuels to gain some insight into surrogates' ability to emulate their corresponding real fuel's combustion behavior.

2.4 Program Validation: Pure Component Boiling Points

The first results we simulated were pure component fuels present in the surrogate mixtures evaluated later in this section [9, 10, 29]. Distilling these fuels should yield a linear line with a slope of zero. The value of the line should correspond to the component's normal boiling point (at atmospheric pressure). This set of data is presented in Table 1 and is representative of all species that future computed distillations will consist of with the exception of Decalin. Referenced work used a mixture of cis- and trans- isomers, which have different boiling points [10, 45].

Table 1

Comparison of Pure Component Normal Boiling Points to Calculated Results. Data From [45]

Species	NPB (°C)	Calculated BP (°C)
n-heptane (nC7)	98.35 +/- 0.3	98.60
n-octane (nC8)	125.55 +/- 0.5	125.81
n-decane (nC10)	174.05 +/-0.6	174.54
n-dodecane (nC12)	215.85 +/- 2	216.76
n-hexadecane (nC16)	280.85 +/- 10	287.24
iso-octane (iC8)	99.25 +/-0.2	99.90
iso-cetane (iC16)	240.05	247.75
Ethanol	78.35 +/- 0.2	80.06
Toluene	110.65 +/- 0.2	111.38
1,3,5-Trimethylbenzene	164.65 +/- 0.8	166.77

The pure component distillation data generally corresponds well to the published normal boiling point (NBP) values. This indicates that the distillation program is accurately emulating species' vaporization characteristics. Some other basic tests were performed on varying number of component fuels which verified reasonable distillation behavior when compared to other established vapor-liquid equilibrium distillation programs [9, 10, 29, 45]. Confident in the program's ability to accurately distill fuel mixtures, we proceeded to examine the multicomponent surrogate fuels which are the focus of this study.

2.5 Program Validation: Optical Engine Comparison

Confident in the program's ability to accurately distill multicomponent mixtures, we wanted to examine if the distillation program's methodology of resolving combustion properties along distillation trajectory can indicate a fuel's ability to emulate target properties and associated combustion behavior. To do this, we examined surrogates and optical engine testing presented in Violi et al. [32]. The surrogates are formulated by the Violi group in Kim et al. [10] using prevaporized species property targets and blending rules to match certain CPTs in a similar fashion as surrogates ([9] and [29]) experimentally tested later. The Violi group tested their surrogates against the corresponding real fuels using a compression-ignition optical engine and broadband UV chemiluminescence which they describe in [32]. The comparison between the surrogate and real fuel in the optical engine serves as a benchmark to test whether our distillation-resolved results can differentiate a surrogate that may emulate its corresponding real fuel well and one that may not.

The Violi et al. study examined three surrogates corresponding to the real jet fuels Jet-A POSF-4658, coal derived Sasol IPK POSF-5642, and natural gas derived Syntroleum S-8 POSF-4734, which were chosen for their use in aero-propulsion engines [10]. In this study, we will focus on the IPK and S-8 surrogate. To reduce repetition and provide clearer correlations between distillation-resolved CPs and optical engine results. The surrogate compositions and combustion property targets are described in Table 2 [10].

Table 2

Combustion Property Targets, Calculated Surrogate Properties, and Recipe for the IPK and S-8 Surrogates Evaluated Using an Optical Engine in [32]

(Target/Surrogate)	IPK Surrogate	S-8 Surrogate
Derived Cetane Number	31.2/31.9	60.5/61.1
H/C Ratio	2.119/2.121	2.152/2.173
MW [g/mol]	156/149.6	168/163.9
LHV [MJ/kg]	44/44.21	44.1/44.42
Components (mole fraction)		
n-decane	-	0.4234
n-dodecane	0.1416	0.3073
iso-octane	0.4016	0.0384
iso-cetane	0.3141	0.2309
Decalin	0.1427	-

Note. The two surrogates are not designed to be equivalent to each other.

Before making comparisons to the Violi et al. chemiluminescence measurements, we first wanted to observe how the surrogate's distillation compares to the real fuel's. Real fuel distillation behavior was determined using an advanced distillation method (akin to ATSM D86) [46, 47] and overlaid onto our simulated surrogate's distillation curve at atmospheric pressure. The results are presented in Figure 10 (a), and (b).

Figure 10

Experimental Distillation Curves of Kim et al. [7] (Symbols) For Real Fuels Tested in Violi et al. Chemiluminescence Studies [32] Compared to Computed Distillation (Present Work) for Surrogate Fuels Suggested by Violi et al. (a) IPK [32], (b) S-8 [10]

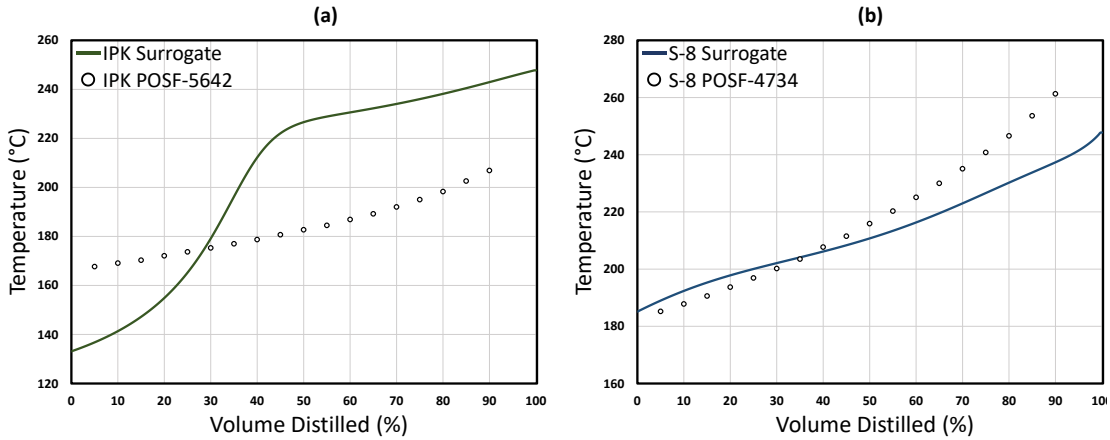

The distillation curve's temperature range indicates that this data is within an acceptable range for use of the Antoine equation, specifically, temperature does not exceed 85% of critical for any individual chemical component (Appendix B). Accepting that the program is operating correctly, observing panels (a) and (b) we can see that the S-8 surrogate appears to be a better match to its real fuel compared to the IPK surrogate. While this observation is interesting, it is not as informative as it may seem. The distillation curve is a compilation of many multidimensional factors and can only indicate that some volatility related vectors are well matched. Matching distillation curves will not directly indicate accurate real fuel emulation due to its multi-faceted nature, but rather give some idea of what may occur. We believe, to gauge a surrogate's ability to emulate its corresponding real fuel, distillation-resolved CPs must be compared to real fuel CPTs throughout the fuel's distillation trajectory.

To calculate meaningful CPs from our distillation program for comparison against optical engine data we had to adjust our D86 model framework because the optical engine does not operate at atmospheric pressure. The engine has a compression ratio of 15:1 and using Equation 10 we can calculate an approximate pre-ignition operating pressure at top dead center (TDC).

$$P = P_0 * r^k \tag{10}$$

Setting P_0 to atmospheric, compression ratio (r) to 15 and specific heat ratio (k) to 1.3 (representative of an air-fuel mixture), we extract a pressure of approximately 33 atmospheres, or 3424 kPa. Solving the program's core algorithm (Equation 5) with P_T equal to our pre-ignition pressure will yield the fuel's distillation behavior within the engine. Applying linear blending rules to this data will yield CPs at engine operation which could serve as a better indicator of real fuel behavior emulation as compared to the atmospheric D86 distillation curve. It should be noted that the increased pressure of the combustion environment produces higher distillation temperatures which brings us out of the Antoine equation 85% critical temperature restriction by a significant margin. Nonetheless, we continue with our qualitative observations accepting the margin of error to see if the program can still be an indicator of real distillation behavior.

The optical engine setup is capable of detecting HCHO (formaldehyde) and OH* emissions, from which it constructs chemiluminescence images generated via probability density functions over 50 cycles at 1200 RPM, as described in [32]. The HCHO emissions are representative of low temperature combustion and heat release that occurs early in the combustion process. The OH* emissions indicate autoignition, high temperature

combustion, and heat release which occurs during the expansion stroke [32, 48]. To create a meaningful comparison between the optical engine chemiluminescence data and combustion properties derived by the distillation program, we will focus on the OH* chemiluminescence data and surrogate's distillation-resolved DCN. This comparison is reasonable being that DCN is a measure of reactivity and is used to gauge a fuel's ignition propensity, with a lower DCN indicating a fuel that is less reactive, requiring higher temperatures and pressures (time into compression stroke) to autoignite [1, 3, 7, 16, 26]. Figure 11 (a) shows the vapor stage distillation-resolved DCN, prevaporized target value, and literature's predicted value. Panel (b) displays the OH* chemiluminescence data for the coal derived Sasol IPK POSF-5642 real fuel (left) and surrogate (right). We consider the DCN "effective" here since linear blending only offers an approximation of how the DCN's stratification may unfold during vaporization.

Figure 11

(a) Distillation Resolved Progression of the IPK Surrogate's Vapor Stage Effective DCN Compared With Target and Calculated Prevaporized Values Indicated. (b) Optical Engine OH Chemiluminescence Comparison [32] of the Surrogate (Right) and Corresponding Real Fuel (Left)*

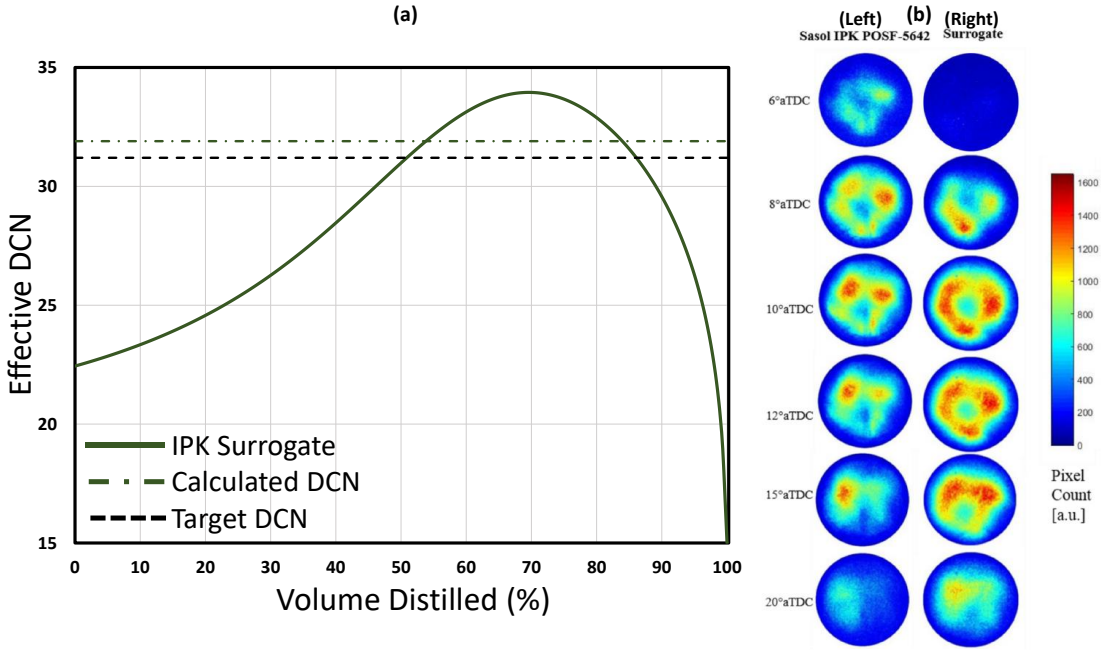

To have a true appreciation for the distillation-resolved CP figure presented here and for future figures, we incorporate a simple understanding of the d^2 Law of droplet vaporization to create a general relation to time. The law states that the square of a vaporizing droplet's diameter decreases linearly with time, and further, the time to complete vaporization decreases quadratically with droplet size [22]. To crudely apply this to our distillation-resolved results we could consider it as a stretching of the curve for the early stages of vaporization and a compression in the later stages. The volume percent distilled to time relation thus indicates that the majority of vaporization takes place while the droplet is large and has the most surface area. This relation will have implications on

emulation, specifically during early stage evolution of CPs for these surrogate mixtures. It is difficult to directly correlate volume distilled to total vaporization time because the calculation relies on temperature and pressure dependent properties such as thermal conductivity, enthalpy of vaporization, and density, as well as conditions within the combustion chamber. Therefore, for the purposes of this investigation we will accept that vaporization time and crank angle progression are loosely correlated and that this chemiluminescence comparison will be purely qualitative.

In panel (a), we observe that the distillation-resolved DCN exhibits deviation from the design CPT as well as the prevaporized calculated value from [10]. This CP behavior may indicate that the surrogate will be less reactive than the real fuel until it is about 50% distilled by volume. The low DCN behavior is caused by the less reactive, more volatile chemical species rapidly vaporizing. As distillation progresses the more volatile species are consumed and their chemical energy release increases temperature of the system. Temperature and composition will cross a threshold where the less volatile, more reactive species will begin to vaporize and influence CPs which can be seen in the mid to late range reactivity increase. The tail end reactivity depression occurs due to the concentration of iso-cetane which is the least volatile and least reactive species, although, considering the d^2 Law this period is relatively short lived. Overall, the IPK surrogate's distillation resolved behavior compared to the real fuel could be interpreted as initially less reactive and less prone to ignition, followed by a period of vigorous reactivity, ending with a heavy tail that may linger in the combustion chamber. Generally, we would predict that this surrogate will not emulate the real fuel's behavior well due to its vast shifts in distillation-resolved combustion properties.

Comparing our broad distillation-resolved combustion behavior interpretation to the chemiluminescence data in panel (b) we can determine if the distillation-resolved CP methodology is able to indicate a surrogate's ability to emulate its corresponding real fuel's behavior. Panel (b) describes the real fuel's (left) and surrogate's (right) autoignition and high temperature combustion heat release behavior through OH* chemiluminescence optical imaging, which DCN is correlated to. What we observe is very similar to our computational based behavioral predictions. Crank angles 6 through 8 degrees aTDC indicate, through color, that the surrogate is initially less reactive than the real fuel, following this, crank angles 10 to 20 degrees aTDC indicate a rapid jump in surrogate reactivity. Had images been taken, it can be inferred from the chemiluminescence results that after 20 degrees aTDC the surrogate could potentially linger in the cylinder longer than the real fuel. These qualitative observations of real data closely correspond to our hypothesized computational results, disregarding the lack of a unified time scale. Within a reasonable degree of skepticism, it could be said that the distillation program correctly predicted that the surrogate would not emulate the real fuel well. Being that the program's distillation behavior is based on volatility via the Antoine equation, the underlying cause of poor real fuel emulation could be attributed to combustion property stratification resulting from preferential vaporization due to mismatched volatility characteristics. It appears that this technique of distillation-resolved CP evaluation enabled the prediction of combustion behavior which closely correlated to real data. Moreover, this methodology seems to offer more insight into the fuel's behavior as opposed to the distillation curve (Figure 10 (a)).

To further test the phenomenology of our distillation-resolved CP comparison technique, we will examine the S-8 fuel surrogate from [10] which was tested in the same engine and manner as the IPK fuels [32]. The distillation program was run at-pressure with the S-8 formula found in Table 2. As with the Sasol IPK surrogate, the at-pressure results exceed the Antoine equation's critical temperature restriction, but again, we continue with our CP evaluation regardless. Figure 12 (a) shows the vapor stage distillation-resolved DCN and (b), the OH* chemiluminescence data for the natural gas derived Syntroleum S-8 POSF-4734 real fuel (left) and surrogate (right).

Figure 12

(a) Distillation Resolved Progression of the S-8 Surrogate's Vapor Stage Effective DCN With Target and Calculated Prevaporized Value Indicated. (b) Optical Engine OH Chemiluminescence Comparison of the Surrogate (Right) and Corresponding Real Fuel (Left)*

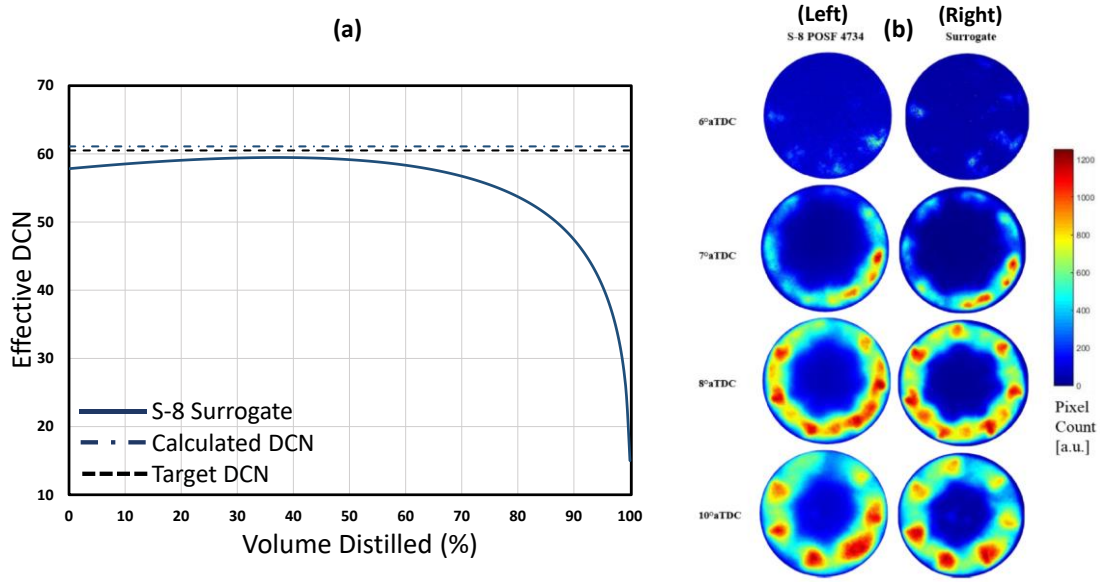

The distillation-resolved DCN of this surrogate closely correlates to the target and calculated values from Kim et al., which may indicate good potential for accurate real fuel emulation. The reactivity conformity persists through approximately 60-70% of the distillation progression, which by the d^2 Law, represents an even greater portion of the total vaporization time. Following this period of close property emulation, the heaviest and least reactive component (iso-cetane) begins to influence CPs, although, this behavior is only prevalent for the comparatively short duration tail end of the distillation process. The distillation-resolved CP evolution to real fuel CPT conformity of this surrogate suggests that for the majority of the combustion process the surrogate and real fuel reactivity will closely correlate. If this behavior analysis holds true, the OH* chemiluminescence of the surrogate and real fuel should look visually similar.

The chemiluminescence data in panel (b) between the surrogate (right) and real fuel (left) indicates a close reactivity correlation. Throughout the entire progression of data we observe, through color, very similar OH* behavior for the two fuels which demonstrates that the surrogate is closely emulating the combustion behavior of the real fuel. Further, it offers evidence that not only can the distillation program's method of evaluating CPs predict a non-conforming surrogate, but it can also predict a surrogate that will emulate its corresponding real fuel's combustion behavior well.

2.6 Literature Surrogates: Distillation Comparison

The optical engine data shows that the distillation program's methods to resolve combustion properties along distillation trajectory may, to a degree, indicate a surrogate fuel's ability to emulate target real fuel properties and associated combustion behavior. Based on these promising findings we investigate the surrogate fuels from the literature [9, 29] which will be experimentally evaluated later in this study. These two sets of surrogates were chosen for their ability to be readily synthesized and tested using facilities which will be discussed in later chapters. We believe these surrogates are most suitable for our study because they

(1) are made of a limited number of pure components (less than 6), and

(2) they present two different surrogates of the same real fuel, which permits both surrogate-real fuel and surrogate-surrogate comparison.

This second point is highlighted in the surrogates we examined in the previous section [10], where only one surrogate was formulated for each real fuel. We believe this to be problematic because as discussed earlier, fuels have an inherent variability, which is part of the motivation for creating surrogate fuels. It would be difficult to determine if any burn results are a cause of the surrogate's inability to emulate the real fuel, or simply a degraded batch of real fuel. For this reason, only studies with multiple surrogates designed to emulate the same real fuel were chosen. This lends itself to an apples to apples comparison of the two surrogate fuels, being that, if they both emulate the real fuel, they should also emulate each other. This reasoning ensures that the fuels tested are to the exact specifications described in the literature.

A good example for this approach is evidenced in the gasoline surrogates formulated by Pera et al. Here, the real gasoline fuel chosen is not a single batch of 95 RON pump gasoline; instead the CPs were obtained from a fuel they describe as ULG95 which is an average of numerous gasoline samples [9]. Furthermore, surrogates comprised of either blends of different real fuels such as those presented in [49-51], or surrogates made of numerous species such as those formulated in [28] neither offer a consistent recipe of pure species nor reduce the complexity of the reaction pathway significantly enough to be useful. Considering this, the surrogates presented by Won et al. [29] and Pera at al. [9] fit our criteria well. These studies formulate multiple mixtures designed to emulate the same fuel and are composed of only a few components. Additionally, their components are not particularly exotic, allowing their formulation in our facility. Lastly, these surrogates are synthesized by matching single point (prevaporized) combustion property targets as discussed earlier.

To analyze these fuels we will first observe their distillation curve, then briefly examine their composition progression, ending with the re-collapsing of their discrete compositions to extract the distillation-resolved CP evolution. While both of these studies present three surrogates, we will only examine the two that we formulated and tested in later sections to reduce conveying unnecessary information and consolidate comparisons to better appreciate the preferential vaporization effect on property evolution. The third surrogates were not chosen for synthesis due to their significant concentrations of species that are prohibitively expensive (iso-dodecane, Surrogate 3 [29]) and notably toxic (Cyclohexene, Sur95f [9]).

2.6.1 Won et al. Jet Fuel Surrogates

The first set of data we will examine are the Jet-A surrogates made in [29]. These surrogates were formulated to emulate Jet-A POSF 10325 fuel, which is considered a nominal "good" jet fuel [29, 52, 53] making these surrogates quite relevant to real applications. Their recipe and targets are seen in Table 3.

Table 3

Combustion Property Targets, Calculated Surrogate Properties, and Recipe for Two Jet-A 10325 Fuel Surrogates Formulated in Won Et Al. [29] and the Corresponding Real Fuel

	Target real fuel	Jet_LT	Jet_HV
CPTs	**Jet-A POSF 10325**		
Derived Cetane Number	50	50	50.6
H/C Ratio	1.961	1.961	1.947
MW [g/mol]	160.8	143.2	156.9
TSI	25.5	23.8	25.5
Density at 288K [kg/m3]	803	768	777
Components		mole fraction	mole fraction
n-dodecane		0.49	-
n-hexadecane		-	0.365
iso-octane		0.21	0.31
1,3,5-Trimethylbenzene		0.3	0.325

Note. Jet_LT corresponds to Surrogate 1 and Jet_HV corresponds to Surrogate 2 in [29].

The top half of Table 3 displays the prevaporized CPTs that these two fuels are formulated on, the bottom half is their compositions. Note that the only compositional difference between the fuels is a swap of n-dodecane for n-hexadecane in the "heavy" surrogate (Jet_HV). Moving forward we will examine the molecular weight, H/C ratio, and DCN property evolution of these surrogates against each other and the target. These

properties were chosen as the focus of this evaluation because their potential effects on combustion behavior are easily interpreted. Additionally, all properties will represent the species deposited into the vapor envelope at atmospheric pressure as justified in previous chapters, except for the distillation curve as that is always representative of the liquid behavior at atmospheric pressure (ATSM D86). The distillation curve for these surrogate fuels and the real fuel [52] are given in Figure 13.

Figure 13

Distillation Curves of Won et al. Jet-A Surrogates and the Corresponding Real Fuel Jet-A 10325 [29]

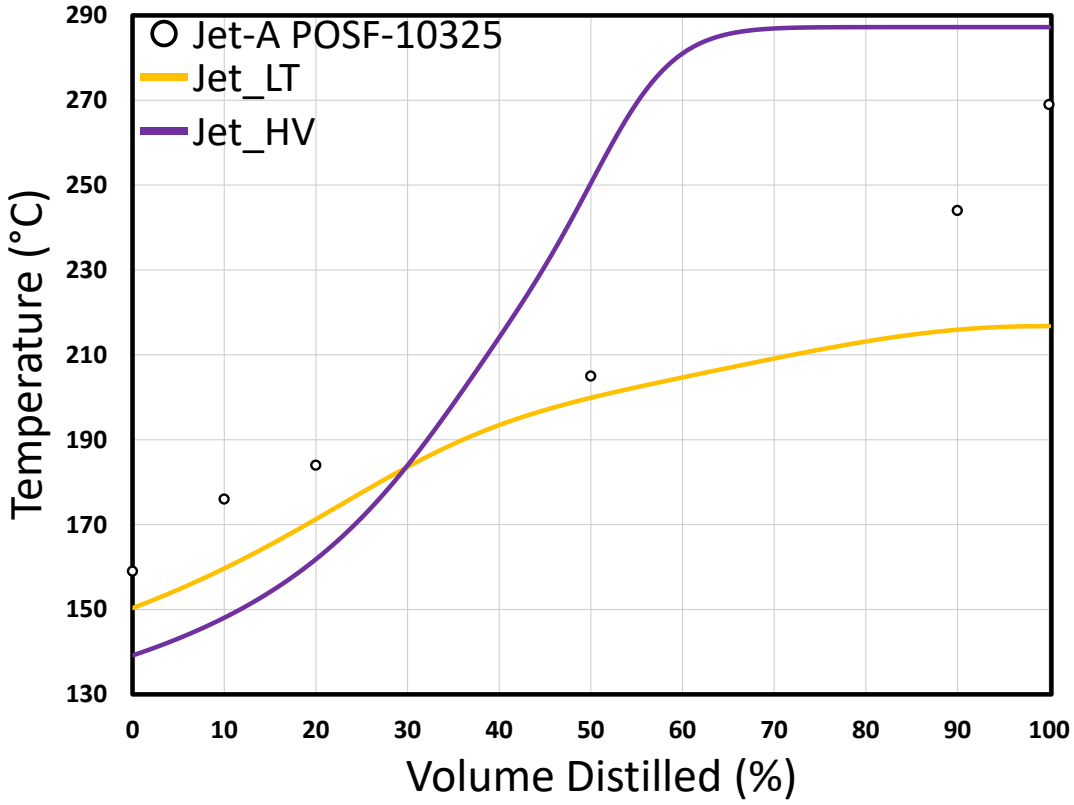

The figure illustrates that these surrogates display significantly different distillation behavior. Comparing the two surrogates we see that their initial behaviors until approximately 40% distilled are well matched, but as distillation progresses these similarities end. Past the 40% mark, we see significant deviation in volatility with neither fuel matching each other or the target distillation profile. Of particular interest is the Jet_HV surrogate which displays noteworthy deviation of up to +70°C from both the Jet_LT surrogate and the real fuel. As with the optical engine surrogates, analyzing the distillation behavior does not give us direct insight into how their combustion properties and associated behavior will evolve. To gain more insight into the combustion behavior of these surrogates, the combustion properties must be resolved along the distillation trajectory. Before making this jump to combustion property resolution, we will first look at how the species evolve throughout vaporization to have a true application for the value gained by resolving CPs. Figure 14 (a) shows the speciation of the Jet_LT surrogate, panel (b) shows the speciation of the Jet_HV surrogate.

Figure 14

Composition Evolution of the Vapor Envelope Along the Distillation Trajectory for (a) Jet_LT and (b) Jet_HV

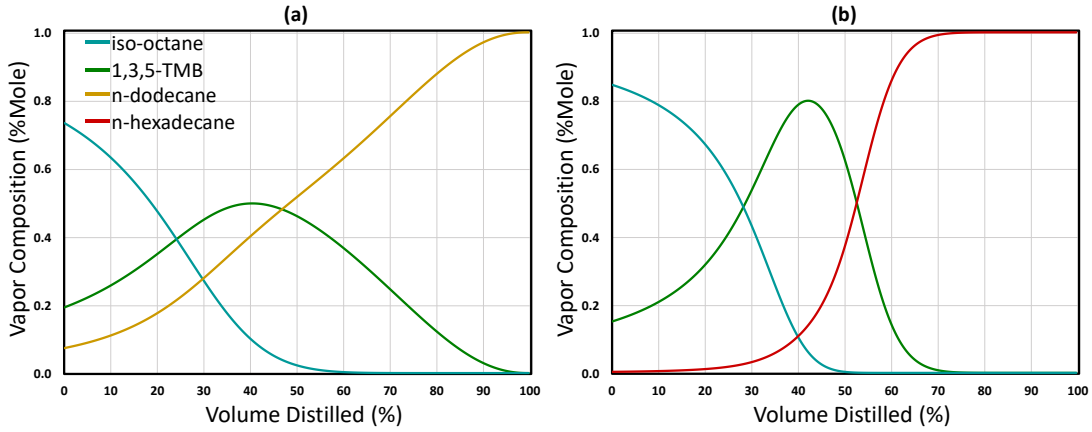

In Figure 14, we are tracking the species deposited in the vapor envelope as the liquid fuel vaporizes; this serves to highlight the effect of preferential vaporization. Iso-octane, which has the lowest normal boiling point of 99°C [43] is initially rapidly deposited into the vapor envelope, followed by 1,3,5-trimethylbenzene (TMB) (164°C [43]) then lastly by n-dodecane/n-hexadecane (216/286 °C [43]). In both cases, we find that towards the end of vaporization the heaviest, highest boiling point (lowest volatility) species dominate composition and thus mixture combustion properties. To gain insight on the mixture's combustion property evolution from the speciation progression, we would need the properties of all species (Table 5), then interpolate the intermediate mixture composition's CPs. A more effective method to represent CPs, as opposed to using Figure 14 with a table of properties and interpolating, is to collapse this data into single CP plots as seen earlier with the Kim et al. [10] surrogates. Doing this will allow us to compare the distillation-resolved CPs to the prevaporized CPTs. Figure 15 displays the resolved CPs of

interest, from top to bottom we have analyzed (a) MW, (b) H/C, and (c) effective DCN which display deviation from the prevaporized CPT for the majority of their respective distillation trajectories.

Figure 15

Distillation-Resolved Progression and Prevaporized Target Values of Jet_LT and Jet_HV for the Combustion Properties: (a) MW, (b) H/C Ratio, and (c) Effective DCN

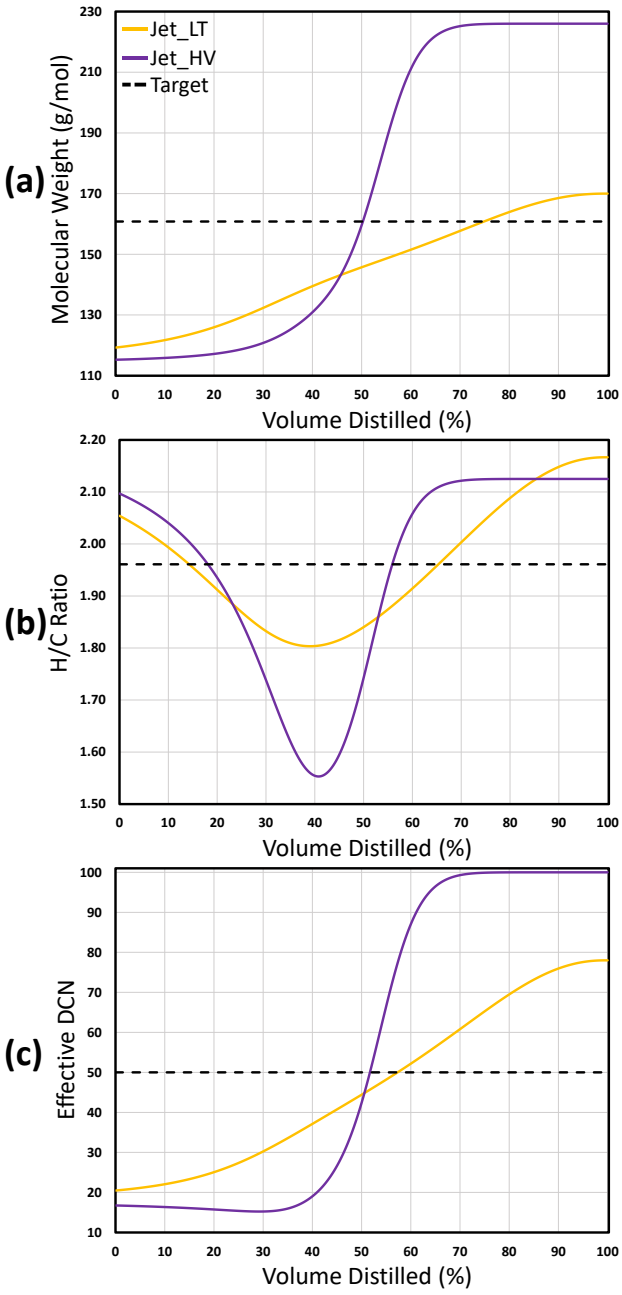

The topmost panel (a) describes the average MW evolution of the surrogates as well as the prevaporized target property. The MW CPT has a large degree of variability as compared to the other CPTs, seen in Table 3, nonetheless, neither of the surrogates display any semblance of a close match to the target property. This has implications on spray dynamics, total enthalpy deposited into the system, as well as various other issues relevant to combustion [1-3, 7, 22, 23, 26, 54]. This plot also serves as an excellent visualization of preferential vaporization where the lightest, most volatile species vaporize first, as corroborated with Chevron's findings (Figure 2 (a)).

The H/C ratio behavior, seen in panel (b) provides information on the local stoichiometric ratio as well as the latent heat of vaporization [1, 7, 22, 23, 26, 54]. The stoichiometric ratio in hydrocarbons is directly correlated to the H/C ratio, therefore it serves as an easy metric to visualize combustion behavior. The CP evolution in (b) displays very interesting non-monotonic behavior where Jet_LT and Jet_HV both cross the target twice starting with an elevated H/C ratio, which is subsequently heavily depressed and ends slightly elevated. If we consider this behavior, along with speciation, and the MW behavior, we observe that the H/C ratio behavior is a result of the n-alkane species which have relatively similar H/C ratios of 2.29, 2.17, and 2.13 (nC7, nC12, nC16 respectively) on the light and heavy ends and the 135-TMB species which has a significantly depressed H/C ratio of 1.34. The speciation progression of the surrogates (Figure (a), (b)) reveals that the 135-TMB is deposited into the vapor envelope in the intermediate stages of distillation which is reflected in H/C space by a mid-range depression. This non-monotonic behavior can have a significant impact on the local stoichiometric ratio. In real applications, this could affect performance such as steady-state liftoff heights, increased susceptibility to

blowout, and flames leaving their design recirculation zone [7, 48, 55-61]. Moreover, this behavior could make any computational simulations or test engine experiments inaccurate considering that the real fuel may have different stoichiometric behavior.

The final CP of significant interest, which can be easily related to combustion behavior, is the effective DCN. Panel (c) displays the distillation-resolved DCN behavior, which as seen with the previous CPs, does not match the target or each other for the majority of the distillation trajectory. As previously discussed, DCN serves as a proxy property for ignition delay time and reactivity [1, 3, 7, 16, 26], which is particularly important for a jet fuels as they require high cetane numbers to achieve their characteristic autoignition and reactivity requirements [1, 3, 21]. Panel (c) indicates that both surrogate's reactivity is depressed for approximately 40% of their early distillation trajectories, which is followed by increased reactivity for the remainder of distillation. The elevated DCN of the surrogates later in their distillations could be considered beneficial, but certainly does not match the real fuel or each other. The depressed initial DCN could have significant consequences in real applications such as an inability to ignite and increased susceptibility to blowout due to reduced chemical reactivity. Furthermore, DCN is a highly non-linear scale [7, 29, 62, 63], which exacerbates the effect of this property stratification on combustion behavior. The analysis of these three combustion properties indicates there is significant qualitative evidence suggesting that these surrogate's combustion behavior will neither emulate the real fuel or each other. The possible distillation-resolved nonconformity among these surrogates – developed assuming prevaporized combustion conditions – could negate any usefulness they may have provided due to their disconnect

with reality where spray nozzles and droplet vaporization are essential in fuel delivery systems [1-3, 40].

2.6.2 Pera et al Gasoline Surrogates

In addition to this set of jet fuel surrogates, a set of 95 octane gasoline surrogates formulated by Pera et al. [9] were experimentally evaluated in the burner rig which will be described in later chapters. These gasoline surrogates were formulated in a similar fashion to the Won et al. [29] surrogates we previously examined with single value prevaporized CPTs and a limited number of components. Based on the encouraging findings revealed in the jet fuel analysis, these gasoline surrogates were analyzed in a similar fashion; although the speciation evaluation (Figure 14) was omitted due to the limited insight that could be extracted from it. The two surrogates denoted Sur95t and Sur95o formulas and CPTs are described in Table 4.

Table 4

Combustion Property Targets, Calculated Surrogate Properties, and Recipe for Two 95 Octane Gasoline Fuel Surrogates Formulated in Pera et al. [9] and the Corresponding Real Fuel

	Target real fuel	Sur95t	Sur95o
CPTs	**ULG95**		
Research Octane Number	95	95	95
Motor Octane Number	85	87.8	86
H/C ratio	1.801	1.801	1.801
O/C ratio	0.011	0	0.011
MW [g/mol]	94.3	102.7	97.5
Density at 298K [kg/m3]	749	750	755
Lower Heating Value [kJ/kg]	42801	42893	42229
Components		mole fraction	mole fraction
n-heptane		13.7	15.8
iso-octane		42.8	34.3
Toluene		43.5	42.3
Ethanol		-	7.6

As with the previously examined jet fuel surrogates, these surrogates are formulated by matching surrogate CPs to an ensemble of single point target real fuel prevaporized CPTs. Additionally, these gasoline surrogates are comprised of similar species with the exception of Ethanol in the Sur95o surrogate. To begin our evaluation into the distillation-coupled behavior of these effectively equivalent surrogates we examine their distillation curves. This is presented in Figure 16; as discussed earlier these surrogates are formulated based on an averaged gasoline blend so the real fuel distillation data is unavailable.

Figure 16

Distillation Curves of Pera et al. [9] 95 Octane Gasoline Surrogates

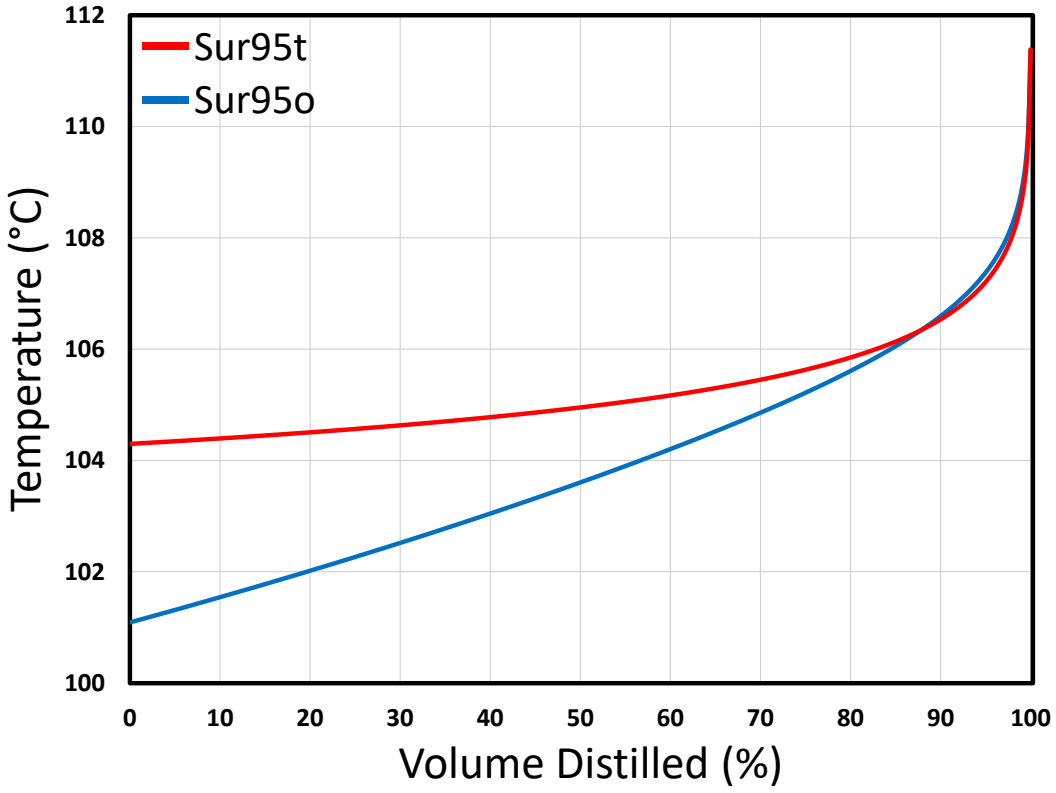

The distillation curves, while not differing as drastically as those seen from the jet fuels (Figure 13) still display inter-surrogate deviation of up to 6 degrees Celsius. If we consider the entire distillation range of 11 degrees this represents a deviation of 55%, which is rather significant. Additionally, deviation of 20% or more persists throughout approximately 50% of the early distillation trajectory, indicating there is cause to investigate these surrogates by applying our distillation-resolved CP methodology. We will limit observation to MW, H/C, and effective RON to allow a more direct relation to combustion behavior and limit repetition. Figure 17 displays the surrogate's distillation-resolved CPs from top to bottom we observe (a) MW, (b) H/C, and (c) RON.

Figure 17

Distillation-Resolved Progression and Prevaporized Target Values of Sur95o and Sur95t for the Combustion Properties: (a) MW, (b) H/C Ratio, and (c) effective RON

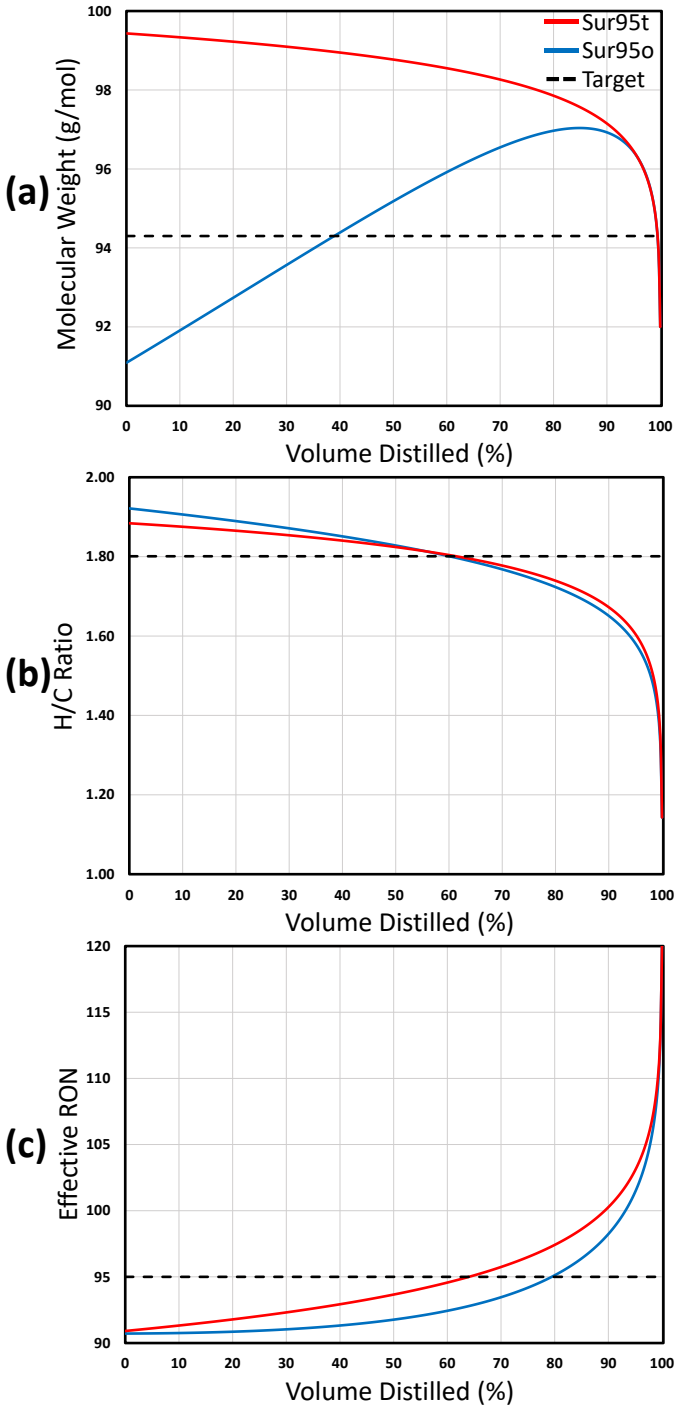

Regardless of particular surrogate formulation, panels (a), (b), and (c) demonstrate stratification of some of the key CPs of the Pera et al. surrogates along the distillation coordinate. These should be identical to each other and the target fuel's CPs under prevaporized conditions. As with the jet fuel surrogates, MW matching was permitted a large degree of variability about the real fuel target which is exacerbated along the distillation trajectory. Looking at panel (a), we observe a large initial nonconformity of approximately 80% with a 40% relative deviation persisting throughout 50% of the distillation trajectory. This deviation indicates a significant inter-surrogate discrepancy of molecular size and associated chemical energy deposited into the system. The Sur95t surrogate consistently deposits greater quantities of larger, less volatile, and more energy dense species into the system.

To better interpret how this may affect combustion behavior we turn attention to panel (b), the H/C ratio. Surprisingly, the H/C ratios of the surrogates are relatively well matched which is due, in part, to ethanol's high H/C ratio of 3.0. The ethanol seems to balance the expected discrepancy in H/C ratio due to the difference in MW caused by the larger quantity of aromatics and alkane isomers present in the Sur95t surrogate. Ethanol's high H/C ratio coupled with its high volatility has equalized the two surrogate's H/C ratio, although not their stoichiometric behavior due to the oxygenated nature of ethanol. Nonetheless, these behaviors still differ significantly from the target. These surrogates display both elevated and depressed H/C ratios for the majority of their respective distillation trajectories, with only about 20% of distillation near the target value.

A final CP of significant interest is the effective RON behavior, which serves as an indicator of autoignition and reactivity. This property is similar to DCN, but RON is

essentially the inverse, with high values indicating reduced autoignition susceptibility. The RON value is of significant importance to spark ignition gasoline applications as a fuel which is too reactive (low RON) can significantly reduce engine operability and cause catastrophic engine damage [2, 9, 16, 17, 40]. Examining panel (c) we see just this, initially both fuels display depressed RON behavior for approximately 50% of their respective distillation trajectories, which by d^2 Law represents an even greater percentage the total vaporization time. The depressed RON indicates that both fuels are more reactive than the real fuel and could be more susceptible to autoignition. Of particular importance is the initial depression in RON, representative of when the fuels are first injected into a combustion chamber (considering direct injection operation). This boost in reactivity could cause the fuel to immediately autoignite resulting in engine knock. Additionally, as with DCN, RON is not a linear scale and minor variations in RON units represent significant differences in ignition susceptibility. For perspective, this depression from the target of 3-5 RON units, which persist for about 40% of distillation, correlates to a price difference of around $0.50 per gallon at the pump. The distillation-resolved CPs, particularly the RON behavior, indicate there is a possibility for these fuels to display divergent combustion behavior from each other and the real fuel.

This chapter has presented computational evidence suggesting that CP stratification due to preferential vaporization in "effectively equivalent" surrogate fuels may lead to significant divergence in combustion behaviors among surrogates and target fuels. These results are considered sufficiently compelling for this work to proceed with experimental combustion tests using a custom built annular burner rig discussed in the following chapters. The following chapter describes the design of test rig; Chapter 4 discusses

experimental validation of the rig; and the results of surrogate burning experiments are presented in chapter 5.

Chapter 3

Spray Burner Rig Design

This chapter will describe the design of the experimental annular spray burner rig platform used to evaluate surrogate fuel combustion behavior. This chapter will document the:

- Initial design criteria.
- Final design of the annular spray burner rig.
- Spray-coupled blowout test.
- Experimental procedure.

3.1 Initial Design Criteria

To incorporate distillation into the combustion environment, an atomizing fuel nozzle was necessary. Atomizing fuel nozzles are a staple in modern combustion applications and their integration into the burner rig creates a distinct relation to actual combustion environments. Incorporation of a standard nozzle used in industrial applications would ensure burn experiments approximate real applications. There are numerous nozzle designs for many varieties of application; in order to determine an appropriate nozzle we considered two primary design criteria: minimizing fuel consumption and selection of a nozzle that is designed to operate at atmospheric pressure. These criteria are essential to keep cost down, as the pure components used in surrogates can be expensive, and to ensure correlation to ASTM D86 and the distillation program. With consideration of the outlined design criteria, the industrial application most applicable was determined to be an oil-fueled home heating furnace. For these systems, there is a wide variety of atomizing fuel nozzles all of which are interchangeable via unified 9/16-24 UNEF thread. The primary

denotation between these nozzles are fuel flowrate and cone shape. A wide range of flowrates are available and after consulting with the industry leader Delavan, the 0.5 gallon per hour (GPH) flowrate nozzle was determined to be the most appropriate as it is the most common low flowrate nozzle used in applications [64]. A diagram of the atomizing fuel nozzle from Delavan is presented in Figure 18.

Figure 18

Delavan Atomizing Spray Nozzle With Some Key Features Indicated [64]

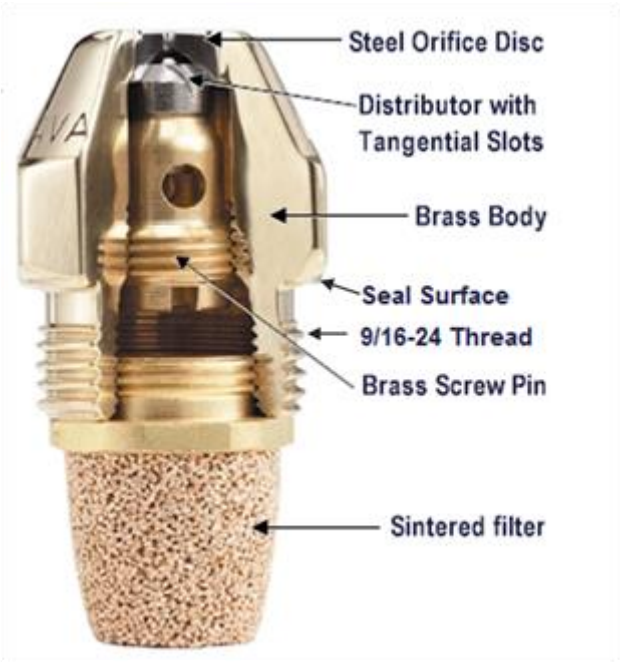

Although the 0.5 GPH nozzle was recommended, we experimented with three types of nozzles: 0.4 GPH solid cone (type B), 0.5 GPH hollow cone (type A) and a 0.5 GPH solid cone. The details and results from these rig qualification experiments can be found in

Appendix C. These initial experiments determined that the 0.5 GPH solid cone nozzle was most appropriate for our experiments. Other initial design features included:

- Use of 1/4" metal tube and tube fittings for connection versatility, ability to handle a wide range of pressures, and fireproofing of the fuel line for safety reasons.
- A high pressure fuel reservoir to handle any possible rapid pressure increase due to unexpected fire in the pressurized fuel line.
- The ability to add flow disruption plates to create uniform flow fields in order to minimize variation due to co-flow fluctuations.
- Versatility, through incorporating interchangeable parts made of stainless steel to increase functionality, improve corrosion resistance, and allow for easy disassembly for modification or repair.

With these desired design features in mind, the Mark II rig was developed.

3.2 Mark II Annular Spray Burner Rig

The Mark II burner rig was developed based on previous trial experiments and design iterations; the full design progression is in Appendix C. A Solidworks rendering of the Mark II spray burner apparatus developed for surrogate fuel comparison is pictured in Figure 19.

Figure 19

Solidworks Rendering of The Mark II Annular Spray Burner Rig

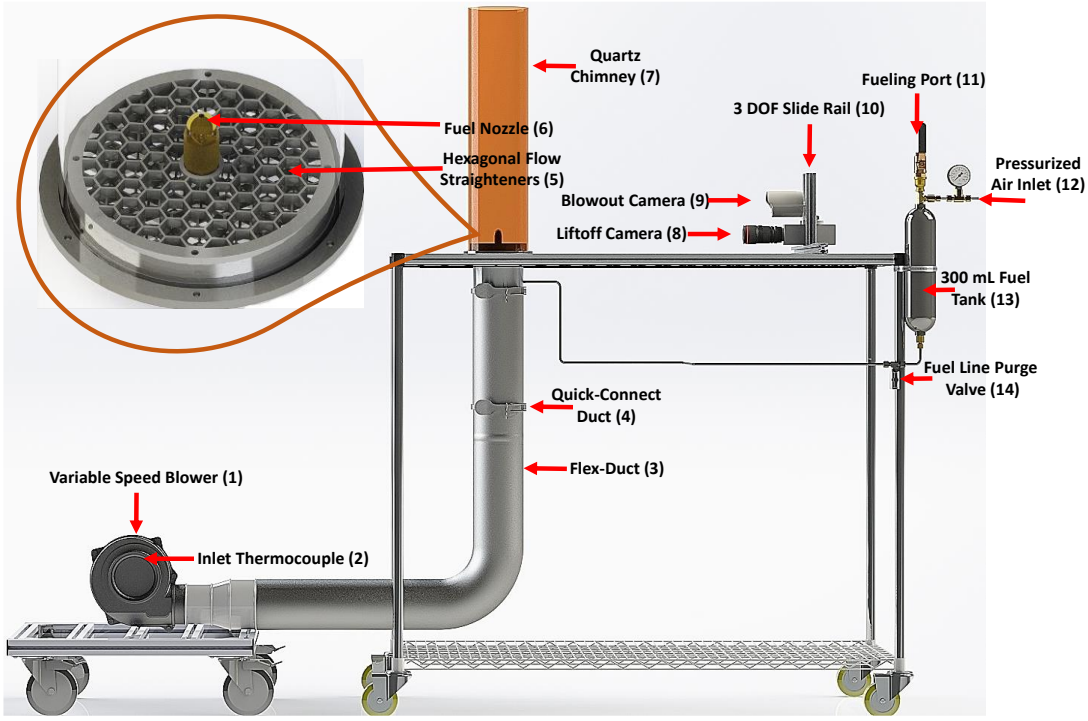

This rig was designed to perform a range of experiments, including determination of flame liftoff height and blowout velocities. For this study, we focus on the blowout experiment which is explained in the following section and is generally more sensitive to distillation properties than liftoff. Briefly, to perform this experiment, the co-flow air velocity must be incrementally increased until the flame extinguishes. To accomplish this, the rig is supplied with an annular co-flow of ambient air through the variable speed air WORX WG520 blower (1). Co-flow velocity is incrementally varied using a Tenma 72-7270 decade resistance box which precisely varies the power delivered to the blower. The air intake charge temperature is measured using a thermocouple (2), which permits flow

rate correction for ambient temperature variation. In this configuration, the user varies co-flow air delivery by resistance adjustment. To convert Ohms to velocity, the blower flow rate was measured with a hand-held anemometer (Holdpeak 866B) and correlated to applied resistance over a broad range of ambient conditions; this can be seen in Appendix D. The blowout threshold (velocity) measurements presented in later chapters result from this correlation.

Isolating the blower from the main cart body and connecting it via flex-duct (3) eliminated any vibration generation, this enabled the optical cameras to pick up clear images of the flame. The quick-connect duct (4) added versatility in rig height for the case of future modifications to avoid a complete redesign of the co-flow delivery system. Co-flow travels through the ductwork and passes through a series of removable and reconfigurable hexagon flow conditioners (5) and into the quartz combustion chamber (7). Within the combustion chamber, a standard interchangeable home heating oil spray nozzle (6) feeds a steady flow of atomized fuel to the system. Fuel is stored in a pressure-resistant stainless steel vessel (13). A dedicated fueling valve (11) enables rapid refueling between tests by providing a larger inlet to allow more air to escape as fuel enters the system. A purge valve (14) permits draining and cleaning of the fuel tank and lines to avoid chemical contamination between tests of dissimilar fuels. Steady fuel flow is delivered to the spray nozzle by supplying a constant, 100 psig regulated air pressure (12) above the liquid in the tank. This pressure is the nozzle's design pressure for all nozzles used herein and is delivered via a dual regulated portable air compressor. Experiments are monitored and recorded using separate optical cameras for liftoff (8) and blowout (9) which can be precisely positioned using the three degrees of freedom slide rail (10) that they are secured

to. Camera outputs can be fed to post-processing software for liftoff analysis, while blowout values are taken from the decade resistance box. This design fulfills all outlined criteria and incorporates various safety features such as relief valves to cut fuel supply in case of process excursion, and hardware for complete remote operation.

While we consider this rig the final design iteration, problems with facility ventilation required additional modification. Consistent laboratory ventilation problems frustrated these experiments, so to rid ourselves of reliance on external systems we designed and encased the burner rig in a custom-built fume hood. This modification can be seen in Appendix C, Figure C8, its operation is identical to the above schematic (Figure 19).

3.3 Spray-Coupled Tests

In the time frame of this study, it was determined that purchasing and waiting for advanced laser diagnostic equipment was not possible. Thus, experiments had to be chosen which could be run with the integrated optical equipment. With optical access to the combustion chamber provided by the quartz chimney, two primary spray coupled experiments were determined to be appropriate: liftoff height measurement and blowout velocity. Although the liftoff experiment and diagnostic equipment was explored in this study, data was not gathered using this experiment, although, information regarding it is in Appendix E. All data presented herein are obtained from the blowout tests explained in the following section.

3.3.1 Blowout Velocity

The data presented in later sections of this study will be strictly from the spray-coupled blowout experiment. This test is dependent on a multitude of combustion properties including, but not limited to volatility, reactivity (DCN/RON), molecular weight, nozzle geometry, fuel pressure, combustion chamber temperature, LHV, H/C ratio, etc. [3, 58, 65-68]. This test was conducted because it suits our experimental requirements well: it is dependent on numerous fuel characteristics, reliant on an atomized fuel spray, thus, droplet distillation, and can be easily measured with our optical equipment. While blowout is an exceptionally multidimensional phenomenon, for the purposes of this study we will consider blowout more simply as the condition where (downward) flame propagation into fresh fuel-air mixture can no longer maintain kinematic balance with the upward velocity of the co-flow air. Figure 20 and 21 presents our simplified understanding of blowout.

Figure 20

A Simplified Illustration of a Flame at Steady State Where the Downward Flame Propagation Velocity is Greater Than the Upward Co-Flow Velocity

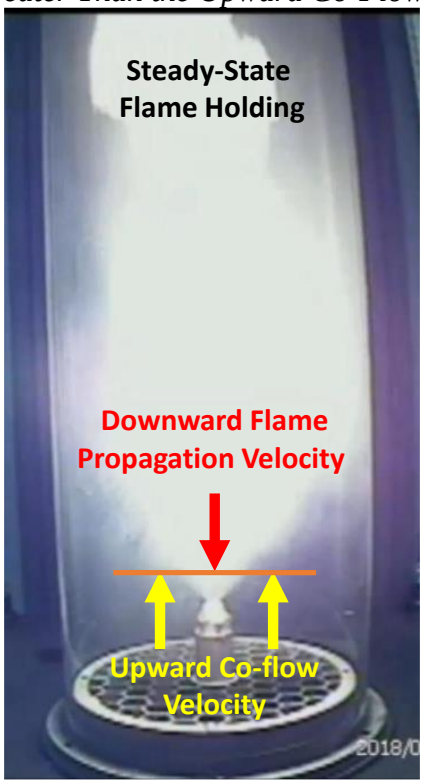

At time-averaged steady state, the downward flame propagation velocity matches the upward co-flow velocity and the flame holds onto the nozzle at some liftoff height within the combustion chamber, demonstrated in Figure 20. Now, if the flame is stressed to just before its blowout limit, and the co-flow velocity is subsequently increased, the kinematic balance will break. The greater upward velocity will sever the flame's hold on the nozzle. The flame front will then proceed to travel up and out of the combustion chamber, as Figure 21 illustrates.

Figure 21

A Simplified Illustration of a Flame at its Blowout Threshold

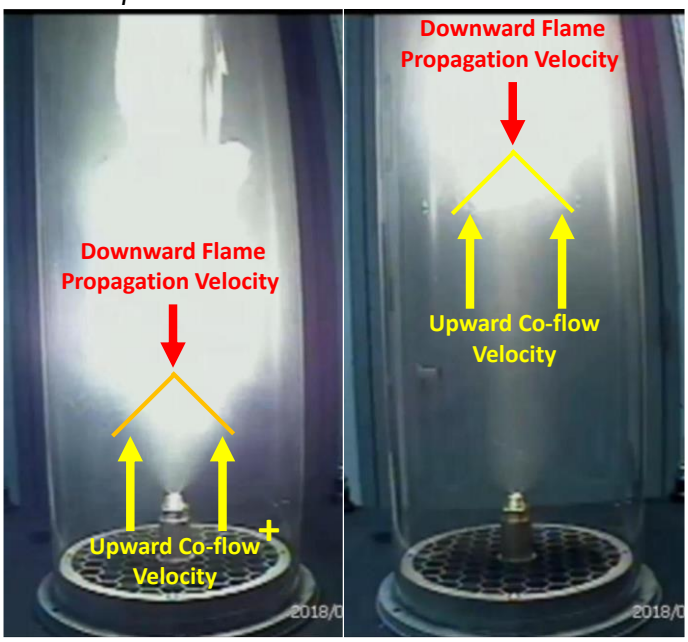

Note. Upward co-flow velocity is incrementally increased, breaking the kinematic balance wherein the upward co-flow velocity is greater than the downward flame propagation speed.

If the surrogate fuels are, in fact, identical, then this balance should be broken at the same co-flow velocity. Any deviation in value would indicate that the fuels are displaying different combustion behaviors. An important note here is that this blowout test is not the traditional lean blowout test (LBO). In the traditional LBO test, co-flow flowrate is kept constant and fuel flowrate is adjusted [69], in this test, fuel flowrate is kept constant and co-flow flowrate is incrementally adjusted using a variable speed blower. While this test is not an ASTM standard, it is still a representation of combustion behavior and can be used to compare two "equivalent" fuels on a one-to-one basis. In sum, utilizing proper

operating procedures, this stress test has the potential to identify nonconformity among "identical" fuels.

3.3.2 Blowout Experimental Procedure

In order to ensure safe and reliable operating conditions and thus, dependable data, the below experimental protocol was developed. This strict protocol is essential to ensure consistent testing procedures and a minimization of cross-species contamination achieved by Acetone wash-downs followed by fuel line purges. Acetone was chosen as the wash-down fluid for three reasons, (1) its solvency making it an ideal fuel line cleaner, (2) its volatility which ensures line purges sufficiently remove any residue, and (3) its use as the baseline test fuel before each set of data on a given day to gauge daily measurement variation (seen in the following chapter). Figure 22 describes the entirety of the experimental protocol.

Figure 22

The Full Blowout Experimental Protocol Used for All Data Sets

Preliminary Information	
This experiment must be run with at least two people	
Any student running this experiment must be fully aware of what every valve on the system does	
Any student operating the blowtorch must familiarize themselves with the device before operating	
Any student operating or viewing this experiment must be wearing eye protection and cotton clothing	
Any student operating the blowtorch in addition to eye protection and cotton clothing must wear welding gloves, welding sleeves and a face mask	
Always have a fire extinguisher within reach	
Never leave experiment unattended when flame is present	
If for any reason a fire cannot be controlled evacuate the area immediately, pull fire alarm and contact appropriate safety personnel	
Return all chemicals and propane to the proper storage location upon completion of testing	
Preliminary Setup	
Check all connections to ensure the fuel delivery system is properly connected	
Ensure the air duct is properly connected with the locking pins securely inserted.	
Align flow straighteners to appropriate positions	
Place the quartz on the flow straighteners	
Set blower control switch to off	
Plug in blower	
Plug in, connect and turn on all four thermocouples	
Plug in camera and control cart to check picture alignment	
Close the Air-In Valve	
Open the ventillation window and turn on the fume hood ventillation blower	
Connect air compressor and turn on, set tool pressure to 120-125 psig, do not proceed until compressor turns off	

Student 1: Valve Control, Resistance Box Control		**Student 2:** Igniter, Refueler, Purger, Safety Checker, Fire Extinguisher, View Screen Monitor	
Close the Air-In Valve			
Close the Relief Valve			
Close the Refueling valve			
Close the Purge Valve		Ensure all valves are closed and the ventillation blower is on	
		Open Refueling Valve & pour 300mL of fuel into tank	
Ensure all valves are closed		Close the refueling valve, remove latex gloves	
Exit Room, leave door open		Exit Room, leave door open	
Turn on blower and set to 800 kOhm (or within 100 kOhm of known blowout)			
Open the Air-In valve when Student 2 is in position with blowtorch		Enter room, open fume hood door and Ignite fuel spray with propane blowtorch	
If spray does not ignite, lower blower speed (increase resistance)		Extinguish and remove propane torch from the room and close fume hood door	
Start Timer			
Set the regulator air pressure to 102-105 psi, record pressure (first run only)		Verify air pressure on downstream pressure dial to be atleast 100 psig (first run only)	
Record air intake thermocouple temperature		Ensure room temperature does not exceed 100 degF	
		Close the door	
Begin stepping down resistance every 10s until blowout occurs		Inform student 1 when blowout has occurred	

Once blowout occurs:			
CLOSE Air-In Valve			
SLOWLY OPEN Relief Valve			
Stop timer			
Record resistance value			
Close Relief Valve		Ensure all valves closed	
Restart procedure after "Exit Room, leave door open" until fuel is depleted		Restart procedure after "Exit Room, leave door open" until fuel is depleted	
Once fuel is depleted, turn blower to 600 kOhm and allow fuel flow until sputtering stops		When sputtering stops enter room and open purge valve, keep open for 10 seconds after air compressor kicks on	
10s after compressor kicks on: close Air-In Valve		Close purge valve after Air-In Valve is sealed	
		Fill fuel tank with Acetone washdown	
		Leave room	
Open Air -In Valve to allow 3 seconds of Acetone flow			
After 3s close Air-In Valve and open Relief Valve			
		Open purge valve and collect Acetone washdown fluid	
		Close Purge valve	
Close Relief Valve and open Air-In Valve			
		Once fuel sputtering stops, open Purge Valve for 10 seconds after compressor kicks on	
10 seconds after compressor kicks on close Air-In Valve, open Relief Valve			
Restart procedure after preliminary setup		Restart procedure after preliminary setup	

After Experimentation	
After performing Acetone washdown, Refill fuel tank with the acetone and burn it off by repeating the ignition process	
Once all the acetone has burned off, Turn on blower at 600 Ohms and let run for 5 minutes	
Close all valves	
Turn off blower and compressor	
Turn off fume hood ventillation blower and close window	
Unplug both blowers, camera, compressor and thermocouples	
Remove quartz from within fume hood	
Return all fuels to necessary storage locations	
Clean up work area	

In addition to Acetone fuel line washdowns and purges, the testing protocol dictates some key procedures to ensure consistent operating conditions. Some of these procedures include a brief 90 second warm-up period between refueling, minimizing time to relight between successive blowout runs, and a time interval of 10 seconds between co-flow rate increases. These features ensure that the quartz and combustion chamber remains at a semi-constant hot temperature between successive blowout runs, and that the kinematic flame balance has ample time to stabilize at a given co-flow flowrate. Lastly, for a species with a known blowout value (measured in Ohms, as this is how the decade box controller operates), the protocol dictates flame ignition should occur at a co-flow flowrate no less than 100 kiloohms from the species' blowout threshold value. This ensures the initial co-flow flowrate does not affect results. All data sets in the following chapters adhere to this protocol, ensuring that data is gathered in a consistent and safe manner.

Chapter 4

Spray Burner Rig Validation

The purpose of this chapter is to assess the responsiveness of the blowout experiment to varying parameters. This exercise is key to ensuring that the experiment can detect the potential effects of preferential vaporization on the combustion behavior of multicomponent fuels due to the spatiotemporal variations in fuel properties. To do this we will explore:

- The day-to-day variations of a base fuel conducted before all data sets over the entirety of experimental proceedings. This will determine the applicability of cross-referencing data sets not taken in quick succession.
- A literature review to select a relevant set of chemical species to gauge experimental sensitivity.
- The sensitivity of the experiment through separately evaluating its response to physical and chemical property variations. This will ensure that the experiment can detect differences in fuels with varying properties.

4.1 Day-to-Day Measurement Variation

To determine day-to-day measurement variation, a test fuel's blowout threshold was taken before each data set. Acetone was determined to be an appropriate calibration fuel, being that, it is used to clean and purge the system, sufficiently volatile, and is relatively inexpensive. Figure 23 below describes four sets of Acetone blowout measurements which correspond to the data that will be seen in later chapters.

Figure 23

Baseline Acetone Results Taken Before all Blowout Trials to Gauge Day-To-Day Measurement Variation

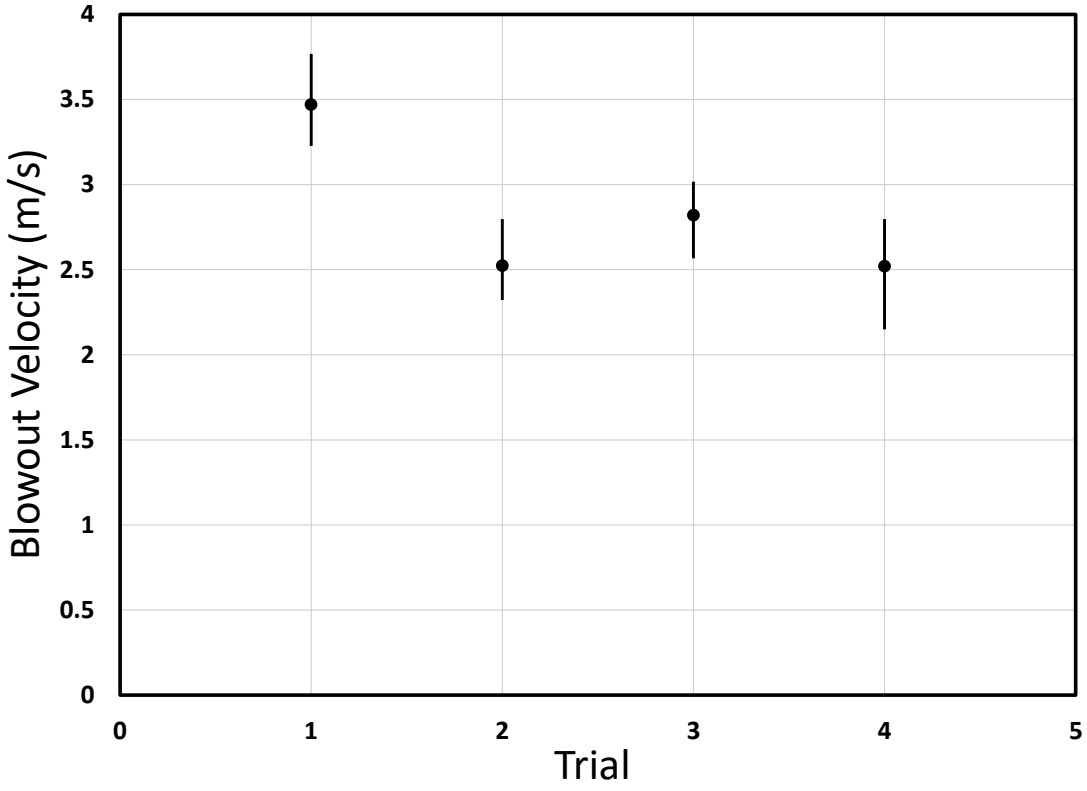

Note. The error bars represent minimum and maximum values for a particular data set.

The baseline Acetone blowout thresholds presented here display significant day-to-day variations which could be a result of a wide range of atmospheric factors such as temperature, humidity, pressure, etc. Although a correlation could be made, attempting to incorporate data sets not taken in quick succession on the same day would result in increased experimental error possibly shrouding any variation in blowout behavior. This inconsistency between test days is further highlighted in the future Figures 28 and 33 where nC8 and nC10 species display significant deviation in blowout behavior for the same

experimental configuration. Based on these findings, all data presented in individual figures will be of data sets taken on the same day in quick succession. In order to continue categorizing the experiment's behavior, a set of fuels are chosen to test the experiment's sensitivity to property variations in the following section.

4.2 Burner Rig Sensitivity Analysis: Species Selection

It is broadly accepted in the combustion community that long-chain alkanes' chemical kinetic behavior is similar [70, 71]. Understanding that these long-chain alkanes are chemically similar is a key theme in this study, but grasping this concept is rather nuanced. We refer to chemical behavior as behavior completely isolated from physical properties ensuring that the only factor influencing behavior is the chemical kinetics of the fuel species. To prove this chemical similarity we will examine various studies where prevaporized long-chain alkanes chemically coupled behaviors are compared. These studies are commonplace in the combustion community to prove this point. Figure 24, 25, and 26 illustrate three separate experimental setups from which four datasets were compiled that all reach the same conclusion.

Figure 24

Illustration of Equivalent Prevaporized, Premixed n-alkane Chemical Dependent Behavior From [70]. Laminar Flame Speeds of (a) nC5, nC6, nC7, nC8, (b) nC9, nC10, nC12 and Extinction Strain Rates of (c) nC5, nC6, nC7, nC8, (d) nC9, nC10, nC12 Across a Range of Equivalence Ratios

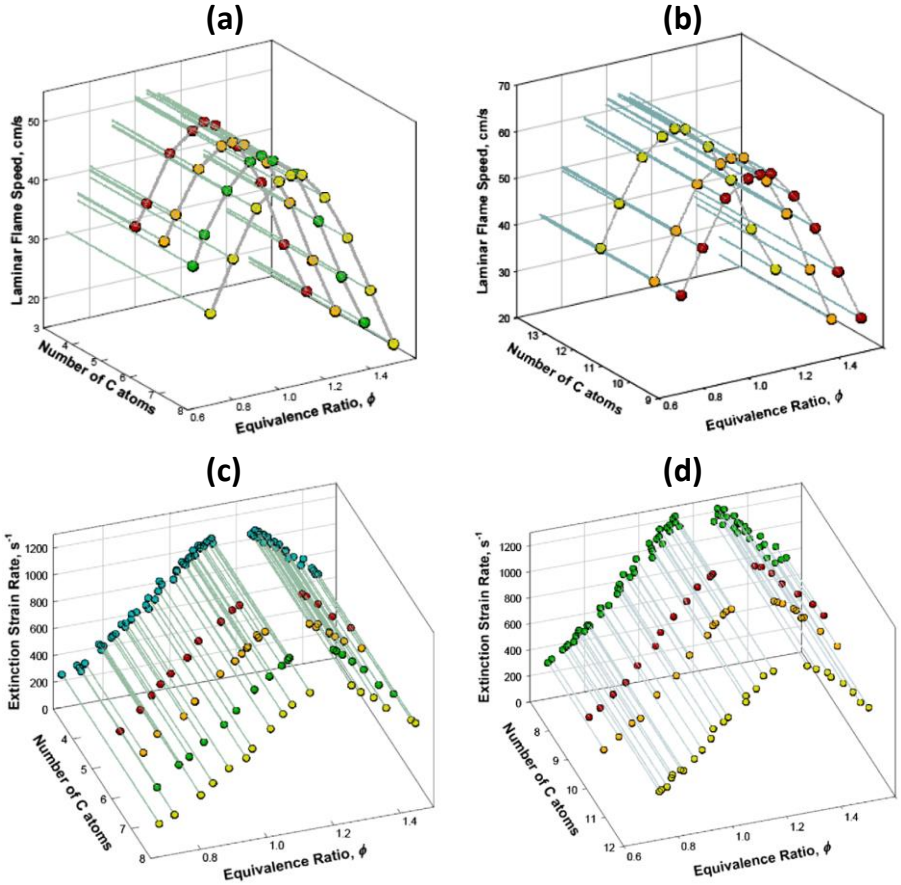

Note. The back set of points on (c) and (d) illustrates the correlation between the data.

The data presented in Figure 24 (a), (b), (c), and (d) are obtained from the same experimental setup [70] wherein two premixed, prevaporized counterflow burners facing each other are used in conjunction with Laser Doppler Velocimetry to measure laminar flame speed (a), (b) and flame extinction rate (c), (d). The experiment was performed at atmospheric conditions over a wide range of stoichiometric (equivalence) ratios for nC5,

nC6, nC7, nC8, nC9, nC10, and nC12, reaching the conclusion that all of these long-chain alkanes display the same prevaporized chemically dependent behavior. A more in-depth explanation of these experiments are described in [70]. The conclusion of this study is that these species display the same prevaporized chemical behavior. This conclusion is further corroborated by [71], with results seen in Figure 25.

Figure 25

Illustration of Equivalent Prevaporized, Premixed n-alkane Chemical Dependent Behavior From [71]. Ignition Delays of nC5, nC6, nC8 And nC9 With a Phi Of 0.5 (a) and 1 (b) Across a Range of Pressures, Normalized to Two Atmospheres

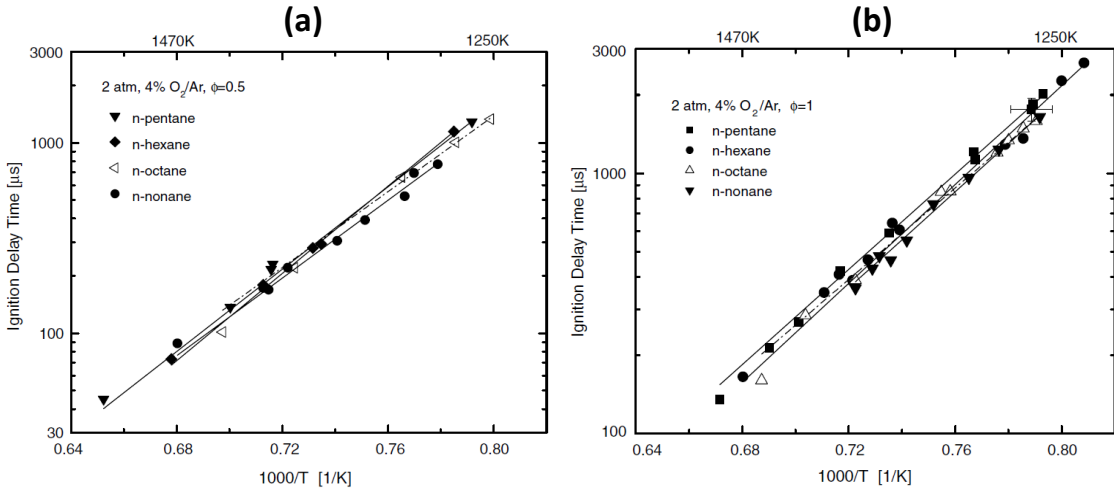

Figure 25 represents data obtained from a premixed, prevaporized, high purity, low-pressure, kinetic shock tube over a range of pressures, normalized to 2 atm. Tests were performed on nC5, nC6, nC8 and nC9 at stoichiometric (phi) ratios of 0.5 (a), and 1 (b). Results indicate that the chemically dependent ignition delay times of these long-chain

alkanes display only small, insignificant variations [71], further validating their chemical equivalence. A final study, seen in Figure 26, performed in [72] using a non-premixed, prevaporized counterflow burner further evidences that long-chain n-alkanes, as well as their permethylated isomers the related homologous series of long-chain methyl esters [73], display the same chemical behavior over a range of fuel flow rates when a constant transport-weighted enthalpy is maintained.

Figure 26

Illustration of Equivalent Prevaporized, Non-Premixed n-alkane Chemical Dependent Behavior From [72]. Extinction Strain Rates of (a) n-alkanes Species nC7, nC8, nC10 and (b) Methyl Esters with C2, C4, C5, C6, C8, C10 Alkyl Chains Over a Range of Fuel Flowrates

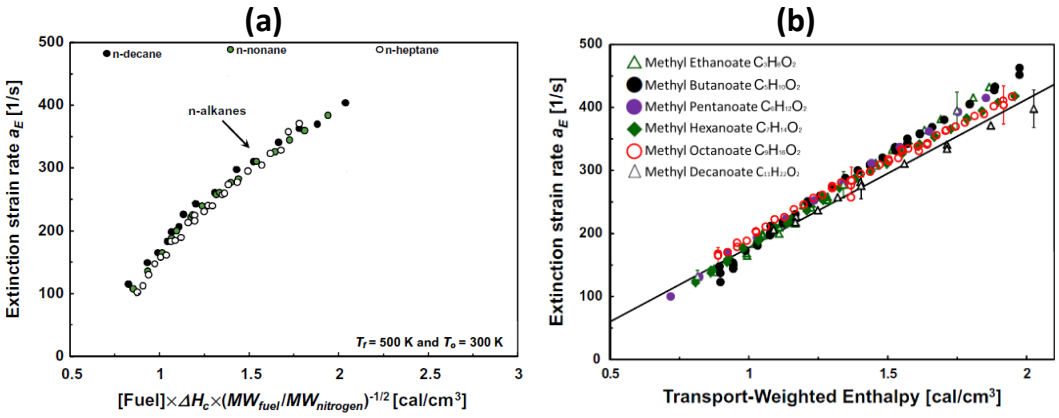

The results of this study are normalized on the x-axis by their transport-weighted enthalpy with units cal/cm^3. This non-premixed study corroborates the results seen in [70] wherein panel (a), the n-alkanes species nC7, nC8 and nC10 have the same flame extinction strain rate. This study goes a step further to show that not only do long-chain n-alkanes

share the same chemically coupled behavior but so do long-chain methyl esters, as evidenced in panel (b).

The consensus among these studies and many others is that long-chain alkanes share the same chemical kinetic behavior in premixed systems. Accepting this, pure component long-chain n-alkanes are easily obtained and serve as excellent benchmarks to test if the spray burner rig is sensitive to physical property variations being that these species share identical chemically coupled behavior yet distill over a wide range of temperatures.

In addition to qualifying the rig's ability to detect physical property variations through comparing n-alkane blowout thresholds as discussed, we wanted to ensure that chemical property variations could be detected as well. This examination is more straightforward; to do this we will investigate the blowout thresholds of nC7, iC8, and to a lesser degree nC8. These species share nearly the same carbon chain length, volatility (boiling point), density, etc. but exist on opposite sides of the Octane Number (chemical kinetic reactivity) spectrum. For ON, nC7 is rated at zero Octane Number (by definition, and with nC8 rated lower) and iC8 defined as 100 Octane Number. These species serve as an excellent case study for species with physically similar properties but drastically different chemistry. Properties of all species used throughout experimentation can be referenced using Table 5 below.

Table 5

Various Properties of all Species Present in Surrogates Recipes That are Experimentally Evaluated. all Data is From [43] Except RON and DCN From [63]

Fuel	MW (g/mol)	H/C	(D)CN	RON	NBP (K)	ρ (kg/m^3)	μ × 10^4 (Pa.s)	σ × 10^2 (N/m)	T_{crit} (K)
iso-octane (iC8)	114.2	2.25	18.0	100	372.4 +/- 0.2	688	4.79	1.84	543
n-heptane (nC7)	100.2	2.29	53.8	0	371.5 +/- 0.3	680	4.14	2.03	540
n-octane (nC8)	114.2	2.25	58.2		398.7 +/- 0.5	698	5.1	2.12	568
n-decane (nC10)	142.3	2.20	65.5		447.2 +/- 0.6	726	8.51	2.34	617
n-dodecane (nC12)	170.3	2.17	78.0		489 +/- 2	745	13.54	2.48	658
n-hexadecane (nC16)	226.4	2.13	100.0		554 +/- 10	770	31.00	2.72	722
Toluene	92.1	1.14	0.2	120	383.8 +/- 0.2	862	5.58	2.79	593
1,3,5-Trimethylbenzene	120.2	1.34	8.0		437.8 +/- 0.8	861	6.00	2.82	639
Ethanol	46.1	3.00	2.2	108	351.5 +/- 0.2	786	10.90	2.19	516

Looking at the n-alkanes in Table 5 we notice that their reactivity, represented by DCN, does vary even though this should be representative of a chemical kinetic driven property. DCN is determined through a normalization of ignition delay time via a correlation calculation to provide a standard value for ignition propensity [6, 7, 15, 16, 62, 63, 74-76].The nonconformity of DCN among the n-alkanes could be due to a nuanced effect in the way low volatility species' DCNs are tested using the ASTM standard ignition quality tester (IQT). The IQT operates by spray injecting a predetermined volume of fuel into a constant volume, preheated, pressurized combustion chamber where the fuel vaporizes, mixes, and autoignites. A pressure trace is used to determine the moment of ignition from which the ignition delay time is extracted by determining the time from when the spray injection valve opens to the moment of ignition [6, 62, 74-76]. This methodology inherently considers physical characteristics of the fuel being that ignition will not occur until all the injected atomized liquid fuel vaporizes. Further nuance in this methodology is that when a fuel is sufficiently reactive (DCN ~60+) it autoignites as the fuel is still spraying in, creating a multiphase reaction system with a diffusion flame likely. Figure 27

displays a dataset from an IQT test performed in [62] for n-heptane to highlight this observation.

Figure 27

Deconstructed IQT Pressure Trace for n-heptane From [62]

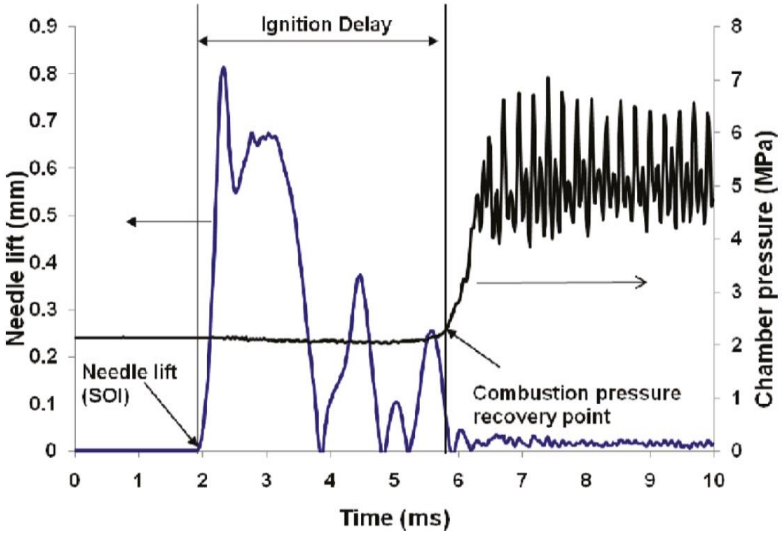

n-heptane has a DCN measured at 53.8, based on the observation of the pressure trace above, one could infer that a more reactive fuel could autoignite as it is still being injected into the system. These observations indicate that this standard test cannot be considered truly prevaporized, and the extrapolated DCN value may include some spray-coupled behavior indicating this measurement may not be driven solely by chemical kinetics. For these reasons, we question the purely prevaporized property of the IQT for species that are determined to have DCNs of about 60 and above. The spray-coupled nature

in IQT determined DCN measurements will be a necessary theme when observing surrogate fuel data in later sections.

Regardless of the n-alkanes DCN behavior, we accept that their prevaporized chemical kinetic behavior is identical. Additionally, we accept that nC7, iC8 and to a lesser degree nC8 share similar physical characteristics. The following section showcases the blowout experiment's sensitivity to physical and chemical property variations by comparing chemically similar species to determine physical property sensitivity and physically similar species to determine chemical property sensitivity.

4.3 Blowout Sensitivity

In order to ensure data collected is both relevant and meaningful, the blowout experiment's sensitivity to different fuel characteristics is validated. To demonstrate the sensitivity of the blowout experiment to physical and chemical property variations the pure component n-alkane series nC7, nC8, nC10, nC12, nC16, and the alkane isomer iC8 were compared against each other to see if we detect a difference in their blowout thresholds. Figure 28 displays the results of this dataset and 1σ error bars.

Figure 28

Pure Component Blowout Thresholds With 1σ Error Bars Used to Determine Blowout Experiment Sensitivity

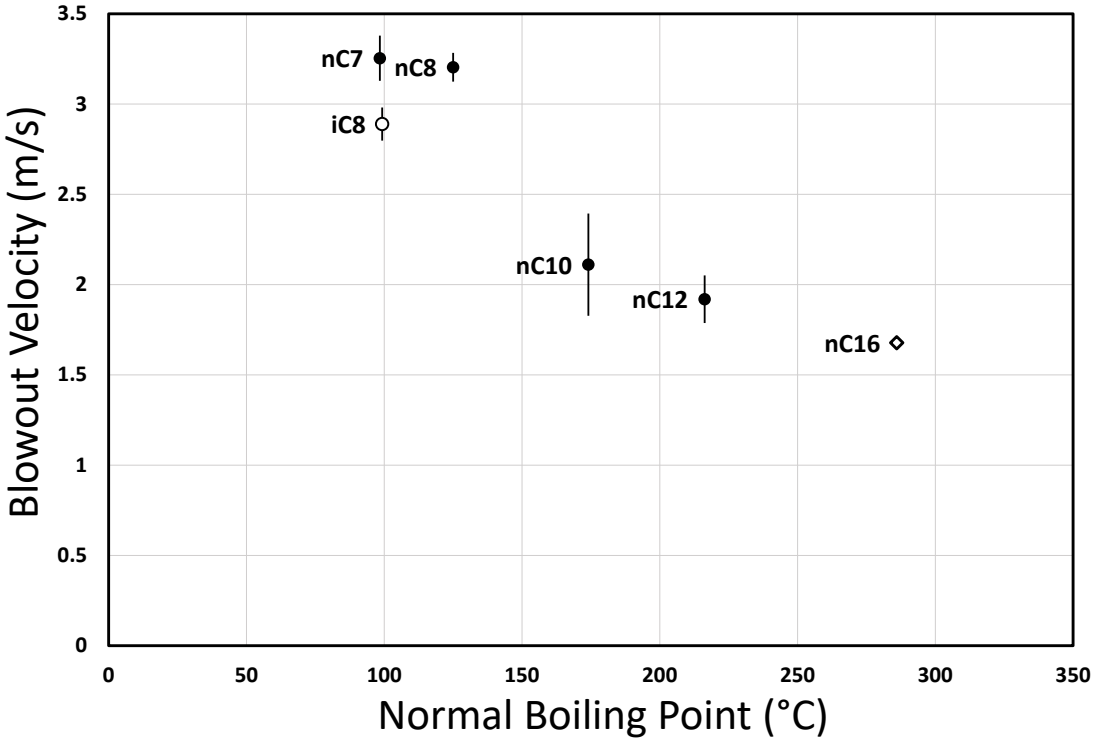

Note. Solid circles are n-alkane species having similar prevaporized chemistry behaviors, though nC16 is represented as a diamond due to difficultly in testing caused by soot formation. iC8 is represented by an open circle to indicate that it does not share similar chemistry to the other species presented here.

This figure simultaneously displays the rig's sensitivity to both physical and chemical property variations. As discussed, the n-alkane series (nC7, nC8, nC10, nC12, nC16) represents species with highly similar prevaporized combustion chemistry and varying physical characteristics (e.g., normal boiling point). Observing these five data points, we see that blowout velocity (obtained through anemometer to decade box

resistance correlation) varies as a function of physical property effects on the complex spray combustion environment. This indicates that, within experimental error, the blowout experiment is sensitive to physical property variation among otherwise chemically identical species. Further, the experiment can differentiate blowout behavior of the physically similar but chemically divergent nC7, iC8, nC8 species dataset demonstrating the experiment's sensitivity to chemical property variation. These datasets (1) demonstrate the experiment's responsiveness to both chemical and physical properties, (2) display its ability to differentiate blowout thresholds of individual species, and (3) support the validity of the experiment, in that it can be used to compare fuels with varying properties.

Additional evaluation of this data reveals that blowout thresholds of the chemically identical species (i.e., the n-alkane species) displays significantly more deviation in their blowout behavior compared to the minor differences in the physically similar species. Taken as a whole, it is evident from Figure 28 that both chemical and physical properties contribute to blowout behavior. However, the influence of physical properties seems to be significantly more influential than the modest variations in blowout thresholds from chemical kinetic variation. The blowout behavior of these pure component species, regardless of physical or chemical similarity, supports the premise that preferential vaporization of more or less volatile species may influence combustion behaviors.

Having confirmed the blowout experiment is sensitive to properties we wish to measure, we now explore the combustion behavior of the multicomponent jet and gasoline surrogate fuels from [29] and [9] that were examined computationally in Chapter 2.

Chapter 5

Spray Burner Blowout Threshold Results

The previous chapters have presented: (1) significant evidence suggesting that the property stratification resulting from the preferential vaporization of multicomponent surrogate fuels may affect their combustion behavior. Moreover, (2), sufficient evidence that the blowout experiment is reasonably sensitive to property variations and thus, can differentiate dissimilar fuels. The findings from previous chapters have provided adequate data to move onto the focus of this study, which is to compare the combustion behavior of surrogate fuels determined to be equivalent based on prevaporized combustion property targets. Adhering to the standard experimental protocol described earlier, this chapter, using the Mark II annular burner rig, equipped with a 0.5 GPH solid cone atomizing spray nozzle, will examine the blowout thresholds of the surrogates presented in Won et al. [29] and Pera et al. [9], as well as a set of n-nonane surrogates developed to highlight the potential consequences of preferential vaporization on multicomponent surrogate fuels. The results of these experiments are described in the following sections, a full table of the raw data can be found in Appendix F. Additionally, other sets of data deemed imprecise are presented in Appendix G.

5.1 Jet-A Surrogate Results

Of the two sets of literature surrogates considered herein, the distillation-resolved combustion property analysis of the Won et al. POSF 10325 Jet-A surrogates seemed to be the more likely candidate to display combustion behavior nonconformity. The two surrogates, Jet_LT and Jet_HV were synthesized in accordance with the recipes seen in Table 3 by using a self-correcting mole fraction to mass excel calculator created to ensure

accurate species ratios. The results of this blowout data along with a partial reiteration of the distillation-resolved results are presented in Figure 29 (a) and (b).

Figure 29

(a) Distillation Curves and Effective DCN Property Stratification Along Surrogate Distillation Trajectories With Target Values Indicated. (b) Jet-A Surrogate's Blowout Thresholds With 1σ Error

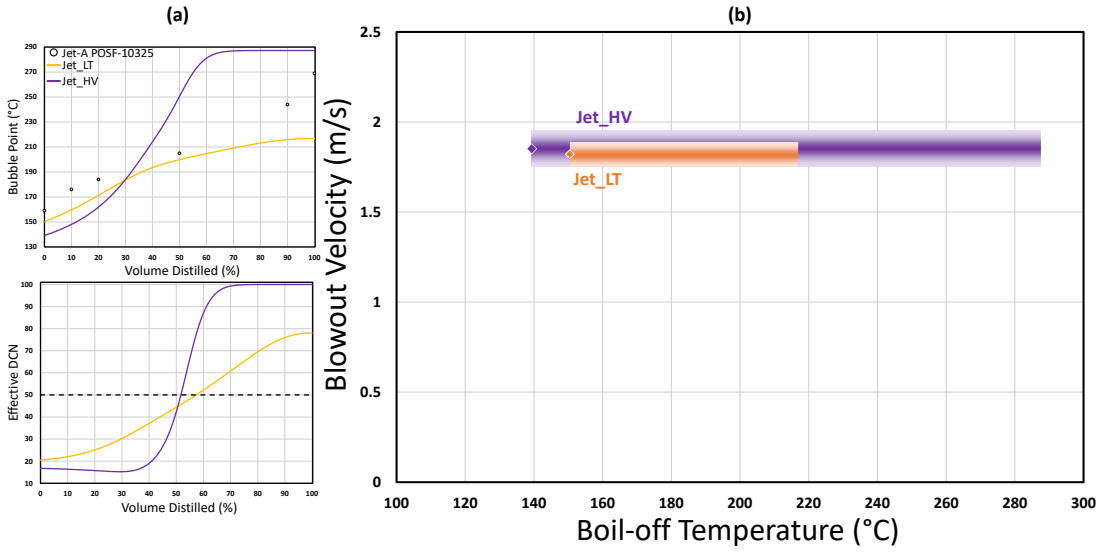

Note. Streak length represents distillation profile and width indicates error.

In Figure 29 (b), the Jet-A surrogate's blowout thresholds are displayed as large streaks with length representative of their respective distillation profiles and width 1σ experimental error. To assist in evaluating the possible role preferential vaporization, panel (a) is presented, which is a reference to the earlier insight achieved through qualifying CP stratification along surrogate distillation trajectories. The effective DCN CP has been isolated to facilitate a more direct comparison of distillation-resolved CPs to combustion

behavior, as reactivity (effective DCN) is an easy CP to correlate to a fuel's resistance to blowout.

The blowout experiment reveals that despite the significant property stratification predicted by the distillation model, the surrogates' blowout behaviors are identical. A parametric analysis to identify exactly what factors are causing this alignment in combustion behavior among these highly dissimilar fuels in distillation-resolved space is not possible given our facility limitations. This is not to say that the prevaporized property matching method is a concrete procedure to formulate surrogates that consistently emulate the corresponding real fuel's behavior, although, it does seem to an admirable job in this case. We cannot definitively point to a cause for this accurate emulation due to the immensely complex physics involved in spray combustion, but we can infer some causes based on previous observations.

If we recall section 4.2, we established that DCN measured in an IQT is not a purely chemical kinetic examination of reactivity. We can infer that the inherent physical and spray dynamic coupling in the DCN measurement may be sufficient to emulate the effects of property stratification expected from preferential vaporization in multicomponent fuels as well as the influence of spray dynamics on combustion behavior. Furthermore, if we take an overarching view of the distillation-resolved CPs in panel (a), we can make a few generalizations. For one, in general, the volatility-reactivity relationship of these two fuels seem to counteract each other at incrementally divergent points, where locally high volatility sections are matched by equally low reactivity and vice versa. This may create an averaging of global combustion behavior. Considering that some cancelation of property discrepancy between these fuels may be occurring, if we observe the Jet_HV surrogate we

see that although is more volatile initially, it is also less reactive, the same observation applies to the later stages of vaporization where it is much more reactive but much less volatile compared to the Jet_LT surrogate. While additional generalizations could be made about the system such as: the effect of n-alkane reactivity driving the ignition characteristics of the system, effects of surface tension and viscosity which may cause convergent or divergent spray characteristics, Heat of vaporization considerations, etc. The multifaceted physics and innumerous factors involved in spray combustion make the system too complex for this experiment to differentiate which factor or factors are driving behavior.

In the scope of this experiment, what we can do is test the fuels and report the data with some applied insight based on literature research and our simple distillation-resolved combustion properties. With that, for the sake of completion, we proceed to test the gasoline surrogates to see if we can differentiate combustion behavior among these "equivalent" fuels.

5.2 Gasoline Surrogate Results

The second set of literature surrogates formulated through prevaporized combustion property matching considered herein are the gasoline surrogate presented in [9]. These surrogates are synthesized and tested in accordance with the previously described mixing methodology and experimental protocol. The results of this data are presented in Figure 30 below, following a similar format as the jet fuel surrogate figure.

Figure 30

(a) Distillation Curves and Effective RON Property Stratification Along Surrogate Distillation Trajectories With Target Values Indicated. (b) 95 Octane Gasoline Surrogate's Blowout Thresholds With 1σ Error

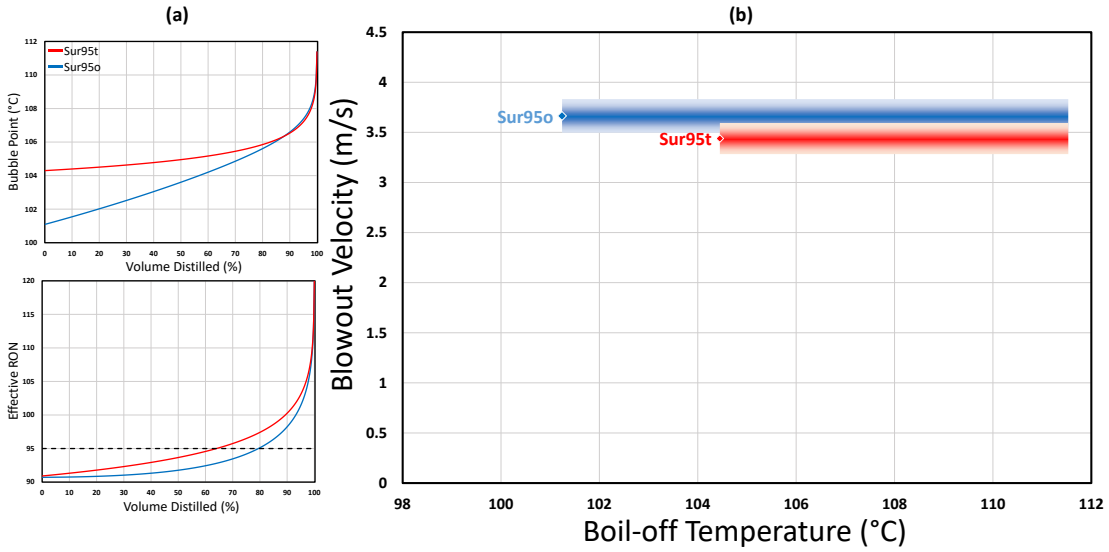

Note. Streak length represents distillation profile and width indicates error.

Interestingly, as opposed to the jet fuel response, the behavior of these surrogates shown in panel (b) displays some deviation from each other, wherein the Sur95o surrogate displays a greater, albeit inconclusive, resistance to blowout. This behavior was unexpected being that the distillation resolved CPs display only minor variation, as opposed to the jet fuel surrogate's dramatic property deviations. The distillation resolved CPs of the gasoline surrogates do not drastically shift through CP regimes, but they do display interesting behavior contrary to the jet fuel's where there is no counteraction of properties. Observing Sur95t's behavior in panel (a) of Figure 30, not only is the surrogate less volatile, it is also less reactive throughout the majority of its distillation trajectory compared to Sur95o. It seems that the reduction in both volatility and reactivity has depressed its resistance to

blowout. This may indicate that property stratification induced by preferential vaporization may influence the surrogate's combustion behavior validating the hypothesis and overarching goal of this study.

While the distillation-resolved CP stratification causality seems plausible, as mentioned earlier, this experimental setup cannot isolate a single metric as governing combustion behavior. Therefore, it is prudent to explore various causes for the observed combustion behavior nonconformity. To further evaluate these surrogates' behavior we explore the counterintuitive equivalence ratio behavior displayed. Taking into account the oxygenated Ethanol species in the Sur95o surrogate, at a given co-flow volumetric flowrate the Sur95o surrogate will have a lower equivalence ratio compared to the Sur95t surrogate. Considering that these fuels should be equivalent this would lead to the assumption that the Sur95o surrogate should be less resistant to blowout since it inherently leans out sooner than the non-oxygenated fuel, although the data shows this is not the case. Table 6 gives a brief description of the global equivalence ratios back-calculated from the average blowout velocities.

Table 6

Global Equivalence (Phi) Ratio of Sur95o and Sur95t

Fuel	Blowout Avg (m/s)	Volumetric Flowrate Avg (m^3/s)	SCFM	Phi Calc
Sur95o	3.664	0.060	128.19	0.0795
Sur95t	3.438	0.057	120.29	0.0856

This exploration does indicate that the equivalence ratios of these surrogates are not equivalent, although, the argument that this is a driver in their combustion behavior cannot be made. The oxygenated species in the Sur95o surrogate may have other effects such as proving a locally stoichiometric mixture which may account for the fuel's resistance to blowout. A final metric directly correlated to gasoline fuel's combustion behavior worth exploring is the Drivability index. This is a global measurement of how well a fuel will operate in a spark ignition internal combustion engine [2, 17]. The formula for this measurement is given in Equation 11.

$$\mathrm{DI°C} = 1.5(\mathrm{T10}) + 3.0(\mathrm{T50}) + (\mathrm{T90}) + 1.33\ (\text{ethanol volume percent}) \qquad (11)$$

Applying this equation, the Sur95o surrogate has a drivability index of 569.73°C and the Sur95t is 577.98°C. These values are relatively indistinguishable considering the United States drivability range for gasoline of 375°C to 610°C (depending on season) [2]. Although interestingly, they approach the limits for driveability based on the Asia-Pacific range of 460°C to 580°C though this is inconsequential. Further, these fuels were designed for use in an autoignition (HCCI) engine [9] as opposed to a spark ignition engine, so this metric is not particularly relevant. Additionally, to a degree, the HCCI design point invalidates the equivalence ratio observations as these engines operate in an excess of air [9, 51, 77] compared to standard spark ignition engines. Although we cannot definitively say the nonconformity in combustion behavior is a cause of property stratification incurred by preferential vaporization, the data does seem to suggest it, and warrants further exploration.

Though some evidence is presented by the gasoline surrogates, neither of the above datasets definitively prove that combustion behavior is affected by stratified combustion properties induced by preferential vaporization. However, they do indicate that these factors must be considered. This is demonstrated by this blowout experiment's sensitivity to volatility. The experiment's sensitivity to volatility is qualified in the pure component testing in Figure 28 where the n-alkanes of divergent volatilities display significant discrepancy in blowout behavior compared to nC7 and iC8 which lie on opposite ends of the reactivity scale (RON in this case), yet share similar volatility characteristics. Further, Figure 31 evidences this sensitivity by plotting the surrogate results on a common plot.

Figure 31

Jet-A and 95 Octane Gasoline Surrogate's Blowout Thresholds With 1σ Error

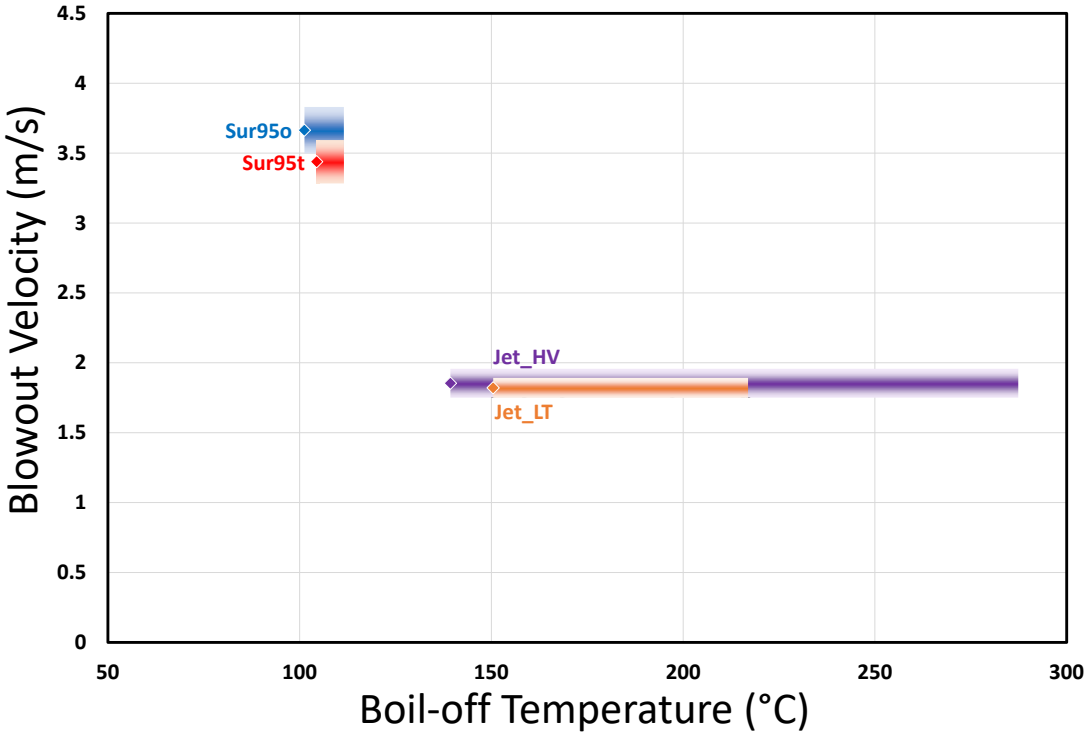

Note. Streak length represents distillation profile and width indicates error. These data sets were taken on different days and cannot be directly correlated.

Keeping in mind this is not an apples-to-apples comparison since these datasets are taken on different days, we observe that the more volatile gasoline surrogates are significantly more resistant to blowout as compared to the much more reactive jet fuel surrogates, even if error is doubled or tripled. This data, coupled with Figure 28, undoubtedly demonstrates that volatility characteristics play a significant role in a fuel's blowout threshold. Although, overall, the data presented in this chapter does not provide a clear-cut answer on preferential vaporization's influence on the combustion behavior of

multicomponent surrogate fuels comprised of species with varying volatility. With that, this experiment is still in its infancy and requires additional data before any definitive conclusions can be drawn.

A final thought experiment was performed in this study to attempt to tease out added insight on how combustion behavior is influenced by volatility. To do this, surrogates comprised of only n-alkanes were formulated. This methodology indicates that if chemically dependent properties are matched, when prevaporized, the fuels should have identical combustion behavior. This experiment is further explained in the following section.

5.3 nC9 Surrogates

Confident that this experiment is sensitive to changes in volatility and in order to gain some additional insight on the role of preferential vaporization on combustion behavior among equivalent prevaporized fuels, we created surrogates for an n-alkane comprised of only n-alkane species. The reasoning behind this dataset is that if we create n-alkane comprised surrogates by matching chemically dependent properties, these surrogates should be identical in prevaporized space since long-chain n-alkanes have equivalent chemically dependent behaviors. In theory, this should isolate the physical property dependence, namely volatility, on combustion behavior among these otherwise equivalent prevaporized surrogates.

Based on chemical availability, nC9 surrogates were created by matching the molecular formula through incorporating varying proportions of nC7, nC8, nC10, nC12, and nC16 species. Formulating surrogates in this fashion couples a matched H/C ratio, average molecular weight as well as CH_2/CH_3 chemical reaction pathways i.e., ability for

the surrogate to react (reactivity). These surrogates are all identical in prevaporized space, the nuance of these formulations lie in that, in some instances and to varying degrees we have loaded the light and heavy distillation endpoints to create surrogates with divergent volatility characteristics. The combustion property targets and surrogate recipes are seen in Table 7 below. It should be noted that this formulation method deviates from the literature's methods of matching CPTs, although, if our n-alkane assumption holds true, these surrogates should all be identical when prevaporized.

Table 7

Chemical Property Targets (nC9), Calculated Surrogate Properties, and Recipe for Four N-Nonane Fuel Surrogates Formulated With Only N-Alkane Components

	n-nonane	Pink	Blue	Green	Black
H/C Ratio	2.222	2.222	2.222	2.222	2.222
CH_2/CH_3	7/2	7/2	7/2	7/2	7/2
MW_{avg}	128	128	128	128	128
Components (mole fraction)					
n-heptane		0.533	0.433	0.68	-
n-octane		-	-	-	0.5
n-decane		0.3667	0.51667	-	0.5
n-dodecane		-	-	0.22	-
n-hexadecane		0.1	0.05	0.1	-

As the table describes, we have matched chemical dependent properties using only n-alkane species, which in prevaporized space should indicate that these fuels are identical. A few noteworthy observations about these surrogates are that the Blue and Pink surrogates are made of identical components in varying proportions. Additionally, the Black surrogate should have smooth distillation characteristics as it is made of equal parts of comparatively similar volatility species. To observe the disparity in volatility among these surrogates, Figure 32 displays each surrogate's distillation curves with nC9's normal boiling point indicated as a target.

Figure 32

Distillation Curves of the nC9 Fuel Surrogates With nC9's Normal Boiling Point Indicated as a Target

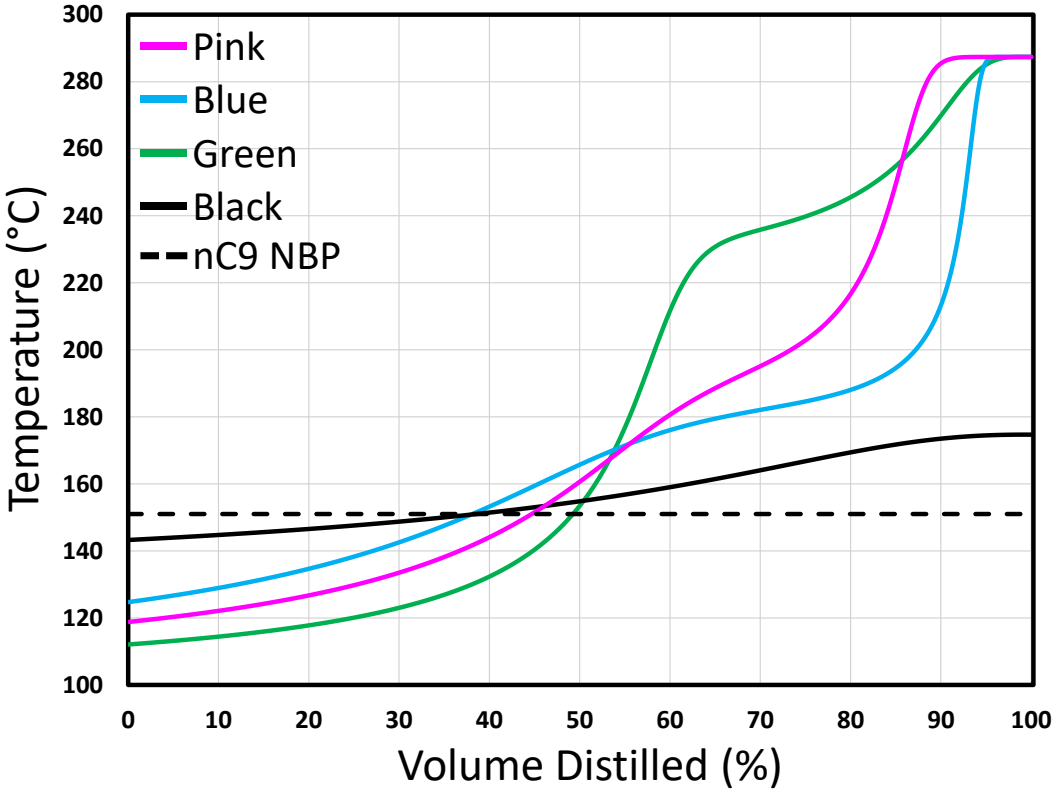

The distillation curves of these surrogates are not well matched to the nC9 normal boiling point target, with the exception of the Black surrogate. This surrogate's smooth, well matched distillation characteristics are expected as it can be considered our baseline fuel being that it is a simple 50/50 mix of nC8 and nC10. The other three surrogates display rather divergent distillation behaviors from the target value. A point to note is that the similar speciation Pink and Blue surrogates have well matched, although slightly offset distillation characteristics. In sum, all these surrogates have identical chemical characteristics but varying volatility. This may provide us with additional insight on the effect of preferential vaporization on blowout behavior, as well as the importance of considering distillation effects when attempting to formulate fuel surrogates. To begin our examination of these surrogate's blowout behavior we qualify nC9's blowout threshold by testing nC8 and nC10 to determine an appropriate range. This was necessary because when this study was conducted nC9 was not on hand to test, so approximating its threshold was the next best thing. This approximation is presented in Figure 33.

Figure 33

Pure Component Blowout Thresholds With 1σ Error Bars Used to Gauge nC9's Blowout Velocity

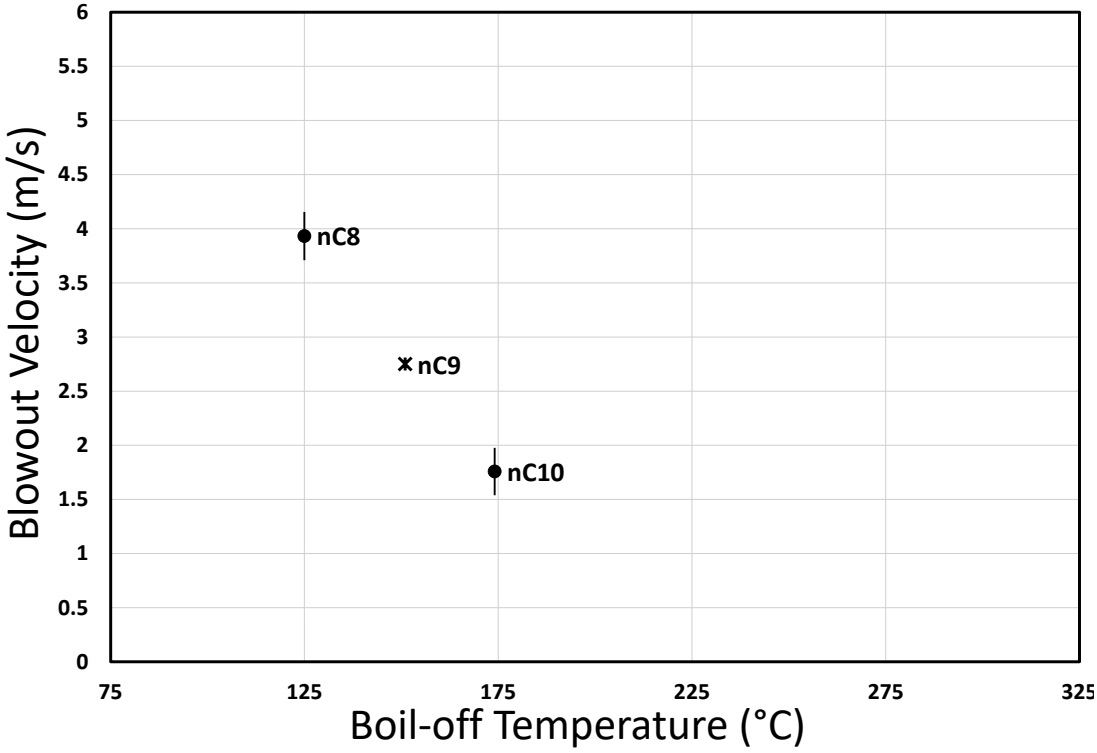

Figure 33 displays a rather straightforward representation of nC9's approximate blowout threshold. It should be noted that the indicated nC9 point is not exact and its blowout threshold could be anywhere between nC8 and nC10. An additional point of interest is the nC8 and nC10 blowout thresholds are about 0.5 m/s greater than the previous values seen in Figure 28. This speaks to the appropriateness of only comparing data which have been tested in quick succession as previously justified in section 4.1. Continuing this experiment, perhaps the most interesting behavior to evaluate is how the Blue and Pink surrogate's blowouts may differ being that they are comprised of the same species. With

that, these fuels were tested in accordance with the experiment protocol, the results are displayed in Figure 34 below.

Figure 34

Identical Component Pink and Blue nC9 Surrogate's and Pure Component's Blowout Thresholds With 1σ Error

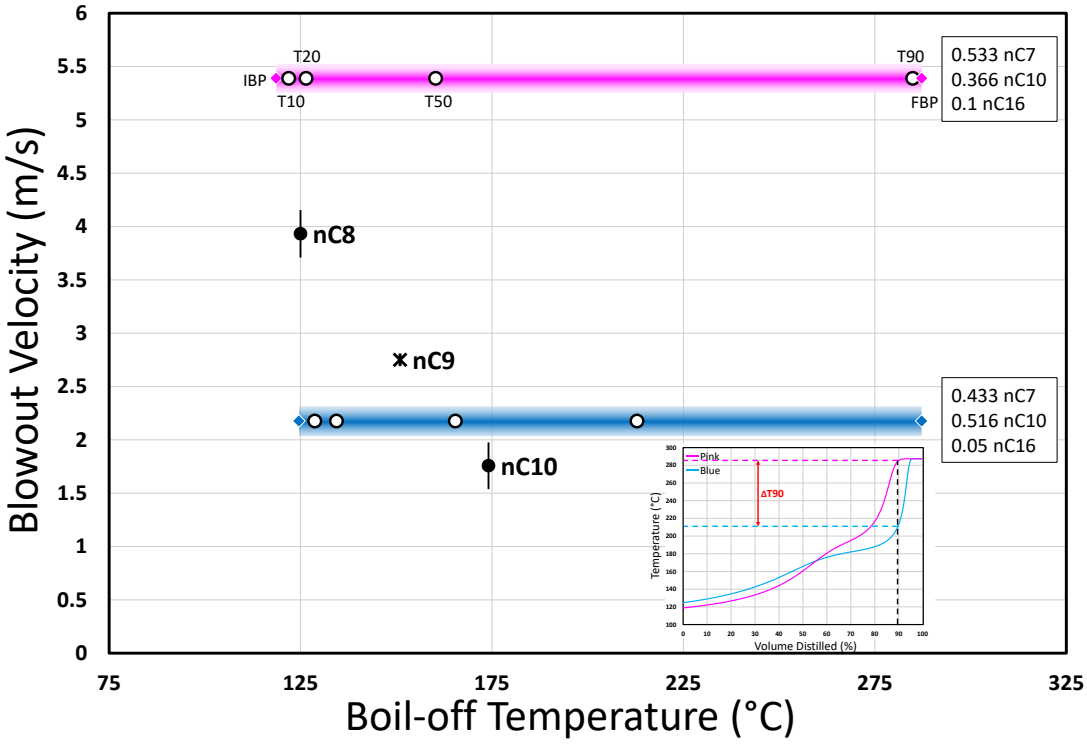

Note. Streak length represents distillation profile, width indicates error, and highlighted points correspond to initial boiling point (IBP), temperatures at 10%, 20%, 50%, and 90% volume distilled (T10,T20,T50,T90), and the final boiling point (FBP). The distillation curves are superimposed to indicate the large T90 temperature difference. Surrogate recipes are superimposed for ease of comparison.

This figure displays blowout thresholds in a similar format to previous blowout evaluations with the addition of highlighting initial boiling point, final boiling point, and temperatures at 10%, 20%, 50%, and 90% volume distilled. Additionally, this figure has the surrogate's composition and distillation curve superimposed onto it. The blowout behavior of these surrogates presents interesting behavior, where these similarly composed surrogates display a vast discrepancy in blowout thresholds even though they should be equivalent when prevaporized. Further, for reasons not fully quantified, the Blue surrogate does a better job emulating nC9's blowout behavior. Since these surrogates have the same reactivity, H/C ratio, MW etc. the only factor affecting blowout should be volatility and perhaps spray dynamics considerations (surface tension, viscosity, etc.). Based on the previous blowout behavior observed in this rig, we conclude that the driving factor is fuel volatility. Observing the intermediate distillation points, we see that the initial boiling point, T10, T20, T50 and the final boiling point are all well matched. The primary deviation in distillation behavior is seen in T90 and may be a driving influencer in blowout thresholds. The T90 relationship is highlighted on the blowout threshold streaks as well as on the superimposed distillation curves. Encouraged by this discrepancy in behavior, the remaining surrogate's blowout thresholds were evaluated to see if this T90 influence hypothesis persists, the results are illustrated in Figure 35.

Figure 35

All nC9 Surrogate's and Pure Component's Blowout Thresholds With 1σ Error

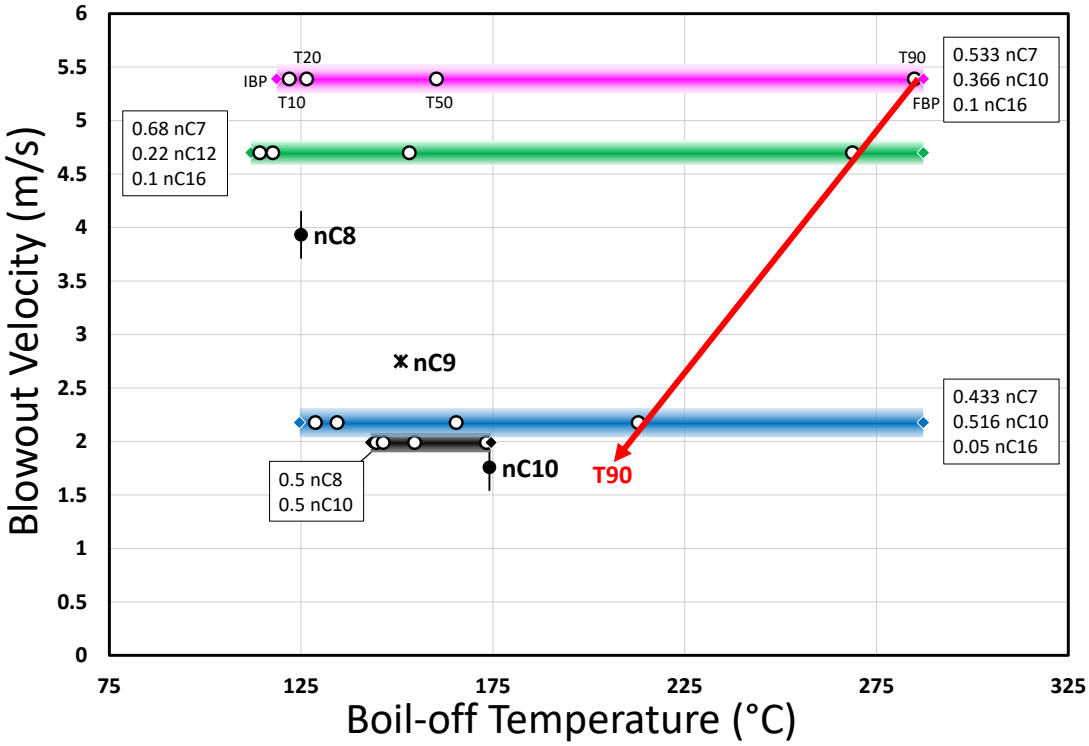

Note. Streak length represents distillation profile, width indicates error, and highlighted points correspond to initial boiling point (IBP), temperatures and 10%, 20%, 50%, and 90% volume distilled (T10,T20,T50,T90), and the final boiling point (FBP). T90 trend is highlighted, as it appears to be a driving factor in blowout thresholds. Surrogate recipes are superimposed for ease of comparison.

Excitingly, the remaining surrogates exhibit divergent blowout thresholds. As mentioned earlier, the Black surrogate is our bland two component surrogate and it is not surprising that it emulates nC9 well, so, we focus on the other three surrogates to attempt to gain some insight into what is influencing blowout behavior. As with the Blue and Pink

surrogates, the Green surrogate displays a comparatively divergent blowout threshold. Among these three surrogates initial boiling point, T10, T20, T50, and final boiling points are all well matched with the primary deviation in distillation behavior being T90. We observe a trend among these surrogates in that lower temperature T90 temperatures correlates to a decreased resistance to blowout. While other trends can be identified in the initial distillation behavior wherein the fuels that emulate nC9's combustion behavior best are initially the least volatile and closest to the target value as compared to the two divergent surrogates, we believe this to be inconclusive. The only clear trend in this data is T90 and may indicate that the blowout experiment is sensitive to this metric. This further emphasizes the importance of considering volatility characteristics when formulating surrogate fuels.

One final metric worth investigating is the surrogates' prevaporized DCN behavior, which was not included in our formulation methodology. Looking at DCN is useful to see if it is the ultimate factor in determining combustion behavior. Each of these surrogates prevaporized DCNs were calculated in accordance with methods in [29] and [9]. The DCN results are displayed below in Table 8.

Table 8

Prevaporized DCN's of nC9 and Surrogates

	n-nonane	Pink	Blue	Green	Black
DCN	60.9	62.69	62.13	63.74	61.85

Note. This was not a CPT when formulating these surrogates

We would expect that the surrogates which emulate the target fuel's behavior best would have particularly similar DCNs to nC9 but this is not the case. The DCN behavior displays some minor correlation in the Blue and Black surrogate's ability to emulate nC9's combustion behavior. Although, this is comparatively insignificant if we consider the small relative DCN difference in the Blue and Pink, yet major deviation in combustion behavior. This indicates that DCN is not the be-all-end-all metric in determining combustion behavior.

All the observations made here are very thought provoking but they are by no means definitive. They do however indicate that distillation behavior may influence the combustion behavior of equivalent prevaporized fuels and thus, should be considered when formulating fuel surrogates.

Chapter 6

Conclusion

The overarching goal of this study was to examine the possible nonconformity among surrogate fuels formulated based on prevaporized single-point combustion property targets. This study has presented some significant evidence that the volatility characteristics of limited specie multicomponent surrogate fuels must be considered due to preferential vaporization effects. This evidence was presented both computationally and experimentally. The computational examination into the effect of property stratification brought on by preferential vaporization was conducted using a simple distillation program underpinned by the Antoine equation and analogous to ASTM D86 batch distillation. This program not only resolves distillation behavior, but also provides insight on the associated property evolution of fuels along their distillation trajectory. The program's algorithm was validated through pure component boiling point evaluation and comparison to calculated distillation curves in published literature. The applicability of this methodology was confirmed through a distillation-resolved combustion property comparison to prevaporized combustion property targets for surrogate fuels tested in an optical engine. The result of this examination indicate that investigating the evolution of combustion properties, which serve as a proxy to combustion behavior, may provide some insight into a surrogate fuel's ability to emulate its real fuel counterpart. Following validation of the model and its efficacy, distillation-resolved property evolutions of surrogates from the literature were assessed. The fuels chosen were from studies where multiple surrogate fuels were formulated for the same real fuel based on prevaporized combustion property target matching allotting a surrogate-to-surrogate comparison. The results from this evaluation

provided sufficient evidence that these surrogate fuels may display nonconformity in combustion behavior from each other and the real fuel.

To explore the model results, an annular burner rig that incorporates distillation behavior via an atomized spray nozzle was conceptualized and built. To compare combustion behaviors, a unique stress test was devised wherein the annular co-flow velocity is incrementally increased until the flame extinguished; the blowout experiment. To ensure consistent data, an experimental protocol was designed to limit cross species contamination, maintain the combustion chamber at a semi-constant hot temperature, and ensure safe operation. Following creation of the experimental methodology, the experiment's sensitivity to physical and chemical property variations was evaluated. The results indicated that the experiment could differentiate physical property variation among chemically identical fuels and chemical property variation among physically identical fuels. Further, to classify experimental consistency, baseline blowout tests were performed over a range of operating conditions to observe the day-to-day measurement variation. The results indicated that only tests performed in quick succession could be compared on a one-to-one basis. With the experiment well classified, the literature surrogates examined in the distillation program were experimentally tested to observe nonconformity in their blowout thresholds.

The blowout results from the jet and gasoline surrogate fuels were inconclusive. The jet fuels, although displaying drastic property stratification in distillation space, seem to have identical combustion behavior. A possible reason for their accurate emulation is the DCN property matching, which, for low volatility fuels is determined in an IQT. This method of measuring DCN may couple distillation and spray characteristics which could

account for the aligned combustion behavior. Additionally, although the distillation data displays drastic shifts in combustion property regimes, they are largely counteractive. For example, periods of increased volatility are matched by decreased reactivity and vice-versa; both metrics we believe influence a fuel's blowout resistance. The gasoline surrogate tested herein did display some inter-surrogate deviation in combustion behavior. Some evidence was presented from the distillation program that may indicate the combustion nonconformity is a result of property stratification brought on by preferential vaporization, although, the results are inconclusive. Furthermore, the oxygenated Ethanol in the Sur95o surrogate may create a region of local stoichiometry that could account for its increased resistance to blowout. Further testing of these surrogates is necessary to definitively determine their emulation ability as well as what factors are driving their combustion behavior. Although these results were inconclusive, they did illustrate that volatility plays a key role in a fuel's ability to resist blowout. This observation indicates that the question of preferential vaporization's effect on combustion behavior is valid and warrants further research.

In order to isolate the effect volatility has on combustion behavior, a set of n-nonane surrogates composed of only n-alkane species with varying volatility characteristics were formulated and tested. The rationale from this experiment is two-fold:

1. n-alkanes have identical chemical behavior, thus, surrogates with the same chemical formula and associated chemical properties should be identical when prevaporized.

2. If these identical prevaporized surrogates display deviation in combustion behavior then it must be a cause of the property stratification brought on by volatility differences i.e., preferential vaporization.

Four surrogates were created, two consisting of identical chemical species, one with a slightly heavier mid-distillation component, and a simple 50/50 mixture considered the nominal surrogate. To vary the volatility characteristics, the light and heavy distillation endpoints were loaded to varying degrees. This ensured a wide range of volatility and associated distillation behavior. This should increase the possibility of combustion behavior deviation due to property stratification. Following experimental protocol, the surrogates' blowout thresholds were determined, interestingly, they displayed significant nonconformity. Overall, the greatest influence in blowout behavior for this experiment seems to be the temperature at 90% volume distilled. This correlation is still in its infancy and requires additional data to definitively prove, but, nonetheless, this behavioral trend indicates that volatility characteristics play a significant role in fuel combustion behavior amongst surrogates considered equivalent under prevaporized conditions.

In sum, both computationally and experimentally, this study has:

1. Developed a simple ideal mixture distillation/linear blending rule model which demonstrates that distillation effects may lead to stratification of key combustion properties (e.g., RON, DCN, MW, H/C, etc.) about the lumped, pre-vaporized "average" target values used to formulate some real fuel surrogates.
2. Shown that distillation-resolved combustion property to target property comparisons can be an indicator of combustion behavior. This indicates that

distillation effects may lead to spatial stratification of relative ignitability, local stoichiometry, etc. in practical applications involving fuel spray atomization.

3. Developed a unique annular spray burner rig that can perform various spray coupled tests designed to highlight the effect of preferential vaporization and associated property stratification in multicomponent fuel surrogates consisting of species with varying volatility characteristics.
4. Verified the sensitivity of the spray coupled blowout experiment to both physical and chemical property variations and their effects on combustion behavior.
5. Obtained blowout data for jet and gasoline fuel surrogates from the literature. Results were inconclusive, but warrant further investigation.
6. Created and experimentally evaluated a set of nC9 surrogates, formulated with only n-alkane species by matching chemical formulas. These equivalent prevaporized surrogates, designed with varying volatility characteristics, displayed significant deviation in combustion behavior. This set of surrogates indicated that property stratification incurred from preferential vaporization effects combustion behavior. Further, preferential vaporization effects must be considered in the formulation of representative fuel surrogates to ensure combustion emulation in real applications where atomized fuel sprays and accompanying vaporization progression is integral.

Chapter 7

Future Work

The design of the Mark II and associated experiments are still very much in their infancy. Numerous improvements are necessary to bring the experiment to optimal operating status. This chapter outlines some of the necessary improvements as well as some future data sets to assist in isolating preferential vaporization's impact on the combustion behavior of fuel surrogates.

- Hardware/Design
    - Syringe pump to allow precise fuel flow control. The current setup relies on the nozzle to control fuel flowrate, this creates issues since physical properties of the fuel may affect the flowrate. The influence of physical properties on fuel flowrate was observed during tests when different fuel's timed flow duration exceeded calculated durations and other fuels. This system can also increase safety by programming a flow direction reversal to rapid cut fuel supply into the combustion chamber.
    - Proper recording equipment to allow accurate determination of the liftoff height. The current optical camera does not have the proper focal length to focus on the entirety of the flame front. Additionally, the current DVR equipment generates a shaky image and requires a higher quality device. Further, optical issues with this test may occur when different fuels are tested. The different liftoff heights could affect the measurement since the camera may pick-up the underside of the flame as opposed to a front on view. This issue has not been fully resolved, but an option would be to

adjust the camera height using the 3 DOF slide rail and incorporate software to calibrate the nozzle tip as the zero point.

- Advanced measurement equipment to take more detailed readings of the combustion environment. This is a vast subject, but in general, incorporating laser measurement for a variety of combustion behaviors will provide more detailed results such as liftoff heights, droplet size distribution, and species distribution in the exhaust stream.
- Advanced co-flow blower to allow more accurate and precise control over the co-flow air. Laboratory grade blowers would allow for far greater control over the co-flow, such as the Nautilaur Variable Speed Blower from Ametek. This blower is designed for combustion air delivery and can be precisely controlled with either a 0-10VDC, 4-20mA, or PWM electrical signals with built-in PID control. Furthermore, a Leister hot air blower system would be robust enough to deliver pre-heated co-flow regulated by its built-in PID heater controller.
- Three way valve to improve safety and ease of use. This value will eliminate the need to simultaneous manage two values in order to cut fuel delivery. This will greatly increase safety by minimizing user error.
- Swirl plates to enable better mixing within the combustion chamber. In the current experimental setup, there is a possibility that not all the fuel is participating in combustion. As co-flow increases in the blowout experiment, it is possible that the less volatile fuels are simply being blown

out of the exhaust. This may minimize their influence on the combustion behavior of a particular fuel and affect results.

- Safety Improvements
    - Internal CO_2 extinguisher system to improve emergency protocols. Integrating a CO_2 extinguisher system into the fume hood will ensure any unmanageable fires can be effectively extinguished even if fuel continues to flow. Additionally, this will increase "red button" effectiveness.
    - Dedicated automatic fuel kill valve to further improve to "red button" procedures. A pneumatic value or electronic solenoid will enable complete, automated, and remote fuel flow control. This, coupled with an extinguisher system will offer the user complete control in emergency situations. This value should not be the fuel kill switch used during blowout or normal testing, it should be a redundant system for emergency purposes. If electronic, it should have a battery backup, or integrated to the UPS currently used to power the blower.
    - Auto-ignition system so students minimize contact with unburnt atomized fuel. Having an auto-ignition system will also allow the fume hood to remain sealed at all times, minimizing exposure to emissions.
    - Pressure transducer to detect rapid pressure drop which would indicate a fuel line leak or burst. This system further increases readiness for emergency situations. Coupling this with the automatic lighting and fuel flow systems could mitigate the possibility of an explosion or fire from a fuel leak.

- Experimental/data gathering with minor modifications
    - Additional rounds of literature surrogate testing. The current results are inconclusive and require further blowout and liftoff height measurements. Moreover, other surrogates from the literature which fit criteria should be investigated to ensure concrete conclusions can be drawn.
    - In a similar fashion to the nC9 surrogates, longer chain, heavier surrogates should be formulated and tested such as nC10 or nC12. The heavier surrogates will allow loading on light end, this will provide additional insight on the T90 trend. This evaluation will determine if the trend persists for surrogates with a wide range of front end volatilities and relatively similar tail ends.
    - Determination of an appropriate day-to-day baseline correlation to allow cross-trial comparisons. This will allow for a larger view of the data. With the outlined experiment improvements, the data should be consistent enough to cross-evaluate and provide a wider view of trends.
    - With the current setup, little modification is necessary to measure light emissions for soot formation evaluation. To do this, a camera which can capture the entire flame, and some specialized software is necessary. The software would isolate the yellow and red light spectrums of the flame and convert them to an intensity scale. This should give a measurement of soot formation. Additionally, including the blue spectrum will give a total illumination value which may also be useful.

- The final test which can be easily executed with the current experiment is evaluating different configurations with the baseline Acetone fuel. This will provide some information on how the flame's behavior is affected by the combustion environment. Configuration modifications could be done to the fuel nozzle, fuel pressure, flow straightener alignment, co-flow temperature, and swirl plates.

References

[1] J. Bacha, J. Freel, A. Gibbs, L. Gibbs, G. Hemighaus, and e. al., "Diesel fuels technical review," *Chevron Global Marketing,* 2007.

[2] L. Gibbs, B. Anderson, K. Barnes, G. Engeler, and e. al., "Motor gasolines technical review (FTR-1)," *Chevron Products Company, San Ramon,* 2009.

[3] G. Hemighaus *et al.*, "Aviation fuels technical review," *Chevron Corporation,* 2006.

[4] Y. Ra and R. D. Reitz, "A combustion model for multi-component fuels using a physical surrogate group chemistry representation (PSGCR)," *Combustion and Flame,* vol. 162, no. 10, pp. 3456-3481, 2015.

[5] A. Krishnasamy, R. D. Reitz, W. Willems, and E. Kurtz, "Surrogate diesel fuel models for low temperature combustion," *SAE Technical Paper,* no. 2013-01, p. 1092, 2013.

[6] S. Dooley *et al.*, "A jet fuel surrogate formulated by real fuel properties," *Combustion and Flame,* vol. 157, no. 12, pp. 2333-2339, 12// 2010.

[7] D. Kim, J. Martz, and A. Violi, "A surrogate for emulating the physical and chemical properties of conventional jet fuel," *Combustion and Flame,* vol. 161, no. 6, pp. 1489-1498, 6// 2014.

[8] W. J. Pitz *et al.*, "Development of an experimental database and chemical kinetic models for surrogate gasoline fuels," SAE Technical Paper0148-7191, 2007.

[9] C. Pera and V. Knop, "Methodology to define gasoline surrogates dedicated to auto-ignition in engines," *Fuel,* vol. 96, pp. 59-69, 2012/06/01/ 2012.

[10] K. Doohyun, J. Martz, A. Abdul-Nour, X. Yu, M. Jansons, and A. Violi, "A six-component surrogate for emulating the physical and chemical characteristics of conventional and alternative jet fuels and their blends," *Combustion and Flame 179,* vol. 179, pp. 86-94, 2017.

[11] T. Edwards *et al.*, "Development of an experimental database and kinetic models for surrogate jet fuels.," presented at the 45th AIAA Aerospace Sciences Meeting and Exhibit, Reno, Nevada, 2007.

[12] Z. Wang and M. Fingas, "Developments in the analysis of petroleum hydrocarbons in oils, petroleum products and oil-spill-related environmental samples by gas chromatography," *Journal of Chromatography A,* no. 774, pp. 51-78, 1997.

[13] C. S. Robinson, *The elements of fractional distillation*. McGraw-Hill book company, inc., 1922.

[14] W. Leffler, *Petroleum refining in nontechnical language*. PennWell Books, 2008.

[15] J. Burger, T. Lovestead, R. Gough, and B. Thomas, "Characterization of the Effects of Cetane Number Improvers on Diesel Fuel Volatility by Use of the Advanced Distillation Curve Method," *Energy & Fuels,* vol. 28, no. 4, pp. 2437-2445, 2014.

[16] D. Phuong, S. Crossley, M. Santikunaporn, and D. Resasco, "Catalytic strategies for improving specific fuel properties," *Catalysis,* vol. 20, pp. 33-64, 2007.

[17] *Standard Specification for Automotive Spark-Ignition Engine Fuel,* A. International, 2018.

[18] K. Anand, Y. Ra, R. D. Reitz, and B. Bunting, "Surrogate Model Development for Fuels for Advanced Combustion Engines," *Energy & Fuels,* vol. 25, no. 4, pp. 1474-1484, 2011/04/21 2011.

[19] J. Burger, R. Gough, and T. J. Bruno, "Characterization of dieseline with the advanced distillation curve method: hydrocarbon classification and enthalpy of combustion," *Energy & Fuels,* vol. 27, no. 2, pp. 787-795, 2013.

[20] *ASTM D86 Standard Test Method for Distillation of Petroleum Products and Liquid Fuels at Atmospheric Pressure*, 2016.

[21] I. Coordinating Research Council, "Handbook of Aviation Fuel Properties," Society of Automotive Engineers, Inc., Georgia530, 1983.

[22] C. K. Law, *Combustion physics*. Cambridge university press, 2010.

[23] F. L. Dryer *et al.*, "Emulating the Combustion Behavior of Real Jet Aviation Fuels by Surrogate Mixtures of Hydrocarbon Fluid Blends: Implications for Science and Engineering," *Energy & Fuels,* vol. 28, no. 5, pp. 3474-3485, 2014/05/15 2014.

[24] C. J. Mueller *et al.*, "Methodology for formulating diesel surrogate fuels with accurate compositional, ignition-quality, and volatility characteristics.," *Energy & Fuels,* vol. 26, no. 6, pp. 3284-3303, 2012.

[25] S. Dooley *et al.*, "The experimental evaluation of a methodology for surrogate fuel formulation to emulate gas phase combustion kinetic phenomena," *Combustion and Flame,* vol. 159, no. 4, pp. 1444-1466, 4// 2012.

[26] D. Bell, J. S. Heyne, S. H. Won, F. Dryer, F. M. Haas, and S. Dooley, "On the Development of General Surrogate Composition Calculations for Chemical and Physical Properties," in *55th AIAA Aerospace Sciences Meeting*(AIAA SciTech Forum: American Institute of Aeronautics and Astronautics, 2017.

[27] M. L. Huber, E. W. emmon, L. S. Ott, and T. J. Bruno, "Preliminary Surrogate Mixture Models for the Thermophysical Properties of Rocket Propellants RP-1 and RP-2," *Energy & Fuels,* vol. 23, no. 6, pp. 3083-3088, 2009.

[28] T. Gallant *et al.*, "Fuels for Advanced Combustion Engines Research Diesel Fuels: Analysis of Physical and Chemical Properties," *SAE International Journal of Fuels and Lubricants,* vol. 2, no. 2, pp. 262-272, 2010.

[29] S. H. Won, F. M. Haas, S. Dooley, T. Edwards, and F. L. Dryer, "Reconstruction of chemical structure of real fuel by surrogate formulation based upon combustion property targets," *Combustion and Flame,* vol. 183, pp. 39-49, 2017/09/01/ 2017.

[30] M. Mehl, J. Y. Chen, W. J. Pitz, S. M. Sarathy, and C. K. Westbrook, "An Approach for Formulating Surrogates for Gasoline with Application toward a Reduced Surrogate Mechanism for CFD Engine Modeling," *Energy & Fuels,* vol. 25, no. 11, pp. 5215-5223, 2011/11/17 2011.

[31] A. Stagni, L. Esclapez, P. Govindaraju, A. Cuoci, T. Faravelli, and M. Ihme, "The role of preferential evaporation on the ignition of multicomponent fuels in a homogeneous spray/air mixture," *Proceedings of the Combustion Institute,* vol. 36, no. 2, pp. 2483-2491, // 2017.

[32] T. Kim *et al.*, "Experimental Validation of Jet Fuel Surrogates in an Optical Engine," *SAE Technical Paper,* 2017.

[33] C. Allen, D. Valco, E. Toulson, J. H. Yoo, and T. Lee, "JP-5 and HRJ-5 autoignition characteristics and surrogate modeling," *Energy & Fuels,* vol. 27, no. 12, pp. 7790-7799, 2013.

[34] L. Zhang and S.-C. Kong, "Modeling of multi-component fuel vaporization and combustion for gasoline and diesel spray," *Chemical Engineering Science,* vol. 64, no. 16, pp. 3688-3696, 8/15/ 2009.

[35] S. Sazhin, "Advanced models of fuel droplet heating and evaporation," *Progress in energy and combustion science,* vol. 32, no. 2, pp. 162-214, 2006.

[36] I. Glassman, *Combustion 3rd Edition*. Academic Press, 1996.

[37] G.-S. Zhu and R. Reitz, "A model for high-pressure vaporization of droplets of complex liquid mixtures using continuous thermodynamics," *International Journal of Heat and Mass Transfer,* vol. 45, no. 3, pp. 495-507, 2002.

[38] S. Som, A. Ramirez, D. Longman, and S. Aggarwal, "Effect of nozzle orifice geometry on spray, combustion, and emission characteristics under diesel engine conditions," *Fuel,* vol. 90, no. 3, pp. 1267-1276, 2011.

[39] Y. Ra and R. D. Reitz, "The application of a multicomponent droplet vaporization model to gasoline direct injection engines," *International Journal of Engine Research,* vol. 4, no. 3, pp. 193-218, 2003.

[40] K. Reif, "Gasoline Engine Management Systems and Components." Wiesbaden: Springer Vieweg, 2015, p.^pp. Pages.

[41] R. H. Ewell, J. M. Harrison, and L. Berg, "Azeotropic distillation," *Industrial & Engineering Chemistry*, vol. 36, no. 10, pp. 871-875, 1944.

[42] G. W. Thomson, "The Antoine equation for vapor-pressure data," *Chemical reviews*, vol. 38, no. 1, pp. 1-39, 1946.

[43] M. Frenkel, R. D. Chirico, V. Diky, X. Yan, Q. Dong, and C. Muzny, "ThermoData Engine (TDE): software implementation of the dynamic data evaluation concept," *Journal of chemical information and modeling*, vol. 45, no. 4, pp. 816-838, 2005.

[44] W. Yuan, A. C. Hansen, and Q. Zhang, "Vapor pressure and normal boiling point predictions for pure methyl esters and biodiesel fuels," *Fuel*, vol. 84, no. 7, pp. 943-950, 2005.

[45] P. J. Linstrom and W. G. Mallard, "NIST Chemistry WebBook." Gaithersburg MD: National Institute of Standards and Technology, 2017, p.^pp. Pages.

[46] T. J. Bruno and B. Smith, "Improvements in the Measurement of Distillation Curves. 2. Application to Aerospace/Aviation Fuels RP-1 and S-8," *Industrial & engineering chemistry research*, vol. 45, no. 12, pp. 4381-4388, 2006.

[47] T. J. Bruno, E. Baibourine, and T. Lovestead, "Comparison of Synthetic Isoparaffinic Kerosene Turbine Fuels with the Composition-Explicit Distillation Curve Method," *Energy & Fuels*, vol. 24, no. 5, pp. 3049-3059, 2010.

[48] B. Higgins and D. Siebers, "Measurement of the flame lift-off location on DI diesel sprays using OH chemiluminescence," *SAE Technical Paper*, 2001.

[49] C. Allen, D. Valco, E. Toulson, T. Edwards, and T. Lee, "Ignition behavior and surrogate modeling of JP-8 and of camelina and tallow hydrotreated renewable jet fuels at low temperatures," *Combustion and Flame*, vol. 160, pp. 232-239, 2013.

[50] M. Colket *et al.*, "Identification of target validation data for development of surrogate jet fuels," presented at the 46th AIAA Aerospace Sciences Meeting and Exhibit, 2008.

[51] J. Jeon, J. T. Lee, S. I. Kwon, and S. Park, "Combustion performance, flame, and soot characteristics of gasoline–diesel pre-blended fuel in an optical compression-ignition engine," *Energy Conversion and Management,* vol. 116, pp. 174-183, 2016.

[52] J. T. Edwards, "Reference Jet Fuels for Combustion Testing," presented at the 55th AIAA Aerospace Sciences Meeting, 2017.

[53] S. Outcalt, "Compressed-Liquid Densities of Three “Reference” Turbine Fuels," *Energy & Fuels,* vol. 30, no. 12, pp. 10783-10788, 2016.

[54] Y. Ra and R. D. Reitz, "A vaporization model for discrete multi-component fuel sprays," *International Journal of Multiphase Flow,* vol. 35, no. 2, pp. 101-117, 2// 2009.

[55] S.-C. Kong, S. Yong, and R. Rietz, "Modeling Diesel Spray Flame Liftoff, Sooting Tendency, and NOx Emissions Using Detailed Chemistry With Phenomenological Soot Model," *Journal of Engineering for Gas Turbines and Power* vol. 129, no. 1, pp. 245-251, 2005.

[56] N. Peters and F. A. William, "Liftoff characteristics of turbulent jet diffusion flames," *AIAA journal,* vol. 21, no. 3, pp. 423-429, 1983.

[57] J. Chomiak and A. Karlsson, "Flame liftoff in diesel sprays," *Symposium (International) on Combustion,* vol. 26, no. 2, pp. 2557-2564, // 1996.

[58] V. M. Reddy, D. Trivedi, and S. Kumar, "Experimental Investigations on Lifted Spray Flames for a Range of Coflow Conditions," *Combustion Science and Technology,* vol. 184, no. 1, pp. 44-63, 2012/01/01 2012.

[59] D. L. Siebers and B. S. Higgins, "Effects of injection conditions on the flame lift-off length of DI Diesel sprays.," presented at the Thermalfluidynamic Processes in Diesel Engines: Selected Papers from the Thiesel 2000, Valencia, Spain, 2000.

[60] R. Venugopal and J. Abraham, "A review of fundamental studies relevant to flame lift-off in diesel jets," *SAE technical paper,* 2007.

[61] H. Persson, Ö. Andersson, and E. Rolf, "Fuel effects on flame lift-off under diesel conditions," *Combustion and Flame,* vol. 158, no. 1, pp. 91-97, 2011.

[62] G. E. Bogin Jr. *et al.*, "Numerical and Experimental Investigation of n-Heptane Autoignition in the Ignition Quality Tester (IQT)," *Energy & Fuels,* vol. 25, no. 12, pp. 5562-5572, 2011.

[63] J. R. M. A. M. Yanowitz, R.L.; Taylor, J.D.; Murphy, M.J., "Compendium of Experimental Cetane Numbers," NRELNREL/TP-5400-61693, 2004.

[64] Delavan, "Oil Burner Nozzles and Accessories for residental and industrial combustion applications," U. A. Systems, Ed., ed.

[65] G. J. Sturgess, D. G. Sloan, A. L. Lesmerises, S. P. Heneghan, and D. R. Ballal, "Design and Development of a Research Combustor for Lean Blowout Studies," presented at the 1990 International Gas Turbine and Aeroengine Congress and Exposition, Brussels, Belgium, 1990.

[66] E. Corporan *et al.*, "Impacts of Fuel Properties on Combustor Performance, Operability and Emissions Characteristics," p. 0380.

[67] T. H. Scott Stouffer, Jeffrey R. Monfort, Jacob Diemer, Edwin Corporan, Paul Wrzesinski, Andrew W. Caswell, "Lean Blowout and Ignition Characteristics of Conventional and Surrogate Fuels Measured in a Swirl Stabilized Combustor," in *55th AIAA Aerospace Sciences Meeting*(AIAA SciTech Forum: American Institute of Aeronautics and Astronautics, 2017.

[68] M. Akbarzadeh, "An experimental study on the liftoff of a co-flowing non-premixed turbulent methane flame: effect of the fuel nozzle geometry," Ph.d, Department of Mechanical and Manufacturing Engineering, University of Manitoba, 2014.

[69] A. H. Lefebvre, *Gas turbine combustion: alternative fuels and emissions*, 3rd ed. Hoboken, NJ: CRC Press, 2010.

[70] C. Ji, E. Dames, Y. L. Wang, H. Wang, and F. N. Egolfopoulos, "Propagation and extinction of premixed C5–C12 n-alkane flames," *Combustion and Flame*, vol. 157, no. 2, pp. 277-287, 2010/02/01/ 2010.

[71] D. F. Davidson, S. C. Ranganath, K. Y. Lam, M. Liaw, Z. Hong, and R. K. H, "Ignition delay time measurements of normal alkanes and simple oxygenates," *Journal of Propulsion and Power*, vol. 26, no. 2, pp. 280-287, 2010/03/01 2010.

[72] S. H. Won, S. Dooley, F. Dryer, and Y. Ju, "A radical index for the determination of the chemical kinetic contribution to diffusion flame extinction of large hydrocarbon fuels," *Combustion and Flame*, vol. 159, no. 2, pp. 541-551, 2012.

[73] P. Diévart, S. H. Won, J. Gong, S. Dooley, and Y. Ju, "A comparative study of the chemical kinetic characteristics of small methyl esters in diffusion flame extinction," *Proceedings of the combustion institute*, vol. 34, no. 1, pp. 821-829, 2013.

[74] F. M. Haas, A. Ramcharan, and F. L. Dryer, "Relative reactivities of the isomeric butanols and ethanol in an ignition quality tester.," *Energy & Fuels*, vol. 25, no. 9, pp. 3909-3916, 2011.

[75] D. Luning Prak, P. Luning Prak, P. Trulove, and J. Cowart, "Formulation of Surrogate Fuel Mixtures Based on Physical and Chemical Analysis of Hydrodepolymerized Cellulosic Diesel Fuel," *Energy & Fuels*, vol. 30, no. 9, pp. 7331-7341, 2016.

[76] E. Osecky, "An alternative for characterizing the combustion kinetics of low volatility fuels," Ph. d, Chemical Engineering, Colorado School of Mines, 2013.

[77] S. Aceves, J. Martinez-Frias, and G. Reistad, "Analysis of Homogeneous Charge Compression Ignition (HCCI) engines for cogeneration applications," *ournal of Energy Resources Technology*, vol. 128, no. 1, pp. 16-27, 2006.

[78] science-resources.co.uk (Ed.). (n.d.). Fractional distillation of crude oil. http://science-resources.co.uk/KS3/Chemistry/Chemical_Reactions/Hydrocarbons/Distillation.htm

[79] alsglobal.com. (n.d.). Search. Petroleum Fractions by Carbon Range. https://www.alsglobal.com/search?query=Petroleum-Hydrocarbon-Ranges.

Appendix A

Distillation Logic Diagram and MATLAB Code

A.1 Logic Diagram

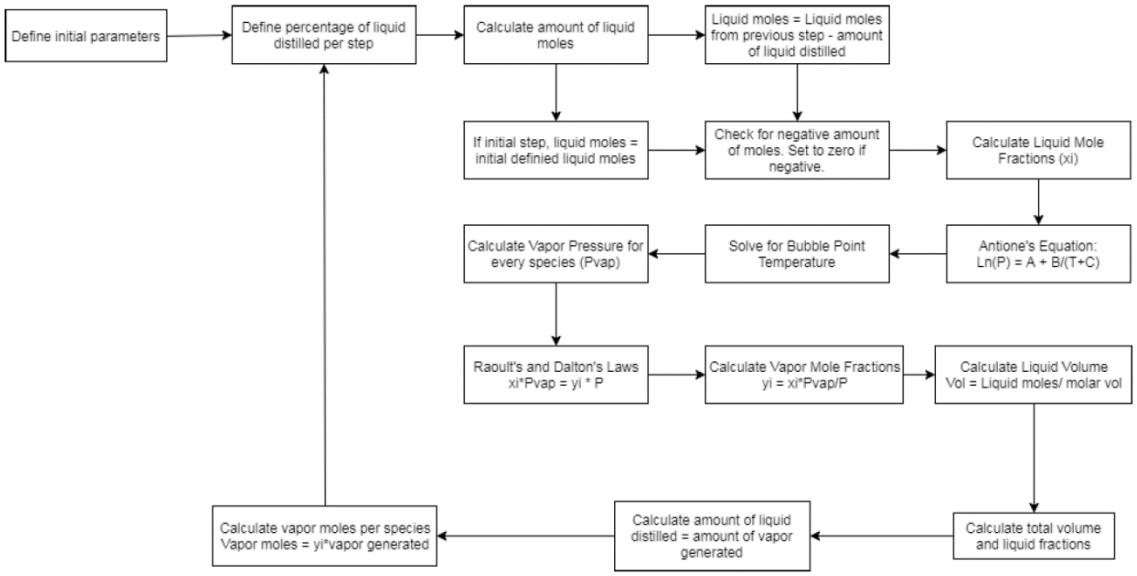

A.2 Front end user interface and graphic generator

```
%This code compares similar surrogate fuels. Create surrogates and save to a .mat file. Use this code to call
the %surrogates and run the distillation.
close all; clc;
clear all;
Pinf_0=101.325; %Initial Pressure in kPa
Step_0=0.0025; %Decimal Form of step --MUST BE DIVISIBLE BY 10, 50, 90 AND 100
D_step=Step_0;
NumSteps=(1/Step_0)+1;      %Number distillation steps taken per surrogate
%_____________________________________________________________________
%Surrogate Design Points
DesignRON(1:NumSteps)=95;      %Input Designed Octane Number
```

```
DesignMW(1:NumSteps)=94.3;      %Input Designed Molecular Weight
DesignHC(1:NumSteps)=1.801;     %Input Designed Hydrogen Carbon Ratio
%_____________________________________________________________________
%Scaling Y Axis for CPT figures (Low,High)
TBubbleAxisLow=365;          %Scaling Temperature K for Bubble Temperature Figure
TBubbleAxisHigh=385;
RONAxisLow =90;                %Scaling RON
RONAxisHigh =120;
MWAxisLow =85;                 %Scaling Molecular Weight
MWAxisHigh =105;
HCAxisLow =1.1;                %Scaling Hydrogen Carbon Ratio
HCAxisHigh=2.1;
SensitivityAxisLow =5;         %Scaling Sensitivity
SensitivityHCAxisHigh=17;
for j=1:3                      %Loop size must match the number of surrogates being compared
   RON0=DesignRON;             %Initializing Design Points
   MW0=DesignMW;
   HC0=DesignHC;
   D_step = Step_0;
   if j==1           % Recipe 1 to distill
     %Calling Files to distill first surrogate
     load('Initialize.mat'); %Recipe reset
     load('JetFuel_Figure_3Comp1.mat'); %Recipe
     D_step = Step_0;          %Passing user step size
     Pinf=Pinf_0;              %Passing user initial pressure
     run('SixComponent_VerifiedBase_Program.m');
     VolD_1=VolD; %Passing values back for figures
     T_BubbleK_1=T_BubbleK;
```

```
    LocalGasRON_1=GasRON;
    LocalGasDCN_1=GasDCN;
    LocalGasMW_1=GasMW;
    LocalGasHCRatio_1=GasHCRatio;
    LocalGasS_1=GasS;
    Di_C1=Di_C;
end
if j==2                    % Recipe 2 to distill
    load('Initialize.mat');
     load('JetFuel_Figure_3Comp2.mat');
    D_step = Step_0;
    Pinf=Pinf_0;
    run('SixComponent_VerifiedBase_Program.m');
    VolD_2=VolD;
    T_BubbleK_2=T_BubbleK;
    LocalGasRON_2=GasRON;
    LocalGasDCN_2=GasDCN;
    LocalGasMW_2=GasMW;
    LocalGasHCRatio_2=GasHCRatio;
    LocalGasS_2=GasS;
    Di_C2=Di_C;
end
if j==3                    % Recipe 3 to distill
    load('Initialize.mat');
    load('JetFuel_Figure_3Comp3.mat');
    D_step = Step_0;
    Pinf=Pinf_0;
    run('SixComponent_VerifiedBase_Program.m');
```

```
        VolD_3=VolD;
        T_BubbleK_3=T_BubbleK;
        LocalGasRON_3=GasRON;
        LocalGasDCN_3=GasDCN;
        LocalGasMW_3=GasMW;
        LocalGasHCRatio_3=GasHCRatio;
        LocalGasS_3=GasS;
        Di_C3=Di_C;
    end
end
%_____________________________________________________________________
%Post Processing Figure Creation
figure
plot(VolD_1, T_BubbleK_1, 'color',[1.0    0.40    0.00],'LineWidth',2,'MarkerSize',3);
hold on;
plot(VolD_2, T_BubbleK_2, 'color',[0.63    0.13   0.94],'LineWidth',2,'MarkerSize',3);
hold on;
plot(VolD_3, T_BubbleK_3, 'g.','LineWidth',1,'MarkerSize',3);
hold on;
    %title('Bubble Temperature');
    xlabel('Volume Distilled (%)');
    ylabel('Temperature (K)');
%     axis([0 100 TBubbleAxisLow TBubbleAxisHigh]);
%     legend('95t','95o','95f');

saveas(gcf,'JetBubbleTemperature.jpg');          %Saves figure as .jpg
hold off;
%_____________________________________________________________________
```

```
figure
plot(VolD_1, LocalGasDCN_1, 'color',[1.0    0.40    0.00],'LineWidth',2,'MarkerSize',3);
hold on;
plot(VolD_2, LocalGasDCN_2, 'color',[0.63    0.13   0.94],'LineWidth',2,'MarkerSize',3);
hold on;
plot(VolD_3, LocalGasDCN_3, 'g.','LineWidth',1,'MarkerSize',3);
hold on;
plot(VolD,DesignDCN,'k:','LineWidth',1,'MarkerSize',2);
hold on;
   %title('Local Gaseous Octane Number');
   xlabel('Volume Distilled (%)');
   ylabel('DCN');
%    axis([0 100 DCNAxisLow DCNAxisHigh]);
%    legend('95t','95o','95f', 'Target');
saveas(gcf,'JetDCN.jpg'); %Saves figure as .jpg
hold off;
%_____________________________________________________________________
figure
plot(VolD_1, LocalGasMW_1, 'color',[1.0    0.40    0.00],'LineWidth',2,'MarkerSize',3);
hold on;
plot(VolD_2, LocalGasMW_2, 'color',[0.63    0.13   0.94],'LineWidth',2,'MarkerSize',3);
hold on;
plot(VolD_3, LocalGasMW_3, 'g.','LineWidth',1,'MarkerSize',3);
hold on;
plot(VolD,DesignMW,'k:','LineWidth',1,'MarkerSize',2);
hold on;
   %title('Local Gaseous Molecular Weight');
   xlabel('Volume Distilled (%)');
```

```
   ylabel('Molecular Weight (g/mol)');
%     axis([0 100 MWAxisLow MWAxisHigh]);
%     legend('95t','95o','95f', 'Target');
saveas(gcf,'JetMolecularWeight.jpg'); %Saves figure as .jpg
hold off;
%_____________________________________________________________________
figure
plot(VolD_1, LocalGasHCRatio_1, 'color',[1.0    0.40    0.00],'LineWidth',2,'MarkerSize',3);
hold on;
plot(VolD_2, LocalGasHCRatio_2, 'color',[0.63    0.13    0.94],'LineWidth',2,'MarkerSize',3);
hold on;
plot(VolD_3, LocalGasHCRatio_3, 'g.','LineWidth',1,'MarkerSize',3);
hold on;
plot(VolD,DesignHC,'k:','LineWidth',1,'MarkerSize',2);
hold on;
   %title('Local Gaseous Hydrogen Carbon Ratio');
   xlabel('Volume Distilled (%)');
   ylabel('Hydrogen Carbon Ratio (H/C)');
%     axis([0 100 HCAxisLow HCAxisHigh]);
%     legend('95t','95o','95f', 'Target');
saveas(gcf,'JetHCRatio.jpg'); %Saves figure as .jpg
hold off;
%_____________________________________________________________________
% Converting to degrees Celsius
T_BubbleC_1=T_BubbleK_1-273.15;
T_BubbleC_2=T_BubbleK_2-273.15;
T_BubbleC_3=T_BubbleK_3-273.15;
% Writing data to excel files
```

```
xlswrite('JetResults.xls',headers,1,'B1:U1');

xlswrite('JetResults.xls',VolD_1(:),1,'B2');

xlswrite('JetResults.xls',T_BubbleK_1(:),1,'C2');

xlswrite('JetResults.xls',T_BubbleC_1(:),1,'D2');

xlswrite('JetResults.xls',LocalGasDCN_1(:),1,'E2');

xlswrite('JetResults.xls',LocalGasMW_1(:),1,'F2');

xlswrite('JetResults.xls',LocalGasHCRatio_1(:),1,'G2');

xlswrite('JetResults.xls',VolD_2(:),1,'I2');

xlswrite('JetResults.xls',T_BubbleK_2(:),1,'J2');

xlswrite('JetResults.xls',T_BubbleC_2(:),1,'K2');

xlswrite('JetResults.xls',LocalGasDCN_2(:),1,'L2');

xlswrite('JetResults.xls',LocalGasMW_2(:),1,'M2');

xlswrite('JetResults.xls',LocalGasHCRatio_2(:),1,'N2');

xlswrite('JetResults.xls',VolD_3(:),1,'P2');

xlswrite('JetResults.xls',T_BubbleK_3(:),1,'Q2');

xlswrite('JetResults.xls',T_BubbleC_3(:),1,'R2');

xlswrite('JetResults.xls',LocalGasDCN_3(:),1,'S2');

xlswrite('JetResults.xls',LocalGasMW_3(:),1,'T2');

xlswrite('JetResults.xls',LocalGasHCRatio_3(:),1,'U2');
```

A.3 Core Solver Program

Solver Program - SixComponent_VerifiedBase_Program.m

```
if n==1                %If input is only one component; cannot divide by zero on final step
   i_max= (1/D_step);
else
   i_max= (1/D_step)+1; %Number of steps stepping i by 1 indexing begins at 1, +1 for final value
end
%_____________________________________________________________________
%Initializing Arrays
D =zeros(1,i_max);
VolD=zeros(1,i_max);
%Liquid Moles In Mixture
LqMol1 = zeros(1,i_max) ;
LqMol2 =zeros(1,i_max);
LqMol3 =zeros(1,i_max);
LqMol4 =zeros(1,i_max);
LqMol5 =zeros(1,i_max);
LqMol6 =zeros(1,i_max);
LqMolSum=zeros(1,i_max);
%Liquid Mole Fraction
LqMolFract1 = zeros(1,i_max) ;
LqMolFract2 = zeros(1,i_max) ;
LqMolFract3 = zeros(1,i_max) ;
LqMolFract4 = zeros(1,i_max) ;
LqMolFract5 = zeros(1,i_max) ;
LqMolFract6 = zeros(1,i_max) ;
%Gaseous Moles around Mixture
GasMol1 = zeros(1,i_max) ;
```

```
GasMol2 =zeros(1,i_max);

GasMol3 =zeros(1,i_max);

GasMol4 =zeros(1,i_max);

GasMol5 =zeros(1,i_max);

GasMol6 =zeros(1,i_max);

GasMolSum=zeros(1,i_max);

%Gaseous Mole Fraction

GasMolFract1 = zeros(1,i_max) ;

GasMolFract2 = zeros(1,i_max) ;

GasMolFract3 = zeros(1,i_max) ;

GasMolFract4 = zeros(1,i_max) ;

GasMolFract5 = zeros(1,i_max) ;

GasMolFract6 = zeros(1,i_max) ;

%Vapor Pressure CALCULATED (kPa)

VapP1=zeros(1,i_max) ;

VapP2=zeros(1,i_max) ;

VapP3=zeros(1,i_max) ;

VapP4=zeros(1,i_max) ;

VapP5=zeros(1,i_max) ;

VapP6=zeros(1,i_max) ;

%Partial Pressure

PFract1=zeros(1,i_max) ;

PFract2=zeros(1,i_max) ;

PFract3=zeros(1,i_max) ;

PFract4=zeros(1,i_max) ;

PFract5=zeros(1,i_max) ;

PFract6=zeros(1,i_max) ;

PCheck=zeros(1,i_max) ;
```

```
%Bubble Temperature C and K
T=zeros(1,i_max);
T_BubbleK=zeros(1,i_max) ;
T_BubbleC=zeros(1,i_max) ;
%Liquid Volumes and Total(cm^3)
LqVol1=zeros(1,i_max) ;
LqVol2=zeros(1,i_max) ;
LqVol3=zeros(1,i_max) ;
LqVol4=zeros(1,i_max) ;
LqVol5=zeros(1,i_max) ;
LqVol6=zeros(1,i_max) ;
LqVolSum=zeros(1,i_max) ;
%Fractional Volumetric Components
LqVolFract1=zeros(1,i_max) ;
LqVolFract2=zeros(1,i_max) ;
LqVolFract3=zeros(1,i_max) ;
LqVolFract4=zeros(1,i_max) ;
LqVolFract5=zeros(1,i_max) ;
LqVolFract6=zeros(1,i_max) ;
%Volumetric Percentage Vaporized and Calculated Step
VolVapor = zeros(1,i_max) ;
VolVapor_step = zeros(1,i_max) ;
%CPTs
LqHCRatio=zeros(1,i_max) ;
LqMWSurrogate=zeros(1,i_max) ;
LqDCN = zeros(1,i_max) ;
LqTSI = zeros(1,i_max) ;
LqMW = zeros(1,i_max) ;
```

```
LqRON = zeros(1,i_max) ;

LqMON = zeros(1,i_max) ;

LqS = zeros(1,i_max) ;

GasHCRatio=zeros(1,i_max) ;

GasMWSurrogate=zeros(1,i_max) ;

GasDCN = zeros(1,i_max) ;

GasTSI = zeros(1,i_max) ;

GasMW = zeros(1,i_max) ;

GasRON = zeros(1,i_max) ;

GasMON = zeros(1,i_max) ;

GasS = zeros(1,i_max) ;

%Beginning Calculations

for i = 1:i_max

   D(i)=(i-1)*D_step*100;            %Current distillation percentage

   MolSum_0=LqMol1_0+LqMol2_0+LqMol3_0+LqMol4_0+LqMol5_0+LqMol6_0;  %Initial sum of
mixture Moles

   if i == 1 %Initialization Step

      LqMol1(i)=LqMol1_0;

      LqMol2(i)=LqMol2_0;

      LqMol3(i)=LqMol3_0;

      LqMol4(i)=LqMol4_0;

      LqMol5(i)=LqMol5_0;

      LqMol6(i)=LqMol6_0;

   else %After Initial Step

      LqMol1(i)=LqMol1(i-1)-((PFract1(i-1))*(D_step*MolSum_0));     %Determining remaining moles in
the liquid %by subtracting evaporated moles

      LqMol2(i)=LqMol2(i-1)-((PFract2(i-1))*(D_step*MolSum_0));

      LqMol3(i)=LqMol3(i-1)-((PFract3(i-1))*(D_step*MolSum_0));
```

```
    LqMol4(i)=LqMol4(i-1)-((PFract4(i-1))*(D_step*MolSum_0));
    LqMol5(i)=LqMol5(i-1)-((PFract5(i-1))*(D_step*MolSum_0));
    LqMol6(i)=LqMol6(i-1)-((PFract6(i-1))*(D_step*MolSum_0));
  end
        if LqMol1(i) < 0     %Ensuring values do not become negative - A smaller distillation step will
ensure %this does not occur
          LqMol1(i) = 0;
        end
        if LqMol2(i) < 0
          LqMol2(i) = 0;
        end
        if LqMol3(i) < 0
          LqMol3(i) = 0;
        end
        if LqMol4(i) < 0
          LqMol4(i) = 0;
        end
        if LqMol5(i) < 0
          LqMol5(i) = 0;
        end
        if LqMol6(i) < 0
          LqMol6(i) = 0;
        end
    LqMolSum(i)=LqMol1(i)+LqMol2(i)+LqMol3(i)+LqMol4(i)+LqMol5(i)+LqMol6(i);   %Taking the
current %Mole sum to determine mole fraction
    LqMolFract1(i) =LqMol1(i)/(LqMolSum(i));    %Determining Mole fraction
    LqMolFract2(i) =LqMol2(i)/(LqMolSum(i));
    LqMolFract3(i) =LqMol3(i)/(LqMolSum(i));
```

```
LqMolFract4(i) =LqMol4(i)/(LqMolSum(i));
LqMolFract5(i) =LqMol5(i)/(LqMolSum(i));
LqMolFract6(i) =LqMol6(i)/(LqMolSum(i));
%Using Antoine Equation :: Ln(P/P0) = A+(B/(T+C))
%P0 is the pressure the Antione is calculated at (1kPa in verification case)
%P is in [kPa], T is in [K]
syms x
%When the vapors of each component reach stoichiometry (occurs at surrounding pressure) the components %vaporize relative to their mole factions
fun = @(x)((LqMolFract1(i)*(exp((A1+(B1/(x+C1))))))+(LqMolFract2(i)*(exp((A2+(B2/(x+C2))))))+(LqMolFract3(i)*(exp((A3+(B3/(x+C3))))))+(LqMolFract4(i)*(exp((A4+(B4/(x+C4))))))+(LqMolFract5(i)*(exp((A5+(B5/(x+C5))))))+(LqMolFract6(i)*(exp((A6+(B6/(x+C6)))))))-Pinf;
T_BubbleK(i)= lsqnonlin(fun,273); %Input initial temperature here (273K)
%Vapor Pressures
VapP1(i) = exp(A1+(B1/(T_BubbleK(i)+C1))); %Calculating Vapor Pressure using Antione Equation
VapP2 (i)= exp(A2+(B2/(T_BubbleK(i)+C2)));
VapP3 (i)= exp(A3+(B3/(T_BubbleK(i)+C3)));
VapP4 (i)= exp(A4+(B4/(T_BubbleK(i)+C4)));
VapP5 (i)= exp(A5+(B5/(T_BubbleK(i)+C5)));
VapP6 (i)= exp(A6+(B6/(T_BubbleK(i)+C6)));
%Partial Pressures
PFract1 (i) = (LqMolFract1(i) * VapP1(i))/Pinf;
PFract2 (i) = (LqMolFract2(i) * VapP2(i))/Pinf;
PFract3 (i) = (LqMolFract3(i) * VapP3(i))/Pinf;
PFract4 (i) = (LqMolFract4(i) * VapP4(i))/Pinf;
PFract5 (i) = (LqMolFract5(i) * VapP5(i))/Pinf;
```

```
PFract6 (i) = (LqMolFract6(i) * VapP6(i))/Pinf;

    PCheck(i) =  PFract1 (i) +  PFract2 (i) + PFract3 (i) + PFract4 (i) + PFract5 (i) + PFract6 (i); %Should
be 1

    %Moles to Volumetric for Driveability Index

    LqVol1(i)= LqMol1(i)/MolRho1;              %Converting moles to cm^3

    LqVol2(i)= LqMol2(i)/MolRho2;

    LqVol3(i)= LqMol3(i)/MolRho3;

    LqVol4(i)= LqMol4(i)/MolRho4;

    LqVol5(i)= LqMol5(i)/MolRho5;

    LqVol6(i)= LqMol6(i)/MolRho6;

    LqVolSum_0 = LqVol1(1)+ LqVol2(1)+LqVol3(1)+LqVol4(1)+LqVol5(1)+LqVol6(1);      %Initial
Volumetric Sum

    LqVolSum(i)=LqVol1(i)+  LqVol2(i)+LqVol3(i)+LqVol4(i)+LqVol5(i)+LqVol6(i);          %Current
Volumetric Sum

    VolD(i) = (1- (LqVolSum(i)/LqVolSum_0))*100;                %Volume Distilled

    LqVolFract1(i)= LqVol1(i)/ LqVolSum(i);                %Calculating fractional volumes

    LqVolFract2(i)= LqVol2(i)/ LqVolSum(i);

    LqVolFract3(i)= LqVol3(i)/ LqVolSum(i);

    LqVolFract4(i)= LqVol4(i)/ LqVolSum(i);

    LqVolFract5(i)= LqVol5(i)/ LqVolSum(i);

    LqVolFract6(i)= LqVol6(i)/ LqVolSum(i);

%_____________________________________________________________________

%Determining Local Gas Phase Properties -- Not in a closed environment so gas does not accumulate

    GasMol1(i) = PFract1(i)*(D_step*MolSum_0);%Local Gas Phase Moles is the molar vaporization from
the %distillation step

    %Partial Pressure x moles vaporized equals local gaseous molar component

    GasMol2(i) = PFract2(i)*(D_step*MolSum_0);

    GasMol3(i) = PFract3(i)*(D_step*MolSum_0);
```

```
    GasMol4(i) = PFract4(i)*(D_step*MolSum_0);
    GasMol5(i) = PFract5(i)*(D_step*MolSum_0);
    GasMol6(i) = PFract6(i)*(D_step*MolSum_0);
    GasMolSum(i)=GasMol1(i)+GasMol2(i)+GasMol3(i)+GasMol4(i)+GasMol5(i)+GasMol6(i);
%Should be constant since we are distilling the same amount each step
    GasMolFract1(i) = GasMol1(i)/GasMolSum(i);      %Calculating Local Gas Mole Fraction
    GasMolFract2(i) = GasMol2(i)/GasMolSum(i);
    GasMolFract3(i) = GasMol3(i)/GasMolSum(i);
    GasMolFract4(i) = GasMol4(i)/GasMolSum(i);
    GasMolFract5(i) = GasMol5(i)/GasMolSum(i);
    GasMolFract6(i) = GasMol6(i)/GasMolSum(i);
%_____________________________________________________________________________
 %POST PROCESSING CPT
 %Calculating Driveability Index Variables (degC) 375 - 610 C in USA
      if VolD(i) <= 10
         T_10 = T_BubbleK(i) - 273.15;
      end
      if VolD(i) <= 50
         T_50 = T_BubbleK(i) - 273.15;
      end
       if VolD(i) <= 90
         T_90 = T_BubbleK(i) - 273.15;
       end
 %Liquid Hydrogen Carbon Ratio
    LqHCRatio(i)=((LqMolFract1(i)*H1) + (LqMolFract2(i)*H2) + (LqMolFract3(i)*H3) +
(LqMolFract4(i)*H4) + (LqMolFract5(i)*H5) + (LqMolFract6(i)*H6)) / ((LqMolFract1(i)*C12_1) +
(LqMolFract2(i)*C12_2) + (LqMolFract3(i)*C12_3) + (LqMolFract4(i)*C12_4) +
(LqMolFract5(i)*C12_5) + (LqMolFract6(i)*C12_6));
```

```
%Liquid Derived Cetane Number
    LqDCN(i) = (LqMolFract1(i)*DCN1) + (LqMolFract2(i)*DCN2) + (LqMolFract3(i)*DCN3) +
(LqMolFract4(i)*DCN4) + (LqMolFract5(i)*DCN5) + (LqMolFract6(i)*DCN6);
%Liquid Threshold Sooting Index
    LqTSI(i)= (LqMolFract1(i)*TSI1) + (LqMolFract2(i)*TSI2) + (LqMolFract3(i)*TSI3) +
(LqMolFract4(i)*TSI4) + (LqMolFract5(i)*TSI5) + (LqMolFract6(i)*TSI6);
%Liquid Molecular Weight
    LqMW(i)= (LqMolFract1(i)*MW1) + (LqMolFract2(i)*MW2) + (LqMolFract3(i)*MW3) +
(LqMolFract4(i)*MW4) + (LqMolFract5(i)*MW5) + (LqMolFract6(i)*MW6);
 %Liquid RON
    LqRON(i)= (LqMolFract1(i)*RON1) + (LqMolFract2(i)*RON2) + (LqMolFract3(i)*RON3) +
(LqMolFract4(i)*RON4) + (LqMolFract5(i)*RON5) + (LqMolFract6(i)*RON6);
 %Liquid MON
    LqMON(i)= (LqMolFract1(i)*MON1) + (LqMolFract2(i)*MON2) + (LqMolFract3(i)*MON3) +
(LqMolFract4(i)*MON4) + (LqMolFract5(i)*MON5) + (LqMolFract6(i)*MON6);
 %Liquid Sensetivity
    LqS(i)=LqRON(i)-LqMON(i);
%_____
%Gaseous CPTs
%Gaseous Hydrogen Carbon Ratio
    GasHCRatio(i)=((GasMolFract1(i)*H1) + (GasMolFract2(i)*H2) + (GasMolFract3(i)*H3) +
(GasMolFract4(i)*H4) + (GasMolFract5(i)*H5) + (GasMolFract6(i)*H6)) / ((GasMolFract1(i)*C12_1) +
(GasMolFract2(i)*C12_2) + (GasMolFract3(i)*C12_3) + (GasMolFract4(i)*C12_4) +
(GasMolFract5(i)*C12_5) + (GasMolFract6(i)*C12_6));
%Gaseous Derived Cetane Number
    GasDCN(i) = (GasMolFract1(i)*DCN1) + (GasMolFract2(i)*DCN2) + (GasMolFract3(i)*DCN3) +
(GasMolFract4(i)*DCN4) + (GasMolFract5(i)*DCN5) + (GasMolFract6(i)*DCN6);
%Gaseous Threshold Sooting Index
```

```
    GasTSI(i)=    (GasMolFract1(i)*TSI1) + (GasMolFract2(i)*TSI2) + (GasMolFract3(i)*TSI3) +
(GasMolFract4(i)*TSI4) + (GasMolFract5(i)*TSI5) + (GasMolFract6(i)*TSI6);
%Gaseous Molecular Weight
    GasMW(i)=    (GasMolFract1(i)*MW1) + (GasMolFract2(i)*MW2) + (GasMolFract3(i)*MW3) +
(GasMolFract4(i)*MW4) + (GasMolFract5(i)*MW5) + (GasMolFract6(i)*MW6);
%Gaseous RON
    GasRON(i)=   (GasMolFract1(i)*RON1) + (GasMolFract2(i)*RON2) + (GasMolFract3(i)*RON3) +
(GasMolFract4(i)*RON4) + (GasMolFract5(i)*RON5) + (GasMolFract6(i)*RON6);
%Gaseous MON
    GasMON(i)=  (GasMolFract1(i)*MON1) + (GasMolFract2(i)*MON2) + (GasMolFract3(i)*MON3) +
(GasMolFract4(i)*MON4) + (GasMolFract5(i)*MON5) + (GasMolFract6(i)*MON6);
%Gaseous Sensetivity
    GasS(i)=GasRON(i)-GasMON(i);
End
%Calculating Driveability Index
Di_C = (1.5*T_10) + (3*T_50) + (T_90) + (1.33*(LqVolFract6(1)));
```

A.4 Sample Recipe mat file

```
%   User Inputs
%_____________________________________________________________________
%ANTIONE NUMBERS AT 1kPa (P0) TEST VALUE
%Number of species
n=1;
%Initial Liquid Moles of n mole composition
LqMol1_0=0.3;          %1,3,5 Trimethylbenzene
LqMol2_0=0.210;          %iC8 isoOctane
LqMol3_0=0.0;            %nC16 HexaDecane
LqMol4_0=0.49;           %nC12 Dodecane
LqMol5_0=0;            %iC12 isododecane
LqMol6_0=0;
%Antoine Numbers - Fuel Specific
A1= 14.9638 ;          %1,3,5 Trimethylbenzene
B1=-4138.45 ;
C1= -39.8902;
%____________
A2=14.1369;            %iC8 isoOctane
B2=-3170.32;
C2=-39.9794;
%____________
A3=14.7458;            %nC16 HexaDecane
B3=-4683.22;
C3=-97.9643;
%____________
A4=14.5228;            %nC12 Dodecane
B4=-4087.79;
```

```
C4=-77.1903;
%_____________
A5=14.0003;                %iC12 isododecane
B5=-3699.44;
C5=-57.2923;
%_____________
A6=1;
B6=1;
C6=1;
%Number Of Hydrogen and Carbon in each species
C12_1=9;
H1=12;
%_________
C12_2=8;
H2=18;
%_________
C12_3=16;
H3=34;
%_________
C12_4=12;
H4=26;
%_________
C12_5=12;
H5=26;
%_________
C12_6=1;
H6=1;
%DERIVED CETANE NUMBERS
```

```
DCN1=8;

DCN2=18;

DCN3=100;

DCN4=78;

DCN5=16.8;

DCN6=1;

%THRESHOLD SOOTING INDEX

TSI1=1;

TSI2=1;

TSI3=1;

TSI4=1;

TSI5=1;

TSI6=1;

%Liquid Mass Density (g/cm^3)

LqRho1=0.001*864;

LqRho2=0.001*690;

LqRho3=0.001*770;

LqRho4=0.001*750;

LqRho5=0.001*750;

LqRho6=0.001;

%Molecular Weight (g/mol)

MW1=12*C12_1 + H1;

MW2=12*C12_2 + H2;

MW3=12*C12_3 + H3;

MW4=12*C12_4 + H4;

MW5=12*C12_5 + H5;

MW6=12*C12_6 + H6;

%Research Octane Number
```

```
RON1=106;
RON2=100;
RON3=83;
RON4=120;
RON5=83.9;
RON6=130;
%Motor Octane Number
MON1=0;
MON2=100;
MON3=77.2;
MON4=103.5;
MON5=63;
MON6=103;
%Liquid Molar Density (mol/cm^3)
MolRho1=LqRho1/MW1;
MolRho2=LqRho2/MW2;
MolRho3=LqRho3/MW3;
MolRho4=LqRho4/MW4;
MolRho5=LqRho5/MW5;
MolRho6=LqRho6/MW6;
%_____%Save as
mat file to call in program
save('JetFuel_Figure_3Comp1.mat');
```

A.5 Initialize program

```
%Resetting all input values
LqMol1_0=0;
LqMol2_0=0;
LqMol3_0=0;
LqMol4_0=0;
LqMol5_0=0;
LqMol6_0=0;
A1=0;
B1=0;
C1=0;
%_____________
A2=0;
B2=0;
C2=0;
%_____________
A3=0;
B3=0;
C3=0;
%_____________
A4=0;
B4=0;
C4=0;
%_____________
A5= 0 ;
B5=0;
C5= 0;
%_____________
```

```
A6=0;
B6=0;
C6=0;
C12_1=0;
H1=0;
%_________
C12_2=0;
H2=0;
%_________
C12_3=0;
H3=0;
%_________
C12_4=0;
H4=0;
%_________
C12_5=0;
H5=0;
%_________
C12_6=0;
H6=0;
%DERIVED CETANE NUMBERS
DCN1=0;
DCN2=0;
DCN3=0;
DCN4=0;
DCN5=0;
DCN6=0;
%THRESHOLD SOOTING INDEX
```

```
TSI1=0;

TSI2=0;

TSI3=0;

TSI4=0;

TSI5=0;

TSI6=0;

%Liquid Mass Density (g/cm^3)

LqRho1=0;

LqRho2=0;

LqRho3=0;

LqRho4=0;

LqRho5=0;

LqRho6=0;

%Molecular Weight (g/mol)

MW1=0;

MW2=0;

MW3=0;

MW4=0;

MW5=0;

MW6=0;

%Research Octane Number

RON1=0;

RON2=0;

RON3=0;

RON4=0;

RON5=0;

RON6=0;

%Motor Octane Number
```

```
MON1=0;

MON2=0;

MON3=0;

MON4=0;

MON5=0;

MON6=0;

%_____%Save as

mat file to call in program

save('Initialize.mat')
```

Appendix B

Component Properties

Component Properties

Fuel	MW (g/mol)	H/C	(D)CN		RON	NBP (K)	ρ (kg/m^3)	μ × 10^4 (Pa.s)	σ × 10^2 (N/m)	A	B	C	Validity Range (K)	T_{crit} (K)
n-heptane (nC7)	100.20	2.29	53.8	0		371.5 +/- 0.3	680.00	4.14	2.03	14.17	-3086.40	-48.51	210-540	540.00
n-octane (nC8)	114.20	2.25	58.2			398.7 +/- 0.5	698.00	5.1	2.12	14.208	-3291.44	-55.7293	238-568	568
n-decane (nC10)	142.30	2.20	65.5			447.2 +/- 0.6	726.00	8.51	2.34	14.40	-3734.48	-65.86	243-618	617.00
n-dodecane (nC12)	170.30	2.17	78.0			489 +/- 2	745.00	13.54	2.48	14.52	-4087.79	-77.19	263-658	658.00
n-hexadecane (nC16)	226.40	2.13	100.0			554 +/- 10	770.00	31.00	2.72	14.75	-4683.22	-97.96	291-722	722.00
Toluene	92.10	1.14	0.2		120	383.8 +/- 0.2	862.00	5.58	2.79	14.42	-3364.40	-41.46	178-591	593.00
1,3,5-Trimethylbenzene (135 TMB)	120.20	1.34	8.0			437.8 +/- 0.8	861.00	6.00	2.82	14.96	-4138.45	-38.89	221-637	639.00
Ethanol	46.10	3.00	2.2		108	351.5 +/- 0.2	786.00	10.90	2.19	16.72	-3756.75	-41.54	208-514	516.00
iso-octane (iC8)	114.20	2.25	18.0		100	372.4 +/- 0.2	688.00	4.79	1.84	14.14	-3170.32	-39.98	165-543	543.00
iso-cetane (iC16)	226.45	2.13	15.0			513.2	793.00	30.00	2.34	14.79	-4669.14	-61.7704	210-691	692.00
Trans-decalin	138.25	1.80	32.0			460.41	870.00	19.31	2.94	14.16	-3889.51	-53.19	242-687	687.00
Cis-decalin	138.25	1.80	41.6			468.97	897.00	30.00	3.16	13.97	-3793.92	-63.7004	288-702	704.00

Appendix C

Burner Rig Design Progression

C.1 Flame impingement test

- Conducted to determine quartz chimney diameter in order to avoid flame impingement on the side walls.
- Evaluated with an open-air burn test using a 0.5 GPH hollow cone atomizing spray nozzle and adaptor seen in Figure C1 below

Figure C1

0.5 GPH hollow cone atomizing spray nozzle and adaptor

Figure C1. Stainless Steel spray nozzle to ¼” compression tube adaptor.

- Adaptor allows the UNEF nozzle thread to be translated to 1/4" compression tube fittings.
- Adaptor had to be of sufficient length the house the 1/4" NPT thread depth, nozzle threads, and integrated pressed brass fuel filter.

- Adaptor design was used throughout design iterations until it was discovered that the stainless steel was the cause of fuel leakage. The stainless steel was too hard to allow for a proper face seal against the brass nozzle.

- With some additional structure and delivering 100 psig to the fuel system, the test was conducted. Figure C2 shows this preliminary test in progress.

Figure C2

Open-air flame impingement test.

- The results of flame impingement test indicate that a diameter of five inches or greater would provide sufficient room for the flame to burn freely without wall interaction.
- This test also provided valuable lessons:
    - It was evident that we could not stop fuel flow with this setup. Closing the air delivery value did not stop fuel flow. The tank would remain pressurized and fuel would continue to flow until enough fuel was expelled to reduce internal pressure.
        - An air depressurization valve was added to rapidly depressurize the line and immediately stop fuel flow.
    - The fume hood proved inadequate to handle sooty fuels.
        - Particularly sooty fuel such as aromatics will be avoided.
- Lessons learned in this initial experiment provided sufficient knowledge to draft and fabricate a first iteration of the spray burner rig for evaluation; the “Mark 1”.

C.2 Mark 1

- The Mark 1 burner fulfills design criteria, specifically, the ability for easy disassembly and interchangeability.
- This platform is a highly versatile experiment capable of accommodating liftoff and blowout tests. Figure C3 panels (a), (b), and (c) depict the exploded view of the intended final design, the exploded view of the manufactured components and a fully assembled rendering of the manufactured burner respectively.

Figure C3

(a) Exploded view of the original configuration of the Haas Burner Rig, all components are 316 stainless steel with a smooth finish. Not pictured: Quartz outer shell which will sit between 3 and 14. (b) The current configuration of the Haas Burner Rig used for experimental data. Components: Inlet, objects 1, 2, 3, 4, 5, 6, 7, 9, 10, 11, 15, and 16. Objects removed from the original are objects 12, 13, 14 due to specifications needed from further. (c) fully assembled rendering of the manufactured rig.

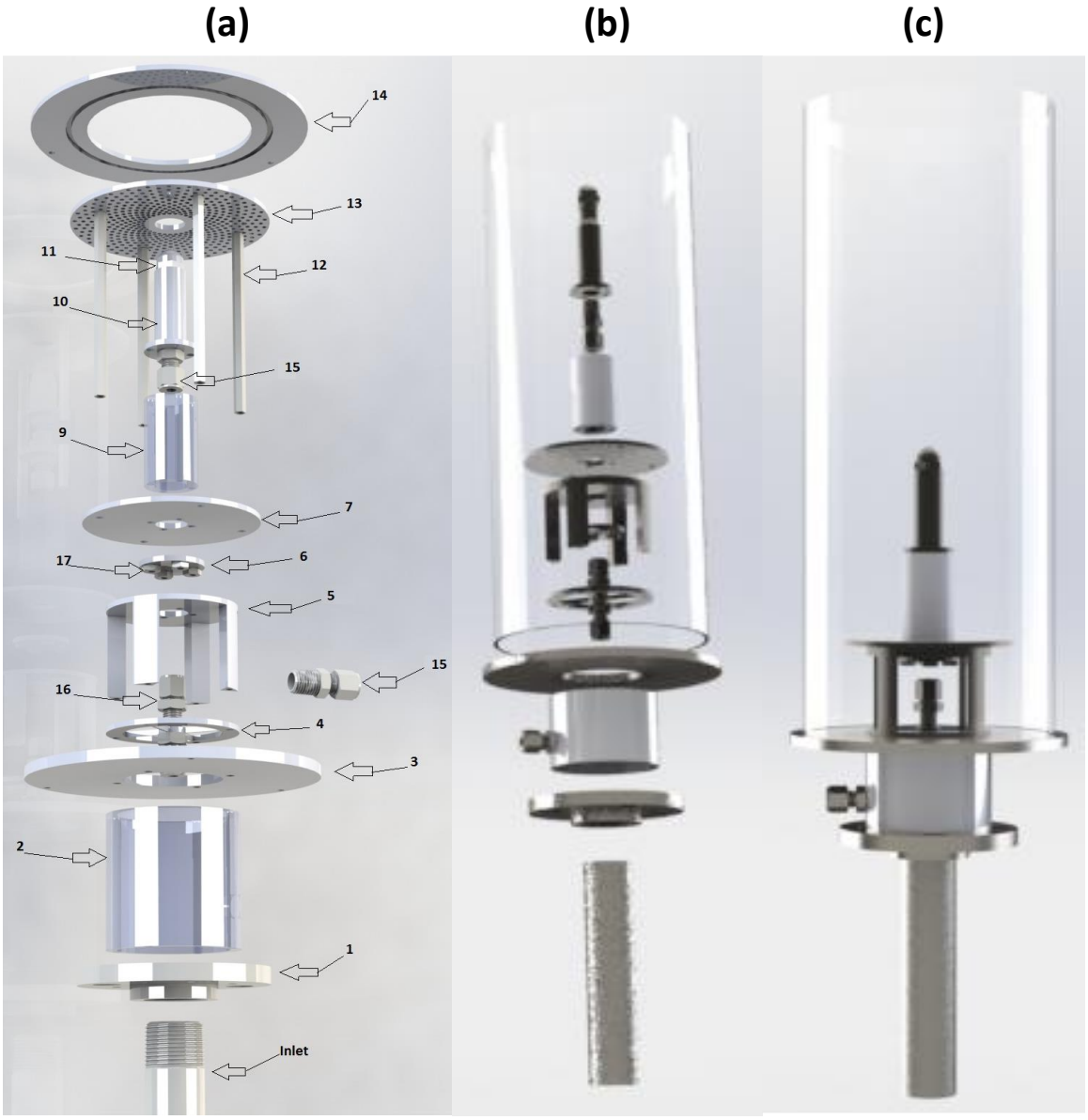

- The overall height of the rig is 21.5 inches and the overall diameter is 6 inches. The following objects correspond to those listed in Figure C3 along with a brief design rational.
    - Object 1: 1 inch NPT flange provides a plug-in for the inlet pipe to supply air to the system.
    - Object 2: The flange standoff creates space for the fuel system components, additionally this section can be filled with porous material such as steel wool to condition the inlet co-flow air.
    - Object 3: The mounting plate provides mounting hard points for the majority of the burner rig components. The stainless steel chimney sits centered on top of it with a 1/8" groove machined for the future quartz chimney to sit in.
    - Object 4: The bulkhead adaptor allows object 16 (bulkhead straight union compression fitting) to mount onto it. This bulkhead adaptor provides a point of stability for the fuel system as well as enables the rig to be disassembled.
    - Object 5: The distributor plate standoff with cutouts allows for wrench access to object 16 for disassembly as well as mounting points for the upper assembly and a pathway for the co-flow air. The four milled cutouts allow air to flow uniformly through the structure while still providing robust structure and wrench access.
    - Object 6: The cutout adaptor seals air out of internal fuel line cavities and allows disassembly.

- Object 7: The distributor plate. Designed to distribute and normalize the air after it interacts with object 5. This distributor is a design point of interest so it can be easily modified to change the flow behavior.
- Object 8: Fuel storage tank; not pictured.
- Object 9: The union standoff, this object allows control over the location of the spray nozzle (11).
- Object 10: The fuel hose union. Serves as an adaptor so the fuel system (15) can connect to the spray nozzle (11). The four holes along the diameter serve as endpoints for the upper assembly mounting hardware.
- Object 11: Delavan spray nozzle delivers fuel to the combustion chamber.
- Object 12: Support for co-flow disruptor plate.
- Object 13: Co-flow disruptor plate to condition air.
- Object 14: Top plate to secure quartz chimney.
- Object 15: YorLok compression tube fitting 1/4" tube to 1/4" NPT male (x2).
- Object 16: YorLok Through-wall bulkhead compression tube fitting. Essential for connecting the rig to the fuel system, this component is key for rig disassembly.

- This experimental platform performs all the design criteria and will be used to determine the final design component specifications such as the quartz tube height, flow straighter need and design, and various co-flow blower options.

C.3 Mark 1 Heat Gun Test

- The tests performed with the Mark 1 heat gun configuration provided insight into:
    - Necessary quartz chimney height to contain the majority of the flame.
    - Fume hood suitability for burn experiments.
    - Necessary blower power and co-flow heating feasibility.
- Setup:
    - Two-speed heat gun for preheated co-flow delivery to provide insight on:
        - Physical representation on how much airflow may be needed to blowout a flame.
        - Feasibility of heating the co-flow air to create an environment more similar to a jet engine combustor.
    - 0.5 GPH type A atomizing spray nozzle supplied with 100 psig
    - Pressure relief valve to enable rapid depressurization of the fuel lines to stop fuel flow into the combustion chamber.
- To accommodate this setup, some superficial structure was created out of aluminum extrusions. This rig configuration is presented in Figure C4.

Figure C4

Mark 1 heat gun test configuration with and without chimney. Note that objects 4 and 16 are not pictured although they are used during the test.

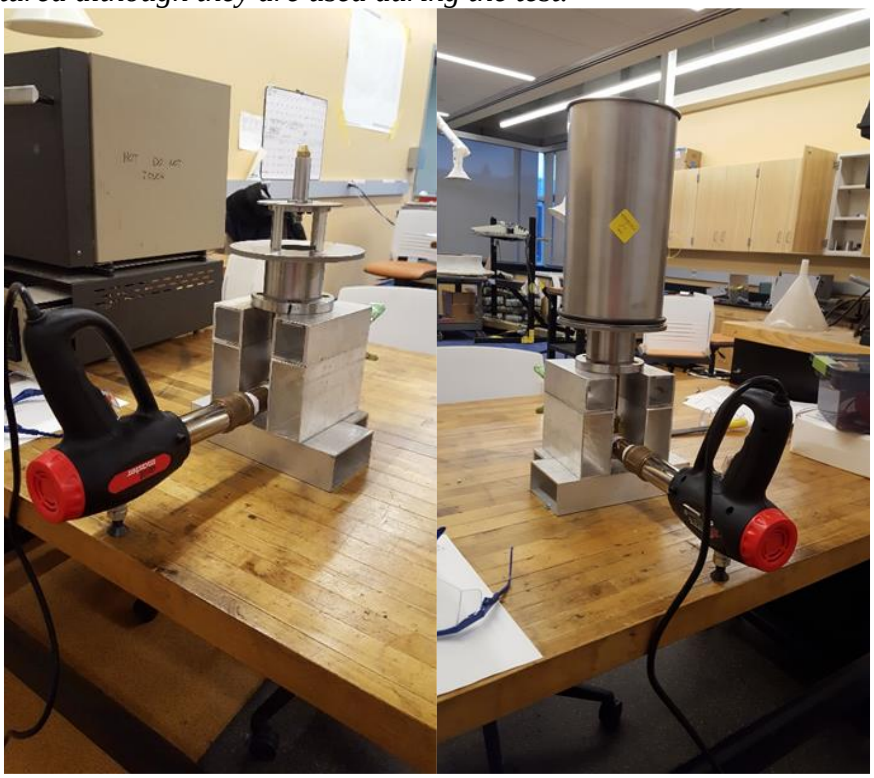

- To further verify no flame impingement on the sidewalls, a mirror was setup to allow visual access to the fuel nozzle and flame. The full running experiment can be seen in Figure C5.

Figure C5

(a) Heat gun test overview. (b) View of the mirror setup and combustion chamber interior. (c) Full length view of flame height.

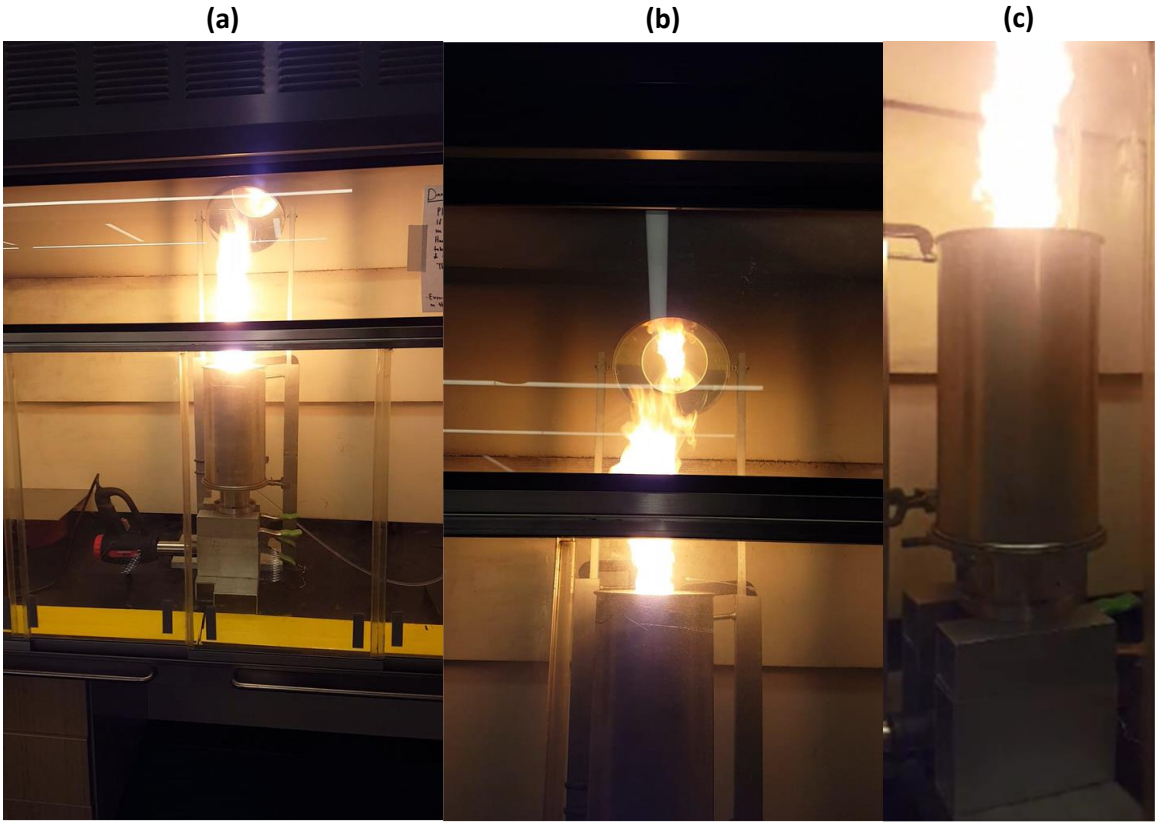

- Panel (a): an overview of the experimental setup, illustrated are the heat gun, fuel line, stainless steel chimney, and mirror.
- Panel (b): The interior of the combustion chamber, we observe that no flame impingement is visible, indicating that our chimney diameter of 5.7 inches is adequate.
- Panel (c): an approximation of how high the flame protrudes from the combustion chamber. The stainless steel chimney is 18 inches, this test displayed that at least

24 inches of chimney is necessary to contain most of the flame, providing the final dimension necessary to order the quartz chimney.

- Key pieces of data from this experiment:
    - The fume hood is hopelessly inadequate. The roof was badly scorched and the internal light was melted and warped; no longer would a standard fume hood be used in experiments.
    - Not surprisingly, the heat gun could not provide adequate flow rates to blowout the flame. It did however give an idea of required flow rates. Stoichiometric flowrate was calculated to be around 13 CFM (depending on fuel) which is close to the heat gun at full speed so a blowout was not expected. This experiment did give an idea of how much 13 CFM actually is (as opposed to some arbitrary number) and the effect it had on the flame.
        - The flame contracted at stoichiometric flow rates, further instilling confidence that the flame would not impinge on the sidewall.
    - This experiment displayed that far more than stoichiometric flow was necessary, further, initial heat input calculations performed near stoichiometric two items became clear.
        - Calculations indicated that at the increased air flow rates, significant heat was necessary to maintain a constant co-flow temperature. This would likely require an expensive heating system and a dedicated 220V power line. This additional complexity did not fit in the timeline of this study.

        - It became clear that maintaining a constant temperature would require significant PID control and time to match heat input to the incrementally increasing flow rates required for the blowout experiment. Compounding this, inconsistent heating of the co-flow air would affect mass air flow by the nozzle due to air expansion making consistent blowout measurements infeasible.
            - These factors indicated that in the timeframe of this study, heating the co-flow was not a reasonable design goal and was abandoned.
- This experiment provided the majority of the information needed for a final design, the only components left to determine were the co-flow blower and an adequate location to perform burn tests.

C.4 Mark 1 b Mobile Platform

- Throughout initial experiments, it became increasingly clear that due to facility limitations a stationary rig would create significant hardship. Thus, the burner rig was modified to the Mark 1 b mobile platform.
- The goal of this modification was to ensure the burner could be run anywhere an electrical outlet was available.
    - The rig was modified to fit onto a rolling cart.
    - Fuel pressure supply was adapted from shop air to a dolly mounted dual regulated high pressure air tank.

- A fully intact oil home heating furnace was acquired from storage. This particular furnace was designed specifically to run off the Delavan 0.5 GPH type A nozzle we had been experimenting with.
    - Being that this blower assembly was specifically designed for use with our nozzle it seemed to be the next logical progression in design iteration.
        - In order to use the blower outside of the furnace heat exchanger assembly, significant modifications were required to bypass built-in safety systems to achieve open-air operation.
            - Thermostat, heat exchanger temperature gauge, and light sensor had to be mimicked to make the system believe it was under normal operating conditions.
            - Failing to correctly input signals with the proper timing would result in complete burner lockout requiring a time-delayed reset.
                - Bypassing these signals was achieved by replacing hardware with simple switches, and the timing was determined via trial and error.
- The fully assembled Mark 1 b can be seen in Figure C6.

Figure C6

(a) Mark 1 b mobile platform. (b) Mark 1 b mobile platform during a burn test.

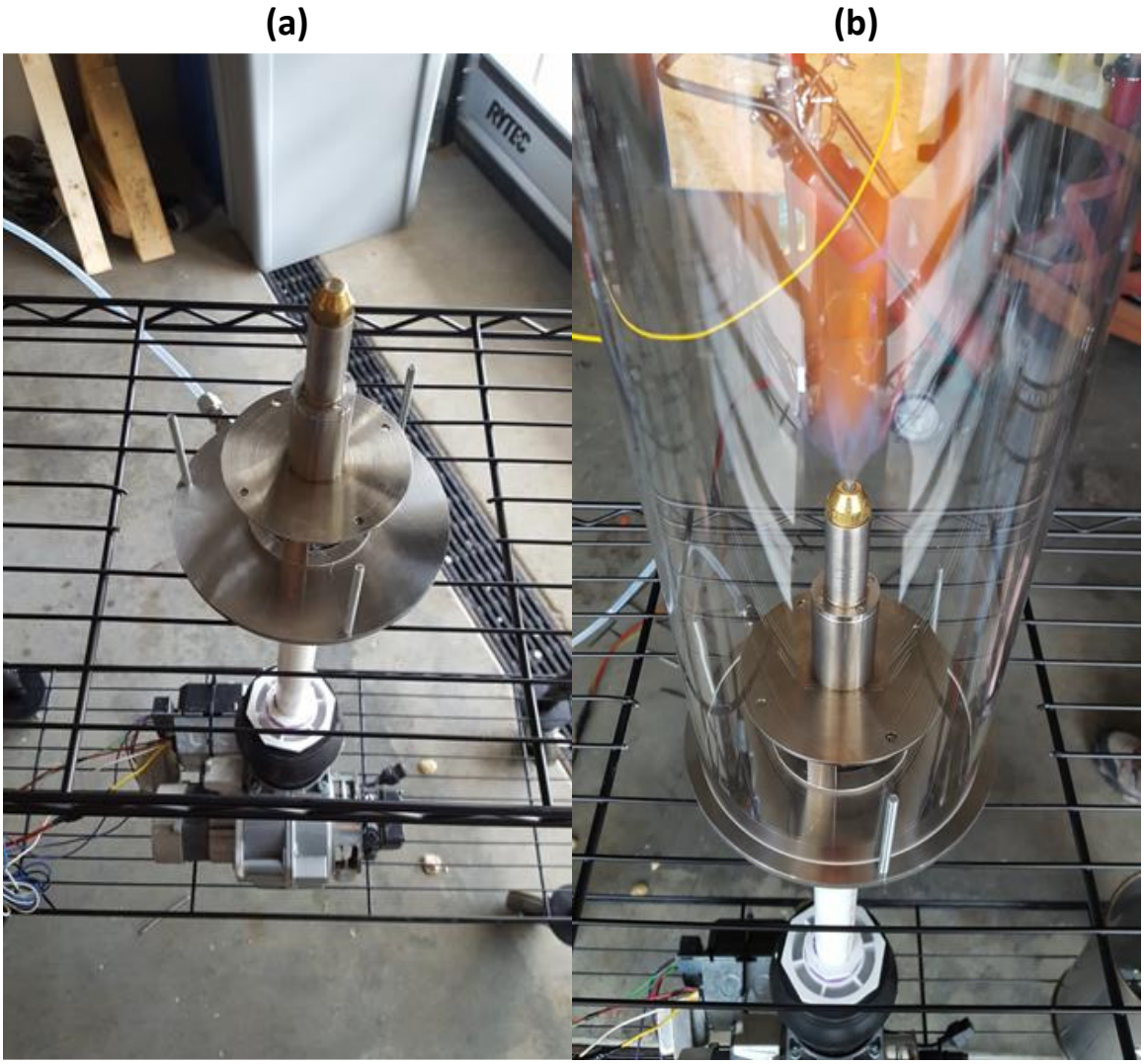

- Oil furnace blower located on the bottom shelf of the cart with co-flow air fed via PVC piping to the combustion chamber.
    - The oil furnace blower is equipped with a mechanical gear pump to pressurize the fuel line.

        - The use of this pump was investigated and it was determined unsatisfactory.
            - The gear pump was designed for use with fuel oil which serves as a lubricant, the intended fuels for this study tend to be solvents and their use deteriorated the gear pump seals as well as the O-rings on the built-in solenoid.
- Blower was designed for stoichiometric use with a 0.5 GPH nozzle, but the blower itself is a universal model capable of use with nozzle flow rates up to 3.0 GPH with air flowrate tuned via inlet vents.
    - For the designed No. 2 fuel oil, the blower at full tilt should be capable of 80 CFM giving our 0.5 GPH flame a stoichiometric ratio of about 0.15.
    - Although, for the blowout test we are consider air velocity to be the primary driver, this stoichiometric gauging should give us some idea of the flow rates necessary to blowout the flame even if it is not a direct correlation.
- Figure C6 (b) displays an active burn test in the open-air automotive bay of Rowan University using a 0.5 GPH type A spray nozzle.
    - Previous to this space, some testing was performed outdoors which was deemed inadequate due to changing atmospheric conditions and wind factors which produced undesirable effects, such as flame flashback into the combustion chamber.
    - The automotive bay testing revealed that the 80 CFM was inadequate to blowout the flame and a larger blower was necessary.

- Conveniently, the furnace came equipped with a second much larger blower designed to blow air over the heat exchanger in order to supply the home ventilation system with heated, unvitiated air. This 1/3 horsepower blower at full power can deliver 1,412 CFM at atmospheric conditions.
    - Unfortunately, this blower did not work out as expected for two reasons.
        - The pressure drop to the rig's 1" inlet proved more than the blower could handle. Connecting this blower to the rig in a similar fashion seem in Figure C6 resulted in a complete flow reversal, even implementing increasingly smooth transitions to the 1" inlet did not remedy the flow reversal issue.
        - The blower has four preset speeds, which we believed would enable variable speed control by adjusting inlet power supply but this was not the case. This blower operates via separate coils to give the different speeds. In order to vary the speed of an AC motor, complex signal alteration was necessary and can only be achieved with high powered and expensive electrical equipment.
- The next design iteration solves these problems by implementing a larger diameter co-flow inlet in order to avoid expensive blowers which can handle large pressure drops.

- The Mark 1 design provided invaluable information which led us to the final design iteration– the Mark II.

C.5 Mark II prototype

- Based off the experimental findings discovered using the Mark 1 apparatus, the Mark II prototype was designed. The Mark II prototype was designed to:
    - Allow for the largest possible inlet diameter to eliminate any back pressure issues allotting the use of a large variety of economically priced blowers.
        - To achieve this, a size 5 steel duct flange was incorporated. This flange was the largest possible option of standard size which is compatible with the 5.7" diameter quartz chimney.
    - Accommodate a new variable speed blower. While there are many options for laboratory grade blowers which accept conditioned 4-20 mA or 0-10 VDC input signals, they are prohibitively expensive. Keeping price and functionality in mind the WORX WG520 variable speed blower ($60.00) was chosen.
        - This blower is traditionally used for leaf blowing, but by modifying the speed controller from a simple potentiometer to a Tenma 72-7270 ($53.20) 1% accuracy decade box enabled precise control over the airflow rate of the blower where decreasing resistance output from the decade box increases blower power and vice versa.
- Integrating these components and some necessary ductwork the Mark II prototype was constructed, the fully assembled rig can be seen in Figure C7 (a) and (b).

Figure C7

(a) Full view of the Mark II prototype. (b) Top view of the Mark II prototype and decade box controller.

- The Mark II prototype is a crude precursor for future versions. The unrefined nature of this design iteration is due to summer renovations of the Rowan University machine shop. Nonetheless, this design serves as a base for the final designs.
    - One design flaw that does persist throughout design iterations is a slight increase in disassembly difficultly. The six mounting bolts have to be removed to access the fuel system.
- This base design fulfills all initial criteria and serves as the platform for the first blowout tests performed.
    - The WORX blower was adequate to blowout various fuels.
        - Blowout values could be differentiated between different test fuels.
- Some flaw addressed in future iterations:
    - Mounting the blower directly to the cart created significant vibrations making liftoff measurements impossible due so camera shake.
        - Various steps were taken to mitigate this vibration such as rubber dampers and counterweights to no avail.
    - Light reflecting off the quartz made it difficult to pick up less sooty fuels such as alcohol creating problems in detecting liftoff and blowout on optical equipment.
    - Time to refuel the system.
        - The small fuel inlet diameter restricted air from leaving the system. This caused refueling to take a considerable amount of time.
- Through modifying and refining this rig, the final version of the Mark II was developed and used to gather blowout data.

C.6 Mark II fume hood modification:

Figure C8

Mark II rig fume hood modification, front and back views. The front has doors that open, close, and seal.

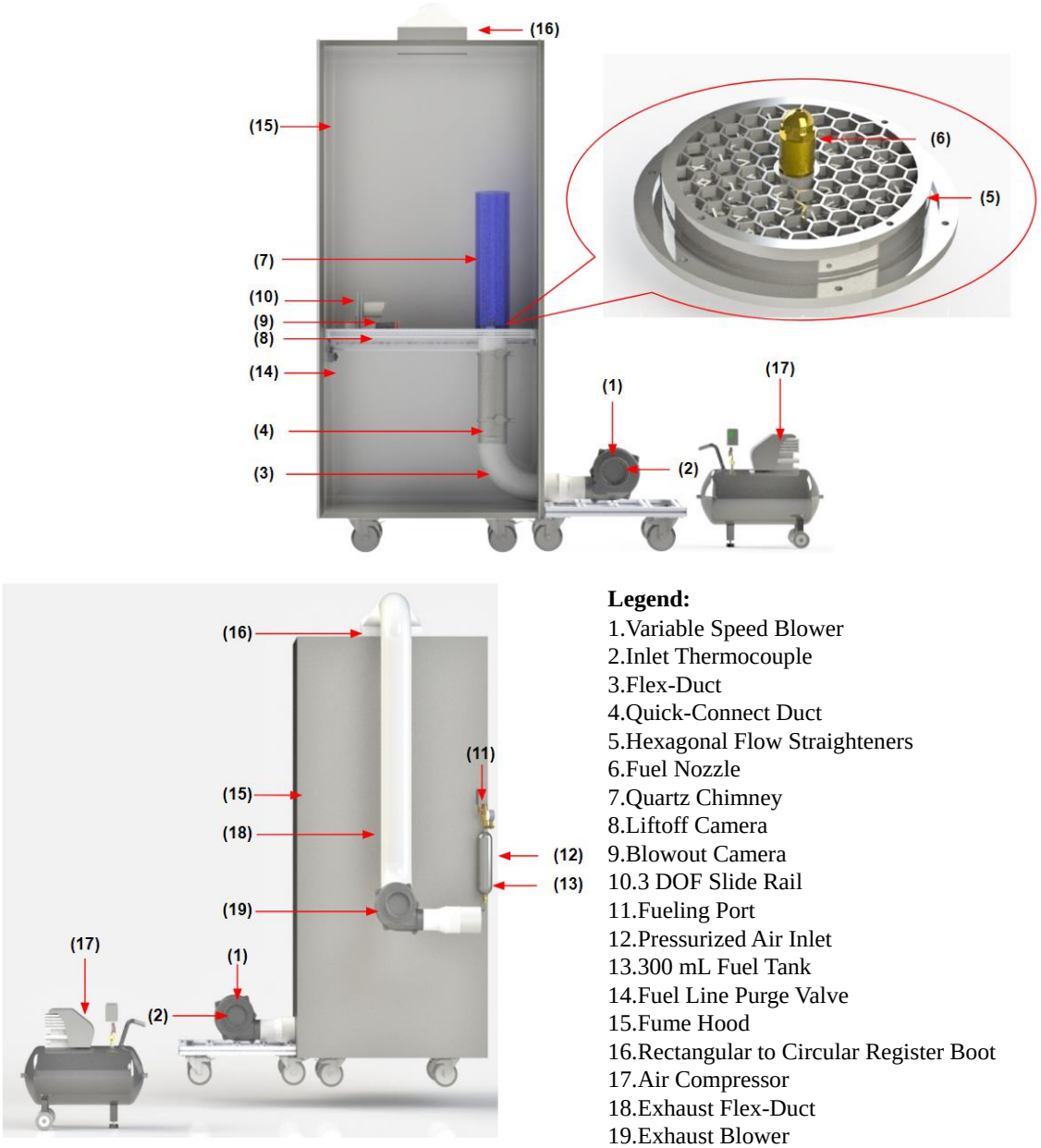

Legend:

1.Variable Speed Blower
2.Inlet Thermocouple
3.Flex-Duct
4.Quick-Connect Duct
5.Hexagonal Flow Straighteners
6.Fuel Nozzle
7.Quartz Chimney
8.Liftoff Camera
9.Blowout Camera
10.3 DOF Slide Rail
11.Fueling Port
12.Pressurized Air Inlet
13.300 mL Fuel Tank
14.Fuel Line Purge Valve
15.Fume Hood
16.Rectangular to Circular Register Boot
17.Air Compressor
18.Exhaust Flex-Duct
19.Exhaust Blower

Appendix D

Anemometer Correlation

D.1 0.5 GPH Correlation

Figure D1

Measured air velocity versus electrical resistance applied to blower (via decade box) adjusted for diameter difference between quartz combustion chamber and Anemometer. The blower performs more consistently at higher velocities.

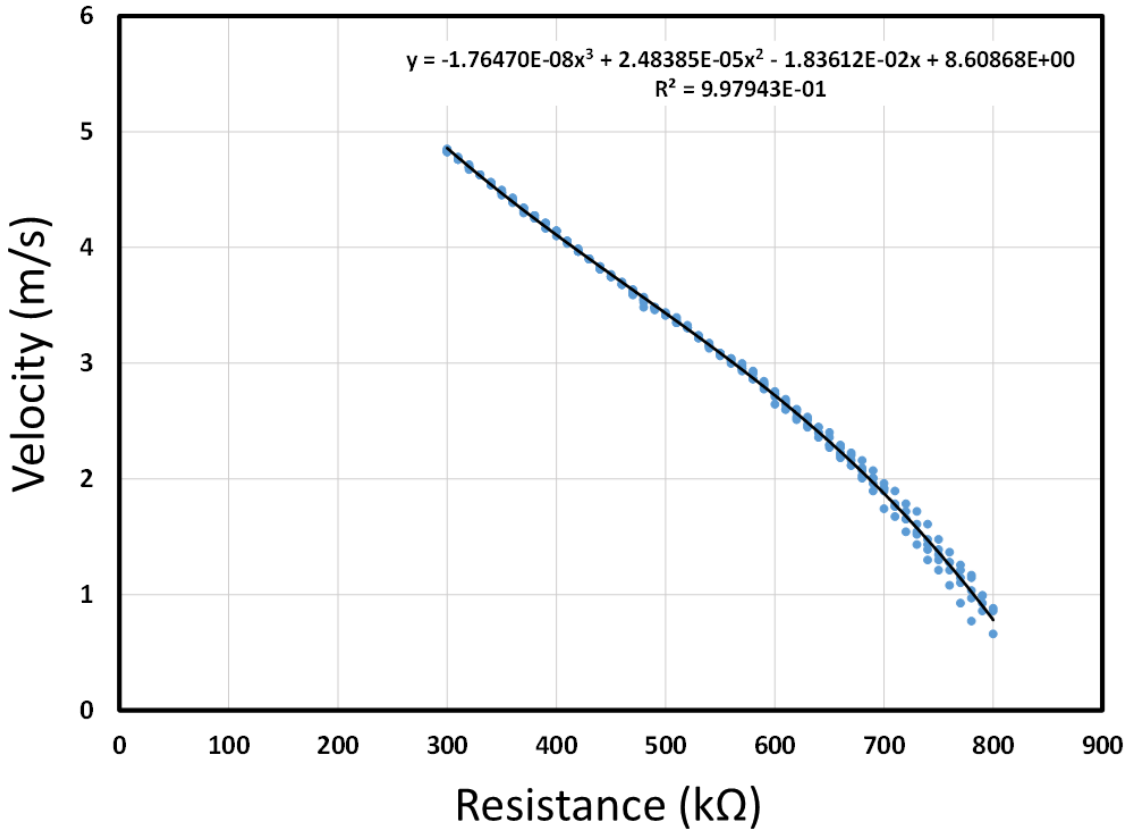

Appendix E

Liftoff Experiment

E.1 Liftoff Test

Liftoff height is of particular interest for direct injection applications such as jet and diesel engines because of its influence on combustion characteristics and emission formation. The liftoff height is defined as the distance from the injection nozzle to the stabilized flame front and can vary depending on combustion conditions and fuel properties [55, 56, 57]. The liftoff height is dependent on numerous factors such as fuel volatility, reactivity (DCN/RON), molecular weight, nozzle geometry, fuel pressure, surface tension, combustion chamber temperature, LHV, H/C etc. [55, 56, 57]. This test suits our experimental requirements well because it is dependent on numerous fuel characteristics, and reliant on an atomized fuel spray, thus, its distillation characteristics. This metric can also be easily measured with our optical equipment with the application of calibrated software. Considering these factors, the liftoff heights of complimentary surrogate sets should be identical, any variation between them could indicate non-conformity amongst "equivalent" fuels. Capturing the liftoff height on film is a rather straightforward process involving a camera and recording equipment, as seen in Figure E1.

Figure E1

Flame front image capture.

The nuance and difficulty with this test comes in the post processing and measurement of the liftoff height. To do this, a custom Matlab program was created to analyze, identify, and measure the flame front in each frame of data. The full computational process is seen in Figure E2.

Figure E2

Liftoff height determination post processing progression with minimum filter.

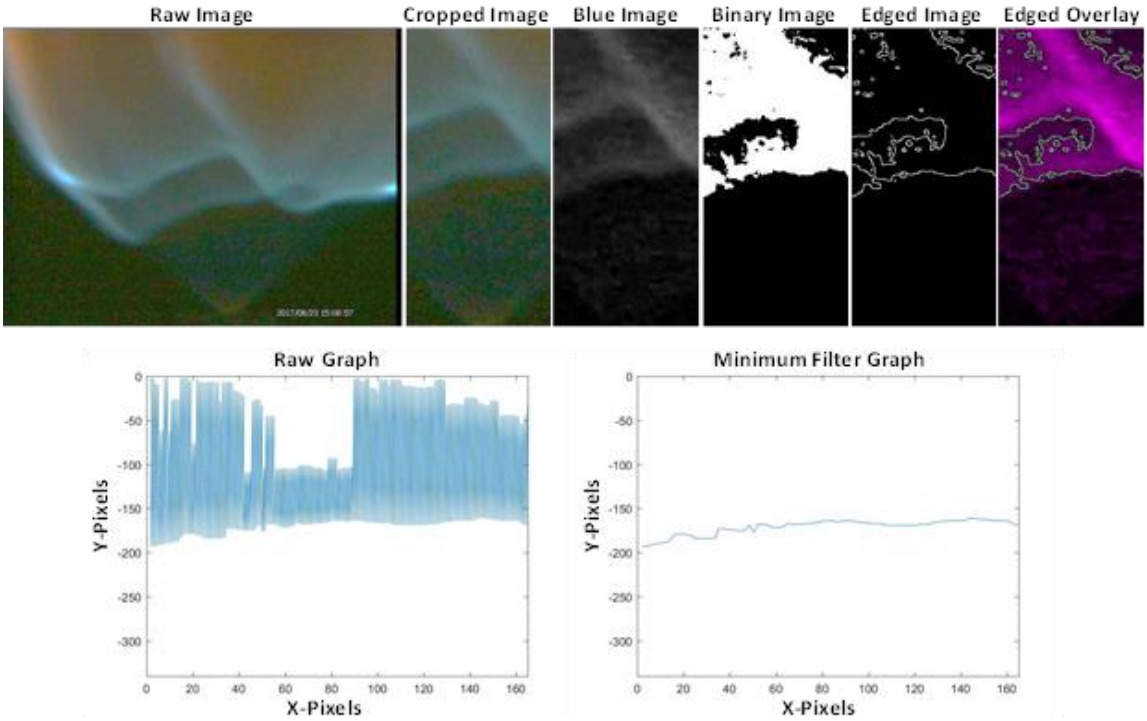

To accurately find the edge, regardless of flame shape or height, numerous manipulations of the image had to be performed. To narrow the sheer amount of data, we first crop the picture. This eliminates the edges of the flame where the front and back of the flame front overlap due to the conical flame shape an atomized spray nozzle produces. Next, the blue spectrum of light is isolated and converted to an intensity based grayscale, as blue flames indicate burning hydrocarbons, while reds and yellow are soot formation. Following this, the image is converted to black and white so it can then be fed into Matlab's built-in image edge detection protocol that has been specially calibrated for this application. The image is then overlayed on the original for quality assurance. Once the

edge is detected, it is mapped to a grid of x by y pixels for measurement. This method often creates edges that do not pass the vertical line test, so these double "x" points are eliminated by selecting the minimum value to isolate the bottom most edge of the flame. From here, numerous statistical operations can be performed on the mapped edge to determine an appropriate single liftoff height value for a given frame. Following this, statistical operations are performed on the thousands of frames which can be extracted from a single video file (depending on length) to reduce the data to a single characteristic liftoff height value. While this method works most of the time, on numerous occasions the edge detection program picks up on droplets close to the nozzle which create artifacts on the mapped edge, skewing the data. To compensate for this outlier elimination was integrated to remove these point. The results of this data smoothing can be seen in Figure E3

Figure E3

Liftoff height determination post processing progression with minimum and outlier filters.

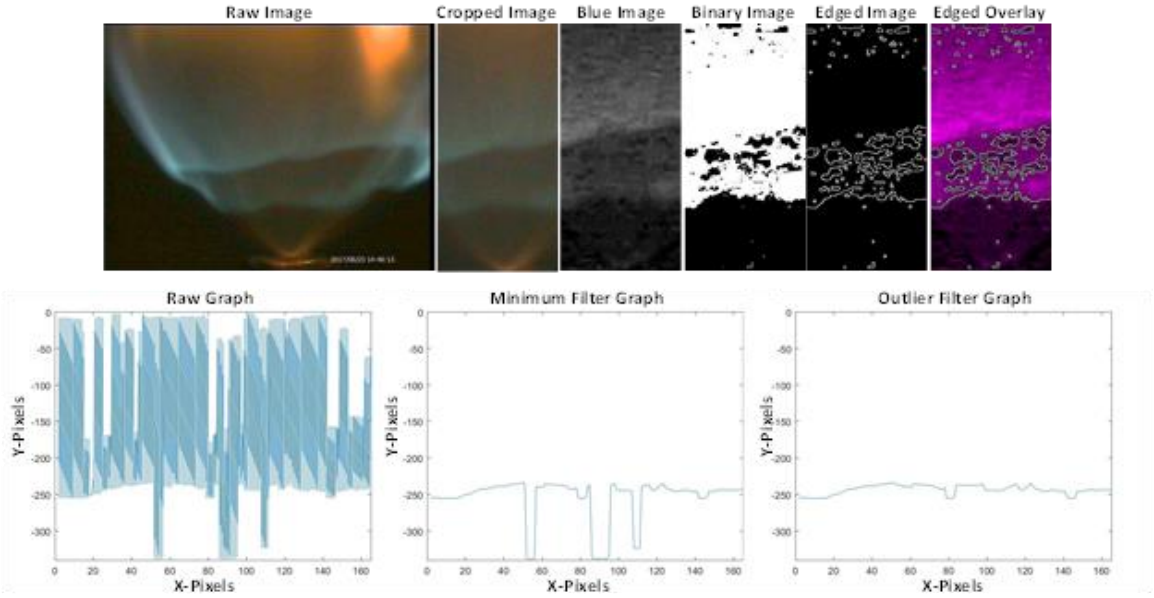

Testing numerous "bad" edge detections have shown that our method of outlier elimination is adequate to reliably find and measure the flame's liftoff. The reliably of the edge detection was determined through visual observation of edge overlays as well robust numerical operations which determine the number of points removed from each frame, tabulation of these values, and removal of frames where 20% (arbitrary) or of the points have been manipulated. These error checking and outlier protocols coupled with the various statistical operations which can be performed on the refined flame edge across numerous sequential or interval (i.e. every 10 frames) frames creates a robust system for determining flame liftoff heights. Moreover, to increase the utility and efficiency of this tool, the code was modified for use on Rowan University's high performance cluster (HPC) due to the immense processing power required to analyze the thousands of images which can be extracted from a single dataset. The full logic diagram and annotated code can be found below in sections E.2 and E.3

With this tool, if combustion chamber conditions and nozzle specifications are held constant, direct comparison of different fuel's liftoff heights based only on the fuel's combustion behavior can be performed. This test serves as an excellent platform to determine preferential vaporization's effect on the aforementioned "equivalent" surrogate fuels.

E.2 Logic Diagram:

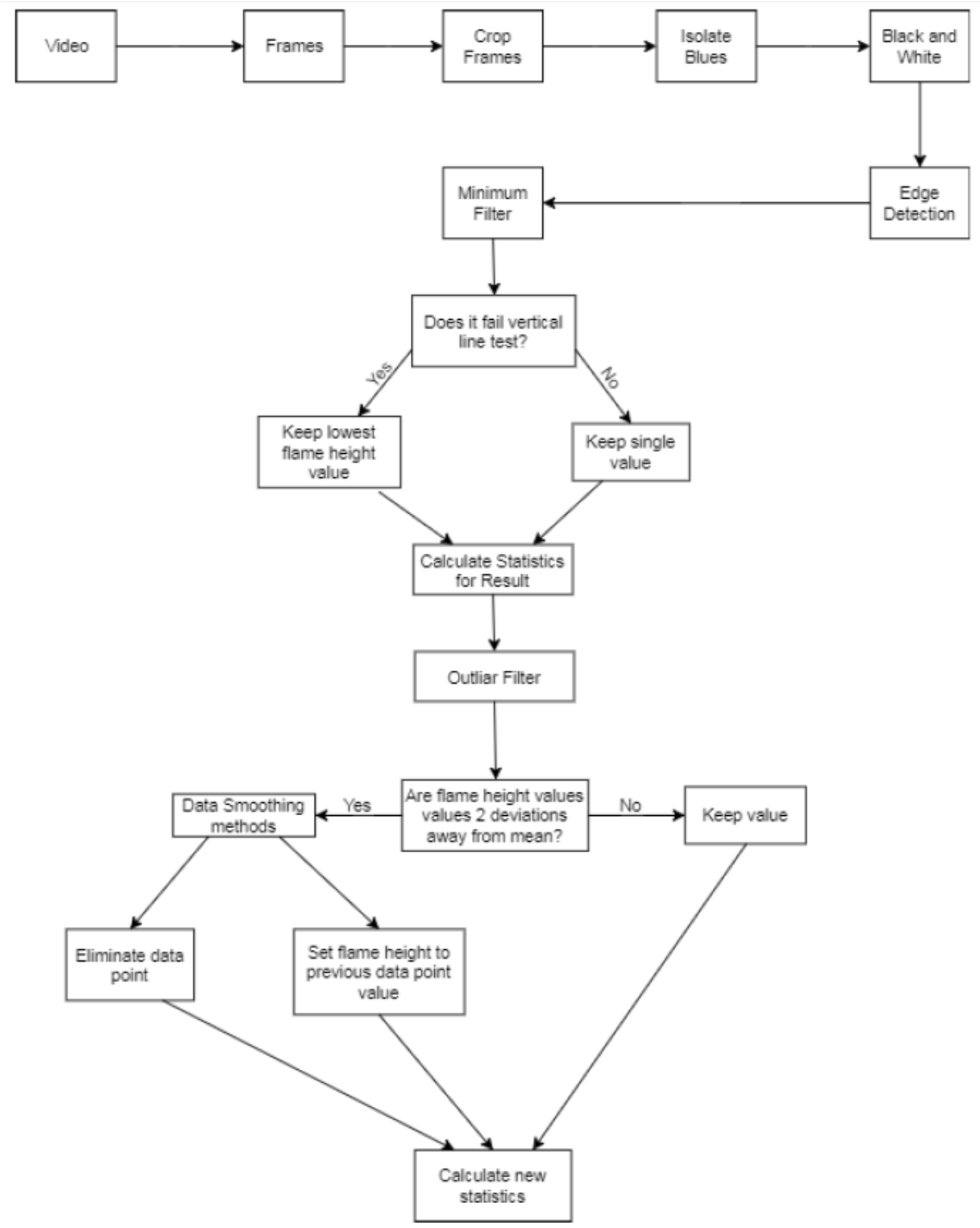

E.3 Liftoff Matlab Code:

```
%This program is designed to analyze the liftoff heights for multiple avi files of the same species in the same
folder
close all;
clear all;
clc;
% setting main directory and counting avi files for Acetone species
mainFolder = '\\rowanads.rowan.edu\home\estadtj4\Documents\Combustion Clinic\Acetone';
avi=dir([mainFolder '/*.avi']); %counting avi files
y_max=size(avi,1); %putting avi files in a matrix to count
date = '7-11-2017'; % user input:('What is the file date? DD-MM-YYY ' , 's');
species = 'Acetone'; % user input:('What is the species? ' ,'s');
% creating a new folder for each video file and moving files to new folder
for y = 1:y_max %For loop to run through all avi files in folder
    cd(mainFolder); % setting directory to main folder
    fileName = [date '_' species '_' num2str(y)]; %writing name of avi file from user input and numbering
    mkdir(fileName); %making new directory for video files
    movefile([fileName '.avi'],fileName); % moving video file to directory
    cd(fileName); % setting directory to new folder
    obj = VideoReader([fileName '.avi']); %reading video files
    vid = read(obj);
    frames(y) = obj.NumberOfFrames; %counting frames of avi file
%analyzing frames 1 to total number of frames with a step size for each avi file
    for x = 1 :50: frames
        imwrite(vid(:,:,:,x),strcat('frame-',num2str(x),'.jpg')); %saving frame image as jpeg
        I=imread(strcat('frame-',num2str(x),'.jpg')); %reading all frames for manipulation
        I2 = imcrop(I,[275 117 165 340]); %cropping, will change based on optical focus
        imwrite(I2,(strcat('Crop-',num2str(x),'.jpg'))); %saving cropped image as jpeg
```

```
Blue= I2(:,:,3); % Isolating blue component intensities
imwrite(Blue,(strcat('BlueCrop-',num2str(x),'.jpg'))); %saving blue image as jpeg
level = graythresh(Blue);  % Computing an appropriate threshold for greyscale
BW = imbinarize(Blue,level); %binarizing blues based on threshold (1's and 0's)
imwrite(BW,(strcat('BW-',num2str(x),'.jpg'))); %saving B/W image as jpeg
EDGE = edge(BW,'Canny'); %Detecting edge using Canny method
imwrite(EDGE,(strcat('EDGE-',num2str(x),'.jpg'))); %saving edged image as jpeg
C = imfuse(EDGE,Blue); %Creating edge and blue overlay image
imwrite(C,(strcat('Overlay-',num2str(x),'.jpg'))); %saving edge overlay image as jpeg
[row,col] = find(EDGE); %Mapping Edge to Grid
D=[col,-row]; %creating edge matrix
 i_max = size(D,1); %Determining x axis edge matrix size
%Vertical line test; keeping the minimum value
for i=1:i_max
   if i>1
      if D(i,1)<=D(i-1,1) %if i has multiples y-values, select lowest
         E(i-1,1)=0; %scaling grid 0-#x points
         E(i,1)=D(i,1); %initializing vertical line matrix x-axis
         E(i,2)= min(D(i,2),D(i-1,2));%select lower y-value
         E(i-1,2)=0; %set larger value to zero
      else %other wise keep the value
         E(i,1)=D(i,1); %x-values
         E(i,2)=D(i,2); %y-values
      end
   else %other wise keep the value
      E(1,1)=D(i,1);%x-values
      E(1,2)=D(i,2);%y-values
   end
```

```
end
% get rid of zeros
E( ~any(E,2), : ) = [];  %rows
E( :, ~any(E,1) ) = [];  %columns
% plot data without minimum filter
U= figure;
set(gcf, 'Visible', 'off');
plot (D(:,1),D(:,2));
xlim([0 165]); %x grid size
ylim([-340 0]);%y grid size
saveas(U,strcat('RawGraph-',num2str(x),'.jpg')); %creating rawgraph image .jpg
% plot data with minimum filter
T=figure;
set(gcf, 'Visible', 'off');
plot (E(:,1),E(:,2));
   xlim([0 165]);%x grid size
   ylim([-340 0]);%y grid size
saveas(T,strcat('MinFilterGraph-',num2str(x),'.jpg'));%creating minimum filter image .jpg
% calculating statistics for minimum filter of individual frame
Min1(x)=min(E(:,2));
Mean1(x)=mean(E(:,2));
Med1(x)=median(E(:,2));
Mode1(x)=mode(E(:,2));
Std1(x)=std(E(:,2));
MinTrans=transpose(Min1); %transposing for csv write and zero removal
MeanTrans=transpose(Mean1); %transposing for csv write and zero removal
% filtering outliers
j_max = size(E,1); %Determining number of points after minimum filtering
```

```
for j=1:j_max
   % if value is over 1.5 std. dev of mean - eliminate point
   if E(j,2) <= (Mean1(x) - 1.5*Std1(x))
      F(j,1)=0;
      F(j,2)=0;
   else %otherwise keep the point
      F(j,1)=E(j,1);
      F(j,2)=E(j,2);
   end
end
% eliminate any zeros from removed points
F( ~any(F,2), : ) = [];  %rows
F( :, ~any(F,1) ) = [];  %columns
% plot data from outlier filter
V=figure;
set(gcf, 'Visible', 'off');
plot (F(:,1),F(:,2));
   xlim([0 165]); %x grid size
   ylim([-340 0]); %y grid size
saveas(V,strcat('OutFilter-',num2str(x),'.jpg')); %creating outlier filter image .jpg
% calculate the number of point eliminated per frame
EliminatedFrame(x) = size(E,1) - size(F,1);
%calculating statistics from filtered data. If too many points are removed, frame is discarded - currently
set at 20%
if EliminatedFrame(x) < 0.2*frames
   Min2(x)=min(F(:,2));
   Mean2(x)=mean(F(:,2));
   Med2(x)=median(F(:,2));
```

```
            Mode2(x)=mode(F(:,2));
            Std2(x)=std(F(:,2));
            P=transpose(Mean2);%transposing for csv write and zero removal
            M=transpose(Min2);%transposing for csv write and zero removal
            % eliminate any zeros from removed frames
            M( ~any(M,2), : ) = [];  %rows
            P( ~any(P,2), : ) = [];  %rows
        else
        end
    end
% saving statistics for each frame as csv files
filename = 'NoFilterStats.csv';
data = [MeanTrans,MinTrans]; %Mean and min of unfiltered frames
csvwrite(filename,data);
filename = 'EliminationStats.csv';
data = [P,M];%Mean and min of outlier frames
csvwrite(filename,data);
%calculate statistics over of all the frames of each avi file
TotMMean(y)= mean(MeanTrans);
TotMMin(y)= mean(MinTrans);
TotOMean(y)= mean(P);
TotOMin(y)= mean(M);
TotEP(y)= sum(EliminatedFrame);
end
%changing directory back to the main folder
cd(mainFolder) ;
% writing statistics for all avi files with outlier filter
filename = 'NoFilterTotalStats.csv';
```

```
data = [transpose(TotMMean),transpose(TotMMin)];
csvwrite(filename,data);
filename = 'EliminationTotalStats.csv';
data = [transpose(TotOMean),transpose(TotOMin)];
csvwrite(filename,data);
% calculating statistics over all avi files for all frames to produce a single value for filter methods vertical
line test %and outlier elimination
MinFilterMean= mean(TotMMean);
MinFilterMinimum= mean(TotMMin);
OutFilterMean= mean(TotOMean);
OutFilterMinimum= mean(TotOMin);
EliminatedPoints = sum(TotEP);
```

Appendix F

Raw Data

F.1 0.5 GPH Raw Data:

Trial 1	
Blowout (Ω)	Velocity ($^m/_s$)
Acetone	
520	3.30
490	3.50
510	3.36
450	3.77
530	3.23
460	3.70
500	3.43
nC7	
520	3.30
540	3.16
510	3.36
550	3.09
510	3.36
nC10	
710	1.78
710	1.78
680	2.06
650	2.32
650	2.32
640	2.41
nC12	
720	1.68
690	1.97
680	2.06
700	1.87
690	1.97
690	1.97
iC8	
560	3.02
580	2.87
590	2.80
580	2.87
nC8	
540	3.16
540	3.16
520	3.30
nC16	
720	1.68

Trial 2	
Blowout (Ω)	Velocity ($^m/_s$)
Acetone	
610	2.65
650	2.32
620	2.57
640	2.41
590	2.80
640	2.41
Jet_LT	
710	1.78
710	1.78
700	1.87
700	1.87
700	1.87
710	1.78
700	1.87
710	1.78
720	1.68
700	1.87
700	1.87
Jet_HV	
690	1.97
700	1.87
700	1.87
720	1.68
690	1.97
700	1.87
690	1.97
710	1.78
710	1.78
710	1.78

Trial 3	
Blowout (Ω)	Velocity ($^m/_s$)
Acetone	
600	2.72
620	2.57
580	2.87
560	3.02
590	2.80
570	2.94
Sur95t	
500	3.43
480	3.57
500	3.43
510	3.36
500	3.43
530	3.23
460	3.70
520	3.30
470	3.63
520	3.30
Sur95o	
470	3.63
470	3.63
470	3.63
480	3.57
490	3.50
430	3.90
490	3.50
470	3.63
420	3.97

Trial 4	
Blowout (Ω)	Velocity ($^m/_s$)
Acetone	
670	2.15
620	2.57
590	2.80
620	2.57
Black	
690	1.97
680	2.06
680	2.06
700	1.87
Green	
330	4.62
310	4.78
Blue	
680	2.06
670	2.15
650	2.32
Pink	
230	5.48
250	5.30
nC8	
440	3.84
430	3.90
450	3.77
440	3.84
370	4.32
nC10	
660	2.24
720	1.68
720	1.68
720	1.68
720	1.68
730	1.58
710	1.78

F.2 0.4 GPH Raw Data:

Trial 1	
Blowout (Ω)	Velocity ($^{m}/_{s}$)
Acetone	
710	1.54
710	1.54
710	1.54
700	1.64
710	1.54
690	1.75
680	1.85
710	1.54
720	1.43
720	1.43
720	1.43
710	1.54
nC7	
740	1.22
750	1.11
750	1.11
740	1.22
740	1.22
750	1.11
740	1.22
730	1.32
740	1.22
740	1.22
740	1.22
740	1.22
nC10	
750	1.11
740	1.22
750	1.11
740	1.22
750	1.11
750	1.11
760	1.00
750	1.11
760	1.00
750	1.11
nC12	
750	1.11
750	1.11
740	1.22
770	0.89
770	0.89
770	0.89
770	0.89
770	0.89
780	0.77
780	0.77
780	0.77
770	0.89
770	0.89
770	0.89
iC8	
800	0.55
800	0.55
800	0.55
790	0.66
800	0.55
790	0.66
790	0.66
800	0.55
790	0.66
790	0.66

Trial 2	
Blowout (Ω)	Velocity ($^{m}/_{s}$)
Acetone	
770	0.89
760	1.00
770	0.89
760	1.00
770	0.89
770	0.89
770	0.89
780	0.77
780	0.77
770	0.89
760	1.00
Sur95t	
760	1.00
670	1.96
760	1.00
690	1.75
660	2.06
760	1.00
Sur95o	
450	3.96
590	2.75
690	1.75
Jet_LT	
830	0.20
850	0
840	0.09
840	0.09
810	0.43
830	0.20
830	0.20
830	0.20
830	0.20
Jet_HV	
890	0
860	0
870	0
850	0
850	0
840	0.09
840	0.09
830	0.20
820	0.32
830	0.20

Appendix G

Unreliable Data

G.1 Mark II 0.4 GPH Solid Cone Sensitivity Test

The below experiments were performed with the Mark II rig equipped with a 0.4 GPH solid cone atomizing spray nozzle. The blowout thresholds using the 0.40 GPH nozzle proved inadequate due to the low chemical energy input and resulting low blowout velocities. These conditions put the WORX blower well out of its designed operating conditions such that the curve fit, which was generated over a range of blower conditions indicated a zero, and in some cases negative velocity. This is further exacerbated by the anemometer's error, velocity pickup range, and resolution. For these reasons this data was considered unreliable but represents a stepping stone in the development of the burner rig, so it is presented here.

- Demonstration of blowout sensitivity to physical and chemical property variations
    - Achieved by evaluation of the pure component n-alkane series nC7, nC10, nC12 and alkane isomer iC8.
    - Figure G1 displays the results of this dataset and 1σ error bars.

Figure G1

Pure component blowout thresholds with 1σ error bars used to determine blowout experiment sensitivity in the 0.4 GPH configuration.

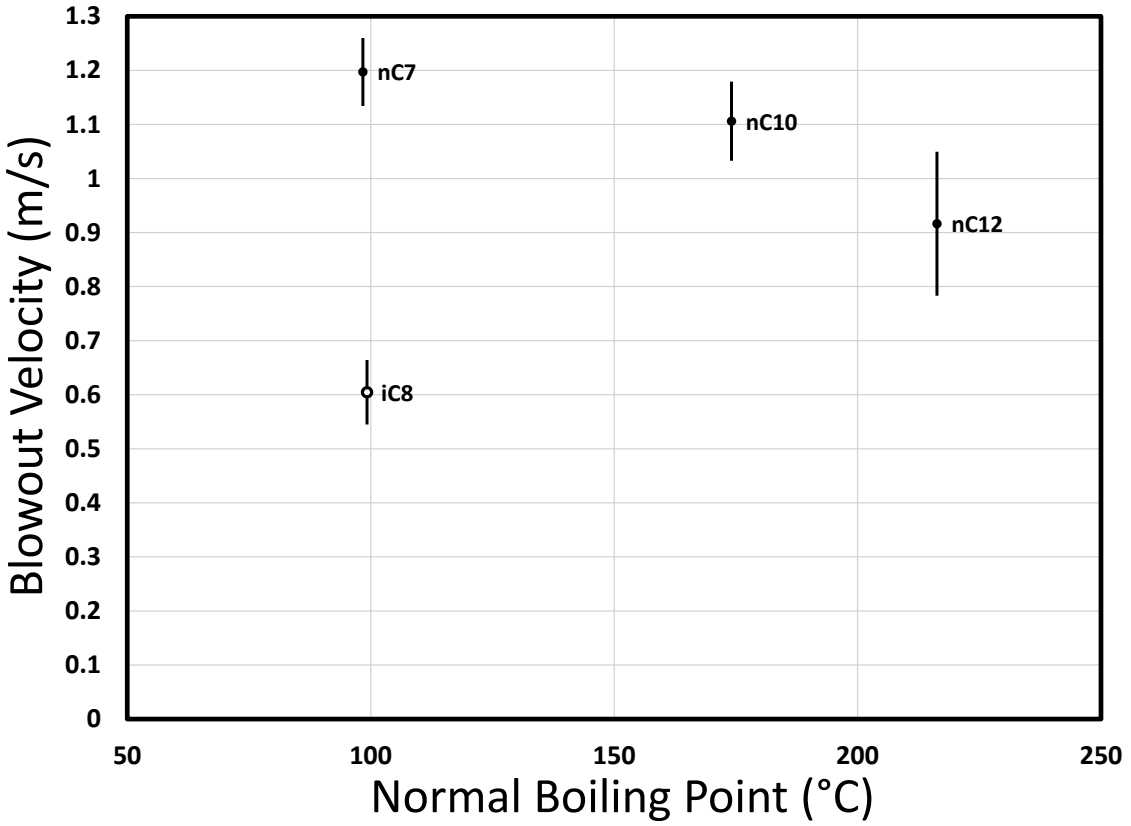

- Experiment is sensitive to both physical and chemical property variations.
    - The n-alkane series (nC7, nC10, nC12) represent species with highly similar prevaporized combustion chemistry and varying physical characteristics (e.g., normal boiling point).
        - Blowout velocity varies modestly as a function of physical property effects on the complex spray combustion environment.

- The blowout experiment is sensitive to physical property variation.

- The experiment can differentiate blowout behavior of the physically similar but chemically divergent nC7 (RON=0), iC8 (RON=100) species.
  - Blowout velocity varies significantly as a function of chemical property effects on the complex spray combustion environment.
    - The experiment is sensitive to chemical property variation.
- This data demonstrates the experiment's responsiveness to both chemical and physical properties, and displays its ability to differentiate individual specie's blowout thresholds.

- Data reveals that blowout thresholds of the collectively higher reactivity (DCN) n-alkane species compared to the iC8 isomer display a higher resistance to blowout. Taken as a whole, both chemical and physical properties contribute to blowout behavior. However, in this experimental configuration, the role of prevaporized chemistry seems to be significantly more influential than the modest variations in blowout thresholds from physical property variation.
  - Evidenced by the severely depressed blowout resistance of iC8 from nC7 as compared to the modest inter-species discrepancies in behavior displayed by the n-alkanes.

G.2 Mark II 0.4 GPH Solid Cone Jet Fuel Surrogates

- Confident in experimental sensitivity, jet fuel surrogates from the literature [29] were evaluated. Data seen in Figure G2 below.

Figure G2

Jet-A surrogate's blowout thresholds with 1σ error in the 0.4 GPH configuration. Streak length represents distillation profile and width indicates error.

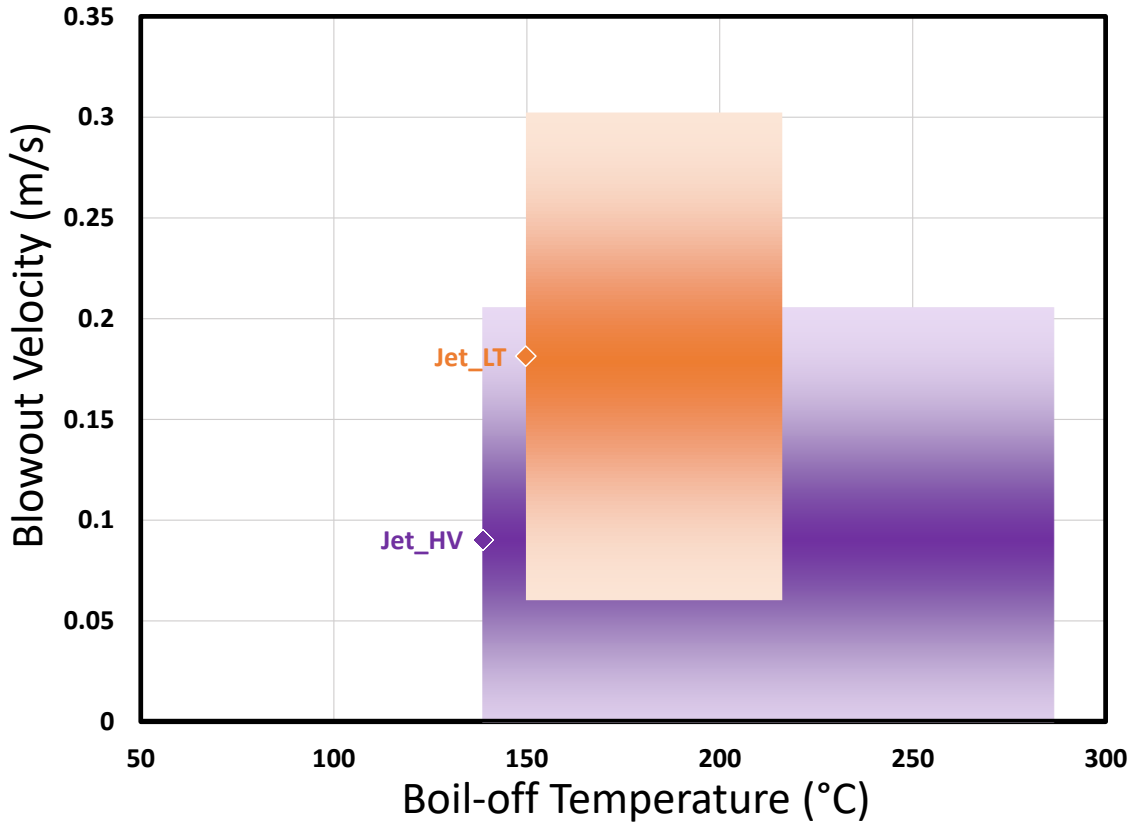

- The Jet-A surrogate's blowout threshold results are displayed as large streaks with length representative of their respective distillation profiles and width 1σ experimental error.
- Inter-surrogate incongruity seen, with the Jet_LT surrogate displaying increased resistance to blowout.
- Results presented here are unreliable
    - Blowouts are seen to be "zero"

- No flames experienced a spontaneous blowout, this zero value is a result of the input resistance-to-air velocity anemometer correlation.
- Low chemical energy input from 0.4 GPH nozzle coupled with the low overall volatility of the Jet-A surrogates seem to create conditions where a minimal bulk flow is sufficient to extinguish the flame.
    - These conditions put the WORX blower well out of its designed operating conditions such that the curve fit, which was generated over a range of blower conditions indicated a zero, and in some cases negative velocity.
    - Exacerbated by the anemometer's error, velocity pickup range, and resolution.
        - Any insight is highly speculative and arguably erroneous.

G.3 Mark II 0.4 GPH Solid Cone Gasoline Fuel Surrogates

- The previous data in Figure G2 apprehensively presents evidence that may indicate the gasoline surrogates developed in [9] which are designed with a similar method as the Jet fuel surrogates in [29] may not emulate the design real fuel's combustion behavior due to property stratification resulting from preferential vaporization.
- The gasoline surrogate fuels blowout thresholds were acquired with the Mark II 0.4 GPH solid cone configuration. The results of this dataset, are presented in Figure G3.

Figure G3

Gasoline surrogate's blowout thresholds with 1σ error in the 0.4 GPH configuration. Streak lengthrepresents distillation profile and width indicates error.

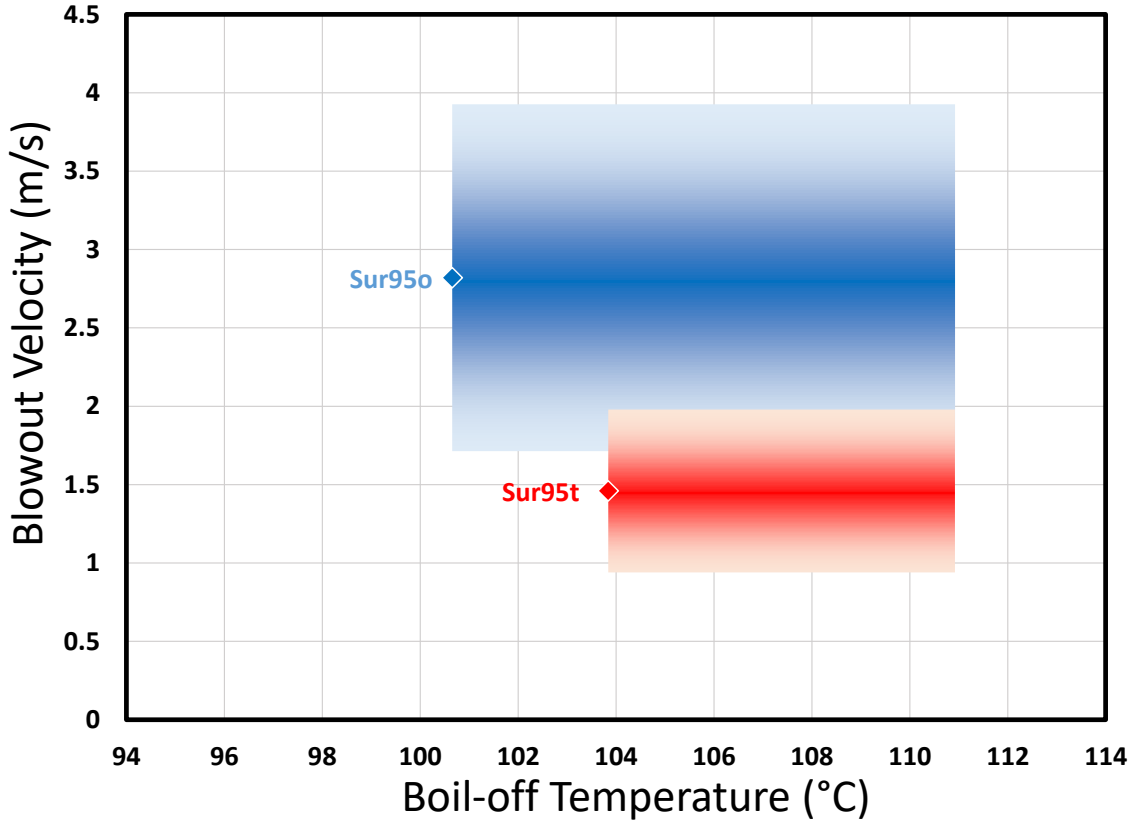

- Dissimilar blowout thresholds were measured for these fuels.
- Error in this dataset is large and results from erratic behavior observed during the blowout test.
    - Trend seen in this data is reflected in Mark II 0.5 GPH solid cone data presented in the main body of this study.
- 0.4 GPH data is unreliable due to erratic flame behavior indicated by large error bars.